UNIVERSITÀ DI PISA

University of Pisa
Department of Energy and Systems Engineering

Novel Haptic Cueing for UAV Tele-Operation

Thesis
Ph.D Course on:
Automation Robotics and Bioengineering
Cicle XXII (2007)

Tutor:
Prof. Lorenzo Pollini
Student:
Samantha M.C. Alaimo

Typeset by the author with the LaTeX Documentation System.
Author email: samanthaalaimo@yahoo.it

Abstract

The use of Unmanned Aerial Vehicles (UAVs) is continuously increasing both for military and civilian operations. The degree of automation inside an UAV has reached the capability of high levels of autonomy, increasing but human participation/action is still a requirement to ensure an ultimate level of safety for the mission. Direct remote piloting is often required for a board range of situations; this is true especially for larger UAVs, where a fault might be dangerous for the platform but even for the other entities of its environment (people, building etc.). Unfortunately the physical separation between pilot/operator and the UAV reduces greatly the situational awareness; this has a negative impact on system performance in the presence of remote and unforeseen environmental constraints and disturbances. This is why this thesis is dedicated to the study of means to increase the level of situational awareness of the UAV operator.

The sense of telepresence is very important in teleoperation, and it appears reasonable, and it has already been shown in the literature, that extending the visual feedback with force feedback is able to complement the visual information (when missing or limited). An artificially recreated sense of touch (haptic) may allow the operator to better perceive information from the remote aircraft state, the environment and its constraints, hopefully preventing dangerous situations. This thesis introdues first a novel classification for haptic aid systems in two large classes: Direct Haptic Aid (DHA) and Indi-

rect Haptic Aid (IHA), then, after showing that almost all existing aid concepts belong to the first class, focuses on IHA and tries to show that classical applications (that used a DHA approach) can be revised in a IHA fashion. The novel IHA systems produce different sensations, which in most cases may appear as exactly "opposite in sign" from the corresponding DHA; these sensations can provide valuable cues for the pilot, both in terms of improvement of performance and "level of appreciation". Furthermore, it will be shown that the novel cueing algorithms, which were designed just to appear "natural" to the operator, and not to directly help the pilot in his task (as in the DHA cases), can outperform the corresponding DHA systems.

Three case studies were selected: obstacle avoidance, wind gust rejection, and a combination of the two. For all the cases, DHA and IHA systems were designed and compared against baseline performance with no haptic aid. Test results show that a net improvement in terms of performance is provided by employing the IHA cuse instead of both the DHA cues or the visual cues only. Both professional pilots and nave subjects were used in some of the experiments. The perceived feelings transmitted by the haptic cues, strongly depend by the type of the experiment and the quality of the participants: the professional pilots, for instance, retained the DHA the most helpful force while they preferred IHA because they found it more natural and because they felt a better control authority on the aircraft; different results were obtained with naive participants.

In the end, this thesis aim is to show that the IHA philosophy is a valid and promising alternative to the other commonly used, and published in the scientific literature, approaches which fall in the DHA category.

Finally the haptic cueing for the obstacle avoidance task was tested in the presence of time delay in the communication link, as in a classical bilateral teleoperation scheme. The Master was provide with an admittance controller and an observer for force exerted by

the human on the stick was developed. Experiments have shown that the proposed system is capable of standing substantial communication delays.

Contents

List of Figures

List of Tables

Chapter 1

Introduction

1.1 Unmanned Aerial Vehicles

Unmanned Aerial Vehicle (UAV) is the name commonly used to describe an airborne vehicle without any pilot on-board, which operates under either remote or autonomous control. UAVs are also referred as Remotely Piloted Vehicles (RPVs), Remotely Operated Aircrafts (ROAs), Unmanned Vehicles Systems (UVSs) or simply Drones. In most instances, the term RPV might be more appropriate as the name suggests that the vehicle is remotely controlled and still rely, to a great degree, on human involvement.

UAVs are mainly employed in military field. Lessons from recent combat experiences in Kosovo, Afghanistan and Iraq have shown that UAVs can provide vastly improved acquisition and more rapid dissemination of Intelligence, Surveillance and Reconnaissance (ISR) data [9]. Over the past several years, a confluence of events and developments has brought the Military Services to change the way of perceiving the UAVs. These include:

- Dramatic increases in computer processing power;
- Advances in sensor technologies that reduce sensor size and

weight, provide high resolution, and permit detection of fixed and moving targets under a variety of environmental conditions;

- Improved communications, image processing, and image exploitation capabilities.

UAVs have the potential to reduce operational and support cost as compared to the use of manned aircraft [8].

Currently UAVs have a permanent position in the military arsenal in the US, Europe, Middle East and Asia. Today UAV development strives toward more peaceful and civil usage [10] such as rescue, border surveillance, disaster monitoring, telecommunications relay, fire fighting, traffic monitoring, pipeline surveillance, agriculture, construction, and public utility operations [61]. Thus, police, forest rangers, fire brigades are very interested on them for public security. UAVs civil employment also includes video-taping for photogrammetric or scientific applications [7].

Communications represent the most important subsystem for UAVs. Bandwidth is needed to support systems that control the UAVs flight, launch and recovery, to transmit the output of on board sensors to both line of sight and beyond line of sight processing centers, and to communicate with air traffic control centers. Equally important is the recognition of a mission area for UAVs acting as communication relays linking tactical forces, including other UAVs, and providing connection to support centers.

The potential benefits of UAVs, such as low operational cost and no risk of losing human lives, make sense when the teleoperation is safe and no mishaps and accidents occur. A crash of a UAV during teleoperation will not only lead to possible damage to the local environment, but could also lead to the loss of the vehicle. Humans in the vicinity of the incident may get injured as well. Therefore, safety in UAV teleoperation is of great importance not only for mission success but also to preserve the sustainability of UAV operations

[12].

1.2 Manual vs autonomous control

Various ways to control UAVs exist. They can be categorized in autonomous control and manual control.

Some of the problems associated with the automatic control are [10]:

- Reduced situation awareness;
- Increased monitoring demands;
- Cognitive overload;
- Mis-calibration of trust in automation (either excessive trust, termed ”complacency”, or, at the other extreme, mistrust of automation);
- Inability to reassume manual control;
- Degraded manual skills through lack of practice;
- The need for new selection and training procedures;
- Increased inter-operator coordination requirements;
- Increased workload management requirements;
- Loss of motivation and job satisfaction;
- Increase in the risk of human error because of the human weakness to maintain vigilance during extended periods of relatively low task demand.

Furthermore, fully-autonomous systems are more suitable for simple missions with, for example, pre-defined targets and far away from inhabited environments. Manual teleoperation could enable more flexibility in controlling a UAV close to inhabited environments and without predefined targets [12]. This is suitable for civil applications such as reconnaissance, surveillance tasks and it is subjected to failures. Focusing on manual control would give to the pilot the freedom to choose the targets step by step (for example because of last minute communication from control towers). Furthermore, the complex scenarios in which UAVs would operate requires the presence of the human operator in the decision making system.

For all these reasons, keeping a human operator in-the-loop is required.

1.3 UAV Mishaps

There are several factors at work contributing to UAV mishaps.

Besides electro-mechanical failures (62%), mishaps and incidents in UAV teleoperation are, for a great part, due to human errors during operation (25%) [8]. This is essentially due to the lack of the natural, multiple-sensory information of the environment. In fact, the remote pilot is inside the Control Ground Station (CGS)(see Figure 1.1) which is characterized by the following troubles:

- Limited Field Of View cameras (i.e. no "look around" possibility, etc.);
- No inertial cues (motion, vibrations, gravity/attitude etc.);
- No auditory cues;
- Video/data communication delays;
- No feedback on control stick of the environment around the remote vehicle (obstacles, disturbances etc.).

Figure 1.1: UAV remote piloting from a Control Ground Station (picture from http://www.flickr.com).

Usually, in order to solve the first mentioned trouble, the UAV operator is supplied with a richer visual information like showing different cameras on various displays. Another alternative is to supply the operator with a continuously updated "augmented reality" or "synthetic vision" produced by a computer resembling reality [21]. As concerning the inertial cues, some steps on the employment of motion cueing to augment UAV operator performance and improve UAV flight training was made [22, 23]. About the auditory cues, augmented reality through multi modal tactile and auditory information displays has been used in other fields to resemble reality [10, 24]. The communication delays, depending on the situation, turn out in the range of 100 to 1600 ms (and even more). This is a considerable amount given that 100 ms delay usually leads to measurable degradation of human performance [29, 27]. Delays of about 250-300 ms quite often lead to unacceptable airplane handling qualities [33]. Other techniques were used in the past to improve the performance of a teleoperator in presence of time delay; for instance, automatic switching for stopping override [26] or the use of the predicted display [25]. As concerning the haptic feedback, tactile cues have shown to complement the visual information (through the visual displays of a remote CGS) and improve the efficiency of the UAV teleoperation [21, 1, 10].

In conclusion, augmented feedback to the operator such as haptic feedback and multi modal displays can compensate, to some extent, for the lack of sensory cues that would be presented to UAV operators [10]. Introducing the mentioned augmented feedbacks in the CGS would hopefully imply a reduction of the UAV mishaps.

Thus, investing in a human machine interface design tailored on the human needs would improve the operator situational awareness and maybe the performances.

1.4 Situational Awareness

By the late 1980s, there was a growing interest in understanding how pilots maintain awareness about the many complex and dynamic events that can occur simultaneously in flight, and how this information was employed to guide future actions. The vast quantities of sensor information available in the modern cockpit, coupled with the flight crew's "new" role as a monitor of aircraft automation, increased interest on Situational Awareness (SA) issue [13]. Through the word "situation(al) awareness", the processes of attention, perception, and decision making that together form a pilot's mental model of the current situation of the aircraft is described [15]. According to [18], the crews knowledge of both the internal and external states of the aircraft, as well as the environment in which it is operating is defined as SA.

In fact, the internal state of the aircraft that is the 'health' of its utility systems and terrain, threats, and **weather** that corresponds to the external environment must be monitored.

To expand upon this definition, Endsley [16], described the three hierarchical phases of SA: perception, comprehension, and projection. The First SA Level, named *Perception of the elements in the environment*, include perceiving the status, attributes, and dynamics of relevant elements in the environment (airspeed, position, altitude, route, direction of flight etc) and also weather, air traffic control clearances, emergency information etc. [16]. The Second SA Level, named *Comprehension*, is based on an understanding of the significance of the First SA Level elements. The Third SA Level, named *Projection*, is based on the knowledge of the status and dynamics of the elements and a comprehension of the situation (both First and Seconds SA Levels).

SA is not synonymous with good performance. In fact, having good SA might bring good performance: a pilot could have a good SA without being a good pilot for the lack of motor skills, because of co-ordination or attitude problems etc. Conversely, under automatic flight conditions it is possible to have good performance with minimal SA [17].

As concerning SA in automation, SA is something that a person creates himself through perception (First SA Level) and it could not be provided by automation which usually exclude the human operator from the control loop. Though automation can be thought in a different way say *supporting SA through decision aids and system interfaces*. And SA can be hindered if designers fail in adequately addressing the SA needs of the operator [17].

Since SA is created through the perception of the situation (Level 1), the quality of SA is very dependent on how the person directs attention and how attention to information is prioritized based on its perceived importance. Jones and Endsley (1996) found that operators were prone to overlooking crucial information in sustaining SA, though all relevant and needed information was present. Actually, this was found to be the most frequent causal factor associated with SA errors [10].

The above definitions are written in case of aviation in general but can be extended to the case of UAV teleoperation as long as the

CGS is, in this case, fixed to the ground. Thus, as seen in subsection 1.3, being aware of the aircraft internal and external state is much more difficult for the pilot. According to [10] haptic feedback can compensate to some extent for the lack of sensory cues that will be presented to UAV operators (see subsection 1.3), this means that a way to improve the situational awareness of a remote UAV pilot and the efficiency of the teleoperation is the addiction of a haptic interface to the visual interface.

1.5 Bilateral Teleoperation

One of the advantages of a teleoperation system is to combine the human capabilities with the robot ones. UAVs have also been referred to as non-anthropomorphic robots [41]. Through the teleoperated systems barriers like distance, hazardness or scaling can be overcome.

Remote teleoperation can be classified into unilateral and bilateral. In unilateral teleoperation no haptic feedback is available to the operator. In bilateral teleoperation, haptic feedback allows the operator to have a better feeling about the remote environment, providing a more extensive sense of telepresence [39].

The word *telepresence* refers to an experience that appears to involve displacement of the user's self-perception into a computer-mediated environment [40]. In particular the word telepresence is employed when the remote environment is real and not synthetic. In this case it is referred as *virtual presence* [40].

In teleoperation, a human operator conducts a task in a remote environment via master and slave manipulators [29]. In particular, in a haptic teleoperation system, a human operator controls a remotely located teleoperator or slave device via a human system interface or master device while receiving haptic feedback of the interaction between the teleoperator and the (virtual or real) environment.

Stimulating a human's sense of touch by managing with sensation of movement or force in muscles, tendons, and joints is referred to as having a kinesthetic or haptic sensory experience [34].

As haptic data from the master site enters the control on slave site and vice versa, a control loop between the subsystems human-master and slave-environment is closed over the communication channel. This poses several challenges for control design, above all in the presence of time delay in the communication links (see section 2.4).

1.6 Goal of the Thesis

The aim of this work is the investigation of possible haptic aids for teleoperated systems. In particular this thesis focuses on the teleoperation of UAVs. The principal issue of remote piloting an UAV is represented by the physical separation between pilot and vehicle which causes an almost complete absence of the sensorial information usually available when on board.

The purpose of this report is threefold. First, it presents a novel classification of the haptic aids present in literature in two classes Indirect Haptic Aids (IHA) and Direct Haptic Aids (DHA) (see Chapter 2). This is a contribution on the research on the enhancing of the UAV pilot Situational Awareness. In fact, by assuming that haptic aids provide an improvement of the SA, this thesis launches a highly important challenge that is to explore which haptic feedback philosophy should be followed in order to better improve the SA. In particular, the main goal of this thesis is to show that the Indirect Haptic Aid philosophy is a valid alternative to the other commonly used, and published in the scientific literature, approaches which mainly fall in the Direct Haptic Aid category. Second, it investigates the potential of using a novel concept of tactile interaction as an information source of the external conditions of the air bone aircraft. Third, it explores the benefits of multi-modal information sources on the flight deck, in terms of improving attention and enhancing flight performance. This work focuses on the investigation of possible haptic cues meant to improve the virtual immersion of the remote pilot. Three novel haptic feedbacks were designed. The first one is a reality-inspired haptic aid since it was built to transmit to the UAV teleoperator a realistic situation which is happening outside the aircraft: the external disturbances such as wind gusts. The second one is an artificial component since it depends on environmental constraints. The third one is both a reality and a virtual reality-inspired haptic aid and it merges the first two haptic feedbacks.

The haptic feedbacks will be provided to the human operator via a haptic control device. As concerning the reality-based haptic feedback, the research resulted in the *Conventional Aircraft Artificial Feel*. As concerning the artificial-based haptic feedback, the research resulted in a novel philosophy of an obstacle avoidance haptic feedback, the *Obstacle Avoidance Feel*, which was built to help the UAV teleoperator in detecting and hopefully avoiding the obstacles. As concerning the mixed reality/virtual reality-based haptic feedback, the research resulted in the *Mixed Conventional Aircraft Artificial Feel/Obstacle Avoidance Feel* which extends the previously described haptic aid systems by merging them into a system capable of aiding a pilot involved in a flight within a constrain environment in the presence of wind gusts.

The above just introduced haptic feedbacks both fall in the class of Indirect Haptic Aids. The mentioned Conventional Aircraft Artificial Feel will be shown to increase the performance in terms of instinctive response to a stimulus in pilots without any previous training on the experiment. It also improves the situational awareness intended as making the pilot to feel as piloting the aircraft on board. The Obstacle Avoidance Feel will be shown to provide a net improvement in the operator sensation with respect to the existing obstacle avoidance haptic aids from the Direct Haptic Aids class. This would improve the safety of the teleoperation by keeping higher the attention of the pilot in the task and improve the situational awareness.

1.7 Thesis outline

The structure of this report is the following: Chapter 2 presents a review about the haptic aids published in literature and classifies them in two classes: Direct Haptic Aid (DHA) and Indirect Haptic Aid (IHA). It also shows the problem of the presence of delay in the communication link of a bilateral teleoperation and it mentions the remedies proposed in literature. Chapter 3 describes in details the Conventional Aircraft Artificial Feel (CAAF) which, as will be shown, belongs to the IHA class. The newly introduced CAAF haptic force was evaluated and Section 3.6 shows the evaluation results. Chapter 4 describes in details the Obstacle Avoidance Feel (OAF) which, as will be shown, also belongs to the IHA class. The newly introduced OAF haptic force was evaluated and Section 4.5 shows the evaluation results. Chapter 5 presents and evaluates (see Section 5.6) the Mixed Conventional Aircraft Artificial Feel/Obstacle Avoidance Feel (Mixed-CAAF/OAF), belonging to the IHA-class as well. It was evaluated as well and Section 5.6 shows the experimental results. Finally, the Chapter 6 considers the introduction of the time delay in the communication link and proposes the application of an admittance-control scheme for the master side with the new introduction of an observer to estimate the human operator force in case of lack of force sensors in the employed haptic device.

Chapter 2

Haptic Systems

As mentioned in Chapter 1, in a general teleoperation setting, the human exerts a force on the master manipulator which in turn results in a displacement that is transmitted to the slave that mimics that movement. If the slave possesses force sensors, then it can transmit, or reflect back to the master, the reaction forces from the task being performed in the remote environment; these enter into the input torque of the master, and the teleoperator is said to be controlled bilaterally (see Figure 2.1) [54].

Although reflecting the encountered forces back to the human operator enables the human to rely on his/her tactile senses along with visual senses, it may cause instability in the system if delays are present in the communication media. This delay-induced instability of force reflecting teleoperators has been one of the main challenges faced by researchers [27, 29, 30, 31, 32, 33].

The teleoperation through haptics has already a 50 years of history. Indeed, in 1950 the first masterslave teleoperator was built by Goertz [38] to remotely handle radioactive substances. Since that work, the number and diversity of teleoperation applications have considerably increased. Today, such systems are used in underwater exploration, manufacturing, chemical and biological industry, and,

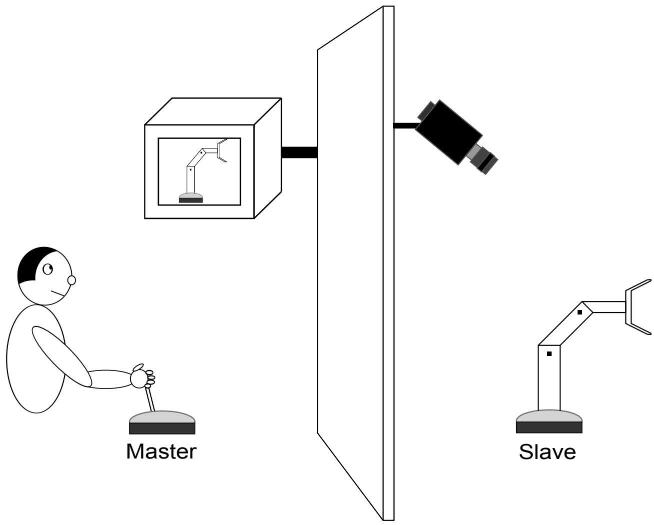

Figure 2.1: Bilateral teleoperation.

more recently, in the medical field. This Chapter focuses in the most recent application: the mobile robot teleoperation.

According to [10] haptic feedback can compensate to some extent for the lack of sensory cues that are presented to UAV operators (see subsection 1.3), this means that a way to improve the situational awareness of a remote UAV pilot and the efficiency of the teleoperation is the addiction of a haptic interface to the visual interface. It is particularly necessary in case of limited visual informations. In the presence of foggy weather conditions, for example, or because of the employment of a limited FOV camera, the haptic feedback provides information through the sense of touch, which can be applied directly on the control device. It is well known that the reaction to the perceived haptic information is faster (3 Hz) with respect to visual information (0.5 Hz). This is due to the spinal cord that acts as a subconscious fast controller [20].

In the next subsection a review of the mobile robot teleoperated systems is presented.

2.1 Robot Bilateral (Tele)operation Review

Some of the numerous applications of teleoperation are operating space robots from ground, commanding unmanned underwater vehicles, handling hazardous materials, maneuvering mobile robots with obstacle avoidance. The present section focuses on the teleoperation of mobile robots.

The following subsections review the Ground Mobile Robots and Manned and Unmanned Aerial Vehicles bilateral teleoperations.

2.1.1 Ground Mobile Robots

This subsection presents a review about the teleoperation of ground mobile robots. Reference [4] makes use of a haptic interface in order to increase the users perception of the workspace of the mobile robot. In particular, a virtual interaction force is computed on the basis of obstacles surrounding the mobile vehicle in order to prevent dangerous contacts, so that navigation tasks can be carried out with generally better performances. When an obstacle is close enough to the mobile robot it exerts a spring damper virtual force on the teleoperator through the haptic device in order to help him/her in avoiding the collision with the obstacle.

Also in [55] the force feedback is based on measured distances from the mobile robot to the obstacles. The force feedback gain is variable based on measured distances to the obstacle and derivatives of the distances. Clearly, the gain is higher when the obstacle and the mobile robot approach each other than when obstacle and robot are moving away from each other.

In [56] the goal location exerts an attractive force on the teleoperator which is proportional to the distance between the goal location and the mobile robot.

References [4, 55, 46] make use of the *Car-Driving Metaphor* which utilizes position-velocity kinematic mapping: the displacement of the end-effector of the haptic device is mapped to the linear and angular velocities of the mobile robot. A 3D approach of the car-driving metaphor is presented in [57]: the Intuitive Haptic Conical Control Surface. Here, the third vertical coordinate provides the current velocity of the robot and so the conical surface allows intuitive haptic detection of the zero speed. For example, a force directed to the zero speed point (the cone's vertex) is a suggestion to the teleoperator to decrease the commanded velocity of the mobile robot.

Also in [46] the obstacle force feedback exerted on the teleoperator is a repulsive one and it is proportional to the distance between the robot and the obstacles.

2.1.2 Manned and Unmanned Aerial Vehicles

The present section presents a literature review concerning operation (remote or not) of aerial vehicles, both manned and unmanned. In [59], 68 actuators form a vibrotactile image that can be updated in real-time navigation, hovering, threat warning, spatial disorientation countermeasures, communication, etc. The actuators are attached to the body and communicate information by vibrating at a specific location. The most simple set-up is when only one actuator vibrates: it is attached to that side of the body that corresponds to the desired direction of movement. Possible applications in land (navigation support and threat warnings for drivers, infantrymen, blind people, etc.), underwater (divers), and in space (astronauts in the International Space Station).

Reference [1] investigated the application of haptic feedback in

UAV teleoperation for collision avoidance in low airspace by mapping of the environmental constraints that can even be outside the visual FOV. In the context of teleoperated systems where visual cues only have usually been used, the adoption of an artificial feel system for the stick appears to increase the situational awareness; this is extremely relevant for UAVs.

Tactile cues have shown to complement the visual information (through the visual displays of a remote CGS) and improve the efficiency of the teleoperation [1]. The task of the experiment was to fly from waypoint to waypoint as accurately as possible in an obstacle-laden environment. Stick deflection tilt the Swashplate (as in a real helicopter). The force on stick was proportional to the distance between the UAV and the obstacles.

They showed with a rather complex remote piloting and obstacle avoidance simulations that an appropriate haptic augmentation may provide the pilot a beneficial effect in terms of performance in its task. The authors extensively studied the problem of force feedback (injecting an artificial force on the stick) and stiffness feedback (changing stick stiffness to oppose less or more strongly to motion). The active deflection of the stick given from the force feedback can be considered an "autonomous collision avoidance" function. In fact, the force feedback can be regarded to yield a "commanded" stick deflection that the operator should follow as much as possible. That is, when yielding to the forces applied on the hand, the operator deflects the stick in a way that satisfies the collision avoidance function. With stiffness feedback instead, the stick becomes stiffer when in the presence of an obstacle, that is, the extra stiffness provides an impedance, resulting in an extra force that depends on the deflection of the stick by the operator. The authors then concluded that a mixed force-stiffness feedback is the best solution. This type of haptic augmentation systems for RPVs was designed in order to help directly the pilot in his/her task by pulling the stick in the correct direction for the achievement of the task, or by changing stick stiffness in order to facilitate or oppose to certain pilot's actions [78, 1].

Another work not about teleoperation but still about haptic augmentation is the one by De Stigter [58]: he suggests to use the haptic device similarly to the artificial horizon with flight director (as in the Instrumental Landing System, ILS, for instance): as bringing the artificial horizon bar in the center would let the aircraft to fly in the desired direction, by bringing the haptic device to the central position the target path will be followed in a close future. In fact, the haptic device moves in the opposite direction with respect to the one required by the target path and about a quantity proportional to the future error with respect the path to follow.

Reference [60] proposes the introduction of an active stick in a manned military aircraft (Alenia Aermacchi M-346). In training aircrafts, the introduction of an active stick in each cockpit would be very useful as long as the two sticks can be electrically connected; thus they could work in a synchronous way as they were mechanically connected. In this way, the trainer gets the chance to supervise the control input of the apprentice pilot. The trainer could also make little corrections to teach the best way to impart some maneuver to the aircraft. The active stick would move also coherently with the autopilot commands to inform the pilot about the approaching of the envelope limits (already present in fly-by-wire aircrafts through the *stick shaker*). This is in line with what is stated in [19]: the active stick in this case makes the system structure and the automation processes visible to the operator. This aid in identifying options for action can help the operator in maintaining SA.

2.2 Haptic aids analysis and classification

Most of the described papers focus on a collision avoidance support to help the pilot in avoiding obstacles. Usually this kind of haptic aids, for example, have always been represented by repulsive forces created by objects in the environment in order to help the operator to avoid them.

When the task is instead a path to follow, a target location to reach or a desired stick position to get, the haptic feedback is instead attractive with respect to the task.

Thus, in all the described papers except for the [58], the haptic force that is artificially injected in the stick has the same sign (i.e. direction) as the one needed in order to achieve the requested task; thus the operator has to be compliant with it in order to avoid the obstacles or to reach the desired position.

As concerning the work [58] instead, the haptic force has the opposite sign with respect to the one desired in order to achieve the requested task and the human operator has to appose the force exerted from the stick by keeping the stick in the center while the haptic force tries to move it away on the sides.

Due to the last considerations, the haptic force used in the bilateral teleoperation of RPV can be divided in two philosophies: Indirect Haptic Aiding (IHA) versus Direct Haptic Aiding (DHA).

Direct Haptic Aid: the class of all Haptic aids which produce forces and/or sensations (due to stick stiffness changes for instance) aimed at "forcing" or "facilitating" the pilot to take some actions instead of others. The operator has to be compliant with the force felt on the stick to achieve the task.

Indirect Haptic Aid: the class of haptic aids where the sense of touch is used to provide the pilot with an additional source of information that would help him/her, indirectly, by letting him/her know what is happening in the remote environment and leaving him/her the full authority to take control decisions. In general, in this case the operator has to oppose to the force felt on the haptic device.

It is clear from the above definitions that these two classes of haptic aids are complementary.

In practice under DHA, the haptic feedback suggests the correct direction the pilot should move the stick in order to achieve the task and the operator has to be compliant with it, while under IHA the haptic feedback is, in general, in the opposite direction and the operator has, in general, to oppose to it.

The stretch reflex, which is a reflex contraction of a muscle in response to passive longitudinal stretching, is an highly automatic motor response that is believed to be the spinal reflex with the shortest latency [77]. The author believe that the stretch reflex is involved when using IHA-based haptic feedback. Thus, a strength point of IHA is that, as a matter of fact, when a haptic input requires a reaction to a stimuli rather than compliance, it might be more "natural" for the human being [77, 3].

Another difference between the two classes is the behavior of the system with the pilot out of the loop: the DHA approach closes the loop itself as long as it is an "almost-automatic-system-concept". The IHA approach instead, as will be clarified later, is more likely to produce a system that requires the presence of an operator in the loop in order to achieve the task. As a matter of fact, with DHA in an obstacle avoidance task the obstacle itself exerts a force on the stick which in turn makes the robot to change the movement direction even if the pilot is out of the loop. While, in the path following task of [58] (which according to the previous definitions would fall in the IHA class) when the stick moves on one side because of a future error in the path following, the error is doomed to rise if an external force (say the pilot) does not bring the stick in the center.

2.3 Reality-Based Haptic Aids

All the papers described so far are based on a haptic aid which does not exist in reality. In fact, they all artificially produce a haptic force linked to environmental constraints or to environmental goals (a specific target location, a path to follow or a desired maneuver).

One study [34] explored, instead, how to provide the UAV pilot with an enhanced indication about a real condition existing outside the aircraft. In fact, the authors examined the value of haptic displays for alerting UAV operators to the onset of turbulence which was identified as being potentially detrimental to safe and effective UAV control by the UAV operators themselves. This is especially true for UAVs that require direct manual control in order to land.

The data in [34] revealed that haptic alerts, conveyed via the UAV operators joystick, could indeed improve self-rated situation awareness during turbulent conditions in a simulated UAV approach and landing task. These improvements might result either from an increase in the operator's "presence" in the remote environment [62], from increased information by effective use of multi-sensory stimulation [63], or a combination of the two.

Before [34], turbulence was indicated solely by an unexpected perturbation of video images being transmitted from a UAV-mounted camera to the operator control station, appearing in the Head-Up Display (HUD).

Due to limitations inherent with reducing all environmental information to the visual channel, UAV operators may fail to perceive, or fail to correctly diagnose this video perturbation as sudden turbulences. In [34] visual feedback was supplemented by haptic feedback applied directly to the pilots control stick, providing a redundant, kinesthetic alert: a force reflection in the axis-direction and scaled-ratio magnitude of the turbulence event.

In the same paper, four different alerts were evaluated and compared: Visual (perturbation of nose-camera imagery in the HUD

Baseline), Visual/Haptic (Visual and additional 1 second, low gain, high frequency vibration of the control stick), Visual/Aural (Visual and 1 second pure tone), Visual/Aural/Haptic (all three cues simultaneously). Data were collected from pilots as they performed simulated landing tasks. Conditions containing the haptic cue (Visual/Haptic and Visual/ Haptic/Aural) resulted in less error than non-haptic cue conditions (Visual and Visual/Aural). Although the aural alert also improved landing accuracy and detection of turbulence direction, performance was best with the redundant kinesthetic feedback. When randomly interrogated regarding the primary direction of the UAV immediately following a turbulence event, participants were more accurate when haptic feedback was present [34].

Interestingly, these results were true despite the fact that the haptic signals were not designed to closely simulate or mimic the veridical haptic information experienced by the pilot of a manned vehicle [10]. In fact, as said, the turbulence was transmitted through a low gain, high frequency vibration of the control stick.

2.4 Time Delays

As mentioned, a teleoperation system in presence of force feedback is referred as bilateral system. In such systems, the human operator controls a remotely located teleoperator. The UAV operator is responsible for the UAV at all times, it is crucial that he/she at all times can understand the UAV. Informational transfers through the datalink have to be without delays that can have an effect on system performance and overall safety. It is vital that control inputs and orders can be executed immediately in emergency situations that require such actions. Datalink delays could be of various magnitude (from 100 to 1600 ms or more) and not always predictable to human operators, and can thus cause a lack of understanding with increased cognitive workload, decreased situational awareness and possible incorrect inputs as result with final failure of the mission

[10].

Different ways to improve the performance of a teleoperated system in presence of time delay exist in literature, starting from the *move and wait* strategy [28], that is initiating a control move and then waiting to see the response of the remote robot until the task is accomplished, to the more advanced control theory. The first methods regard automatic switching for stopping override [26], supervisory control [64] or the use of the predictive display [25, 65]. Beginning in the mid 1980s, more advanced control theoretic methods started to appear, such as Lyapunov-based analysis [66] and internal virtual model [67]. In the late 1980s and 1990s, network theory starts to grow up through impedance representation [68] and passivity theory with [29, 30, 31] and without [32] the scattering variables (wave variables transformation). Reference [37, 36] through the two/four channel architectures and the impedance/hybrid matrix approach started mentioning the trade off between stability and transparency. In the 1990s the teleoperation through Internet started and the problem of packets loss grew up [69]. Other methods overcome the instability problems bilateral teleoperation in presence of time delay are the admittance control [43, 14], the adaptive control [35] and the time domain passivity [36, 71]. Another way to handle the time delay communication and the loss of packets is the sampled Port-Hemiltonian approach [72]. In particular, while the passivity method presents a trade off between the stability and the transparency, the Port-Hemiltonian approach allows both stable and transparent behavior [72].

Chapter 3

Conventional Aircraft Artificial Feel

A typical trouble of remote piloting an RPV is the lack of situation awareness because of the physical separation between the pilot (inside the Control Ground Station, CGS) and the airborne RPV. Visual feedback only is usually provided by UAVs Ground Control Stations; when an external disturbance or a fault, which on a conventional aircraft would produce a perceptible effect on the stick, affects the RPV, the pilot has to understand this situation by looking at the output of the instruments only. When a vertical wind gust disturbance affects a manned aircraft, the change in angle of attack and wing load are practically instantaneous. This has also an immediate effect on a mechanical-linkage based control column. The altimeter on the GCS cockpit will show the resulting change in altitude with a certain delay with respect to the actual disturbance time; as a matter of fact the aircraft dynamics has a low pass behavior and phase lag from angle of attack to altitude (in the simplest linear approximation it behaves as an integrator).

As said in Section 1.4, automation usually does not provide or could hinder SA if the designers fail in adequately addressing the

SA needs of the operator. But automation can also, in many different ways, be created to support good SA through decision aids and system interfaces. IHA-CAAF was introduced to satisfy such a different way to create SA.

Operators where prone in overlooking crucial information to sustain SA, though all relevant and needed informations were present. This was found to be the most frequent causal factor associated with SA errors [10]. Through the IHA-CAAF they do not have to think about their response at the haptic aid because IHA-CAAF is built in a way that their response will be natural and instinctive.

Furthermore, by considering that UAVs pilots are also manned aircrafts pilots, they expect, in presence of external disturbances such as wind gusts or turbulences, a stick cueing which is similar to the one they would feel by piloting the aircraft on board. Thus, a good way to inform the remote pilot about the external disturbances could be perhaps to reproduce, through the haptic feedback, a feeling which mimics the real one.

The IHA-CAAF haptic feedback will be shown to increase the performance in terms of instinctive response to a stimulus in pilots without any previous training on the experiment. It also improves the situational awareness intended as making the pilot to feel as piloting the aircraft on board. This would improve the safety of the teleoperation by keeping higher the attention of the pilot in the task.

3.1 FBW Aircrafts/UAVs Analogy

As said this work is based on UAV feedback augmentation but nonetheless similar techniques could be employed in similar fields like Fly-By-Wire (FBW) piloted commercial aircrafts or helicopters.

A FBW system is an electrically-signaled aircraft control system, a computer-configured controller, that modifies the manual inputs of the pilot in accordance with control parameters. The movements of the flight control, the *sidestick*, are converted to electronic signals, and flight control computers determine how to move the actuators at each control surface to provide the expected response.

FBW aircrafts (Airbus, Boeing 777 and later designs) present, at least as concerning the haptic feedback, similar loss of situational awareness compared to the previous technology, i.e. the mechanically driven aircrafts (see later the Section 3.2).

In fact, FBW system employed both in large airliners and in military jet aircraft, dispenses all the complexity of the mechanical circuit of the mechanical flight control system and replaces it with an electrical circuit. The FBW (also referred as *irreversible* control system [47]) makes use of an electronic passive sidestick, in place of the conventional control stick which was connected to the actual aerodynamic surfaces via mechanical linkages (*reversible* control system [47]). The sidestick is in general implemented as a spring system with constant stiffness that makes the force felt by the pilot stronger as the displacement of the stick increases independently from the particular aerodynamic situation (velocity, load factor). Sometimes the sidestick may provide an artificial vibration of the stick (stick shaker) and some acoustical/visual warning that makes the pilot to know that the limits of the flight envelope (see Section A.2 for details) are going to be reached [74].

The employment of fully powered controls made essential the introduction of completely artificial feel [75]. In that time, a considerable speculation about what elements of natural feel should be emulated, started. It was also coupled with the natural desire to minimize the cost and complexity of the feel devices.

The possibilities included control force variation with dynamic pressure (*q feel*), speed (*V feel*) or control deflection only (*spring feel*). Devices such as bobweights and downsprings which were already familiar on conventional aircraft, were sometime included as well. Mechanical controls also carry out the role of a tactile display: the human hand can interpret loading forces appearing on the handgrip in terms of demands imposed on the system and its expectable response, enabling the pilot to develop a beneficial phase lead [76].

Artificial feel had become more and more fundamental in addiction to the visual cueing in the context of RPVs.

3.2 Mechanically Driven Aircrafts

As said, a meaningful way to inform the remote pilot about the external disturbances is the reproduction, through the haptic feedback, of a feeling which mimics the one transmitted to the pilot on board of a manned mechanically driven aircraft. In this case, the pilot feels all the aerodynamic forces (external disturbances as wind gusts and turbulences) directly on the bar, the control device. The force felt by a pilot on the aircraft control device of a mechanical Flight Control System (FCS) during a maneuver depends in a very complex manner from all the aerodynamics characteristics of the aircraft, the current state of the aircraft (speed, angle of attack etc.) and of course from control device deflection. By taking into consideration the only longitudinal dynamics (pitch and altitude motion), the force felt by the pilot of a mechanically driven aircraft is [47]:

$$F_S = \eta_h C_h q S_e c_e G_e = (C_{h0} + C_{h,\alpha}\alpha_h + C_{h,\delta}\delta_e) \cdot \eta_h q S_e c_e G_e \tag{3.1}$$

where η_h is the dynamic pressure ratio at horizontal tail, C_h is the elevator hinge moment, q is the dynamic pressure of the aircraft which is defined as

$$q = \frac{1}{2}\rho V^2$$

(where ρ is the air density and V is the airspeed), S_e and c_e are the surface and the chord of the elevator and G_e is a gearing factor (with units) to convert moments to force and includes the geometry of the control mechanisms, pulleys, push-rods and cables (see Figure 3.1). C_{h0}, $C_{h,\alpha}$ and $C_{h,\delta}$ are respectively the elevator hinge moment coefficient at zero lift, the elevator hinge moment coefficient derivative with respect to the tail angle of attack (α_h) changes and with respect to the elevator deflection (δ_e) changes.

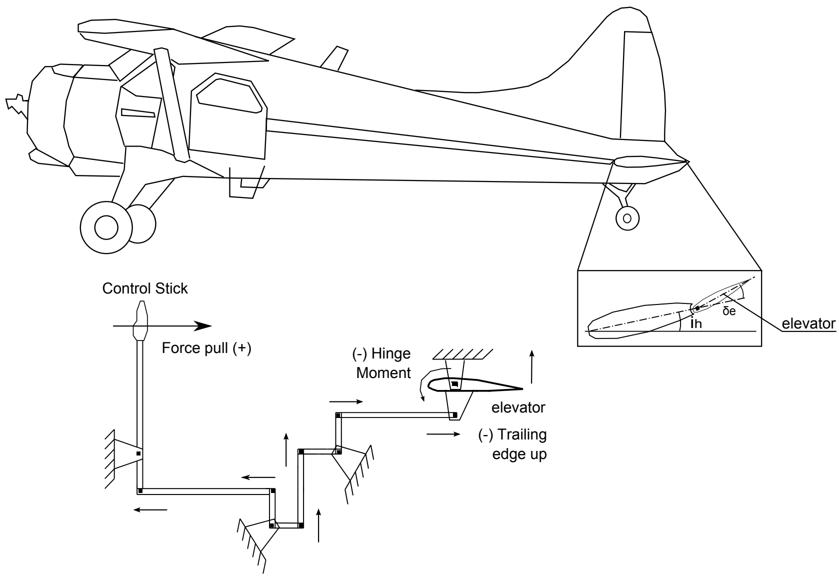

Figure 3.1: Mechanically driven aircraft [47]. i_h is the horizontal tail angle and δ_e is the elevator deflection.

A simplified expression for the force felt by the pilot of a mechanically driven aircraft can be re-written (see Section 3.2.1).

3.2.1 A simplified stick force

A simplified expression for the force felt by the pilot of a mechanically driven aircraft can be re-written as made up, in general, by two different components: a spring-damper component, F_{SD}, and an external force component, F_{WG} (see Equation 3.2).

$$F_S = F_{SD} + F_{WG} \tag{3.2}$$

where:

$$\begin{cases} F_{SD} = K \cdot \Delta\delta_e \\ K = \eta_h S_e c_e G_e |C_{h,\delta}| \cdot q \\ F_{WG} = \eta_h S_e c_e G_e |C_{h,\alpha}| \cdot q(\alpha - \alpha_{trim})(1 - \frac{d\epsilon}{d\alpha}) \end{cases} \tag{3.3}$$

$\Delta\delta_e$ is the change in the commanded elevator deflection with respect to the trim condition deflection. α is the aircraft angle of attack, which is the angle between the direction of motion (relative velocity) and the x-axes of the Body Reference Frame (left-handed frame with origin in the center of gravity of the aircraft, $\mathbf{x_B}$ is in the vertical plane of symmetry of the aircraft and points the nose of it, $\mathbf{y_B}$ axes is in the plane perpendicular to the plane of vertical symmetry and points to the right side), α_{trim} is the angle of attack in trim condition (see later), ϵ is the downwash angle produced on the horizontal tail by the wings airflow. A justification for the approximate expression of Equation (3.3) is given in the Section 3.2.2.

3.2.2 Simplified Stick Force Proof

The longitudinal steady state equations in horizontal flight in Wind Axes (left-handed coordinate system with x_W same direction as the relative velocity and z_W downward, origin in the aircraft center of gravity) are written as [47]:

$$\begin{cases} W = L = C_L \cdot qS \\ 0 = m = C_m \cdot cqS \end{cases} \tag{3.4}$$

where W, L and m are respectively the aircraft total weight, lift and pitching moment; C_L and C_m are respectively the aircraft lift and pitching moment coefficients. c is the mean wing chord. The Equation (3.4) can be re-written by expressing the lift and the moment coefficients as in the Equation (3.5):

$$\begin{cases} mg = (C_{L0} + C_{L\alpha} \cdot \alpha + C_{L,ih} \cdot i_h + C_{L\delta} \cdot \delta_e) \cdot qS \\ 0 = (C_{m0} + C_{m\alpha} \cdot \alpha + C_{m,ih} \cdot i_h + C_{m\delta} \cdot \delta_e) \cdot qS \end{cases} \tag{3.5}$$

In Equation (3.5), C_{L0} and C_{m0} are respectively lift and pitch moment coefficients for zero angle of attack α. $C_{L\alpha}$, $C_{L,ih}$, $C_{L\delta}$ represent the change in lift coefficient with respectively the angle of attack (the aircraft lift curve slope), α, the horizontal tail incidence angle, i_h, and the elevator deflection, δ_e (see Figure 3.1). $C_{m\alpha}$, $C_{m,ih}$ and $C_{m\delta}$ are equivalent variations of the pitching moment coefficient. As usual, q and S are dynamic pressure and the wings area. The solutions of Equation (3.5) are referred as trim condition quantities [47]:

$$\begin{cases} \alpha = \frac{(C_{L,trim} - C_{L0} - C_{L,ih} \cdot i_h) C_{m\delta} + (C_{m0} + C_{m,ih} \cdot i_h) C_{L\delta}}{(C_{L\alpha} C_{m\delta} - C_{m\alpha} C_{L\delta})} = \alpha_{trim} \\ \\ \delta_e = \frac{-C_{L\alpha}(C_{m0} + C_{m,ih} \cdot i_h) - C_{m\alpha}(C_{L,trim} - C_{L0} - C_{L,ih} \cdot i_h)}{(C_{L\alpha} C_{m\delta} - C_{m\alpha} C_{L\delta})} = \delta_{e,trim} \end{cases} \tag{3.6}$$

In general the following is held:

$$\alpha_h = \alpha \cdot (1 - \frac{d\epsilon}{d\alpha}) + i_h - \epsilon_0 \tag{3.7}$$

In Equation (3.7), the average downwash angle caused by the wings on the horizontal tail is often expressed [47] by

$$\epsilon = \epsilon_0 + \frac{d\epsilon}{d\alpha} \cdot \alpha$$

where ϵ_0 is the down wash angle at zero airplane angle of attack and $\frac{d\epsilon}{d\alpha}$ is the change of the downwash angle, ϵ, with respect to the angle of attack, α.

The force F_S that the pilot applies on the bar should be equal to the hinge moment [47] written in Equation 3.1.

By supposing to have a *trimmable stabilizer* that is possible to position to make the force of Equation (3.1) null, i.e. $i_h = i_{h,trim}$ (by considering the Equation (3.7) into the Equation (3.1) and solving for $F_S = 0$):

$$\begin{cases} i_{h,trim} = -\frac{1}{C_{h,\alpha}}\big(C_{h0} + C_{h\alpha} \cdot \alpha_{trim}(1 - \frac{d\epsilon}{d\alpha}) - C_{h,\alpha}\epsilon_0 + C_{h,\delta}\delta_{e,trim}\big) \\ \\ F_S = 0 \end{cases} \tag{3.8}$$

If the aircraft is trimmed (stabilizer deflected by $i_{h,trim}$) and by considering that the pilot could move the bar through the application of the force ΔF_S and thus the elevator by $\Delta\delta_e$, it is possible to write:

$$\begin{cases} \alpha = \alpha_{trim} + \Delta\alpha \\ i_h = i_{h,trim} + \Delta i_h \\ \epsilon_0 = const \\ \delta_e = \delta_{e,trim} + \Delta\delta_e \\ \alpha_h = \alpha_{h,trim} + \Delta\alpha_h \\ \alpha_{h,trim} = \alpha_{trim} \cdot (1 - \frac{d\epsilon}{d\alpha}) + i_{h,trim} - \epsilon_0 \end{cases} \tag{3.9}$$

By considering the Equation (3.7) and that the horizontal stabilizer is deflected by $i_{h,trim}$ and fixed to that value (then $\Delta i_h = 0$), it is possible to calculate $\Delta\alpha_h$:

$$\Delta\alpha_h = \Delta\alpha \cdot (1 - \frac{d\epsilon}{d\alpha}) \tag{3.10}$$

The corresponding stick force changing is obtained by substituting the previous ones in the Equation (3.1):

$$\Delta F_S = \eta_h q S_e c_e G_e \Big(C_{h,\alpha}\Delta\alpha\Big(1 - \frac{d\epsilon}{d\alpha}\Big) + C_{h,\delta}\Delta\delta_e\Big) \tag{3.11}$$

The change in α, $\Delta\alpha$, produced by the change in δ_e, $\Delta\delta_e$, with respect to the trim conditions, α_{trim} and $\delta_{e,trim}$, can be written as:

$$\begin{cases} \Delta\alpha = \alpha - \alpha_{trim} \\ \Delta\delta_e = \delta_e - \delta_{e,trim} \end{cases} \tag{3.12}$$

The second of the Equations (3.12) is obtained by supposing that the THS is fixed in the horizontal trim conditions ($i_h = i_{h,trim}$). As a consequence, the Equation (3.11) can be simply written as:

$$F_S = K \cdot \Delta\delta_e + F_{WG} \tag{3.13}$$

Where:

$$\begin{cases} K = \eta_h S_e c_e G_e |C_{h,\delta}| \cdot q \\ F_{WG} = \eta_h S_e c_e G_e |C_{h,\alpha}| \cdot q(\alpha - \alpha_{trim})(1 - \frac{d\epsilon}{d\alpha}) \end{cases} \tag{3.14}$$

In Equation (3.14), the dynamic pressure and the angle of attack are the only non-constant values. Thus, the simplified stick force equation, was re-written through two components: an elastic term with stiffness (K) which varies with the dynamic pressure and an external component (F_{WG}) which varies with the dynamic pressure and the angle of attack.

3.3 CAAF

A pilot flying a mechanically steered aircraft feels aerodynamic forces on the stick, which are generated on the actual control surfaces. The simple fact that the pilot feels the load factor (ratio between lift and aircraft weight) helps him to avoid flight conditions which might be dangerous for the aircraft structure. As another simple example, stall may happen during a steep climb maneuver; while approaching the stall condition the stick becomes looser informing the pilot of the risk to lose aircraft control. Furthermore, external disturbances like wind gusts which may be very dangerous if not appropriately and suddenly compensated in a constrained mission environment (e.g., a urban canyon), would produce an immediate effect on the stick. Useful information like load factor, "distance" from stall and external disturbances cannot be read by the pilot on the GCS cockpit instruments; thus the Conventional Aircraft Artificial Feel (CAAF) haptic aiding scheme was designed in order to provide the pilot with a richer information with respect to the visual display only. The experiments were performed in order to show and assess analytically that these additional haptic information help the pilot from a performance point of view.

Level 1 SA (see Section 1.4) says that the pilot needs to accurately perceive information about the weather among other elements. Reference [34] followed this principle by creating a haptic sensation linked to the turbulence but in that case the haptic signal was not related to the real sensation experienced by a pilot of a manned aircraft. The present work instead introduces a haptic feedback which mimics aerodynamic forces usually experienced by the pilots of manned aircrafts and it belongs by definition to the class of IHA because it is born, above all, to improve the SA and it is not designed taking into account the right maneuver to perform in order to reject the wind gust.

As mentioned before, the newly introduced haptic feedback has been given the name of *Conventional Aircraft Artificial Feel* (CAAF).

Two different version of the CAAF are presented: the former, named *Variable Stiffness CAAF*, estimates the effect of wind gust as changes in stick stiffness (see Section 3.3.1) while the external force, F_{WG}, is set to zero; the latter, named *Force Injection CAAF*, estimates the effect of wind gust as changes in the angle of attack, α, and dynamic pressure, q, and it produces also an external force, F_{WG} (see Section 3.3.2).

3.3.1 Variable Stiffness CAAF

The Variable Stiffness CAAF estimates the effect of wind gust as changes in stick stiffness according to a weighted sum of the load factor, n, and the dynamic pressure, q. Thus, the force was assumed to be dependent on the two most important variables for defining the flight envelope (see Section A.2 for details). The load factor

$$n = \frac{L}{W}$$

is defined as the ratio of the lift L to the weight W of the aircraft, thus it is a measure of the severity of a commanded maneuver. It was introduced in the stick force equation to make the pilot more conscious about the commanded maneuver and to make more difficult the maneuvers which could be dangerous for the aircraft structure and cause accidents as the loss of wings in the RPV. The external force is set to zero:

$$\begin{cases} F_{CAAF,vs} = F_{SD,vs} + F_{WG,vs} \\ F_{SD,vs} = K_{S,vs} \cdot \delta_S + K_{D,vs} \cdot \dot{\delta}_S \\ F_{WG,vs} = 0 \end{cases} \tag{3.15}$$

$F_{SD,vs}$ is the Spring-Damper component of the force and $F_{WG,vs}$ is the external force component. The Variable Stiffness CAAF, Equation (3.15), is similar to the Equation (3.13) accept for the null external force component, for the introduction of the load factor in the variable stiffness and for the introduction of a damper component as well in order to provide some damping for the future implementation of the CAAF in an haptic device. As long as in Equation (3.13) $\Delta\delta_e$ is the elevator deflection around the trim value, which is *0 deg* with the THS deflected by i_{trim}, and fixed on this value and since the deflection of the elevator is proportional to the bar deflection for mechanically driven aircrafts, in Equation (3.15) δ_S, the stick deflection, was employed instead of $\Delta\delta_e$. Equation (3.16) shows the value of the stiffness expression of the Variable Stiffness CAAF:

$$K_{S,vs} = K_{f,vs} \cdot [K_{q,vs} \cdot q + K_n \cdot (n-1)] \tag{3.16}$$

$F_{CAAF,vs}$ represents the change in the stick force during a maneuver with respect to the stick force in trim conditions ($F_{trim} = 0$). δ_S and $\dot{\delta}_S$ are stick deflection and stick deflection rate respectively. $K_{D,vs}$ is the damping constant.

The Equation (3.16), shows the changes of the stiffness as proportional to the squared velocity, through q, and to the load factor.

$K_{q,vs}$ and K_n are the weights of the dynamic pressure and of the difference between the load factor during the maneuver and the one of horizontal flight respectively $(n-1)$; $K_{f,vs}$ is a constant gain which determines the "amount" of force feedback.

The sign conventions are the same as in [47] (see Figure 3.1). As concerning the sign, the force that the pilot feels on the stick has the same sign as the deflection requested to the elevator (see Figure 3.1). Thus, a positive value is needed as $K_{q,vs}$. As concerning the dynamic pressure component, the goal is to make the pilot conscious about the velocity of the UAV: the higher is the velocity, the bigger is the dynamic pressure component, the bigger is the spring component and more difficult will be to perform a maneuver.

As concerning the load factor component: the load factor is positive for climbing maneuver and negative for diving maneuver but a positive sign of the product $K_n \cdot (n-1)$ is needed, thus K_n should have a negative value for diving maneuvers and a positive value for climbing maneuvers. The goal of the introduction of the load factor in the spring component of the Variable Stiffness CAAF is to avoid the pilot doing a sudden maneuver: the higher is the load factor, the bigger is the stiffness of the stick and more difficult will be to perform a maneuver.

In order to assign meaningful values to the constants $K_{q,vs}$, K_n and $K_{f,vs}$, the dynamic pressure and the load factor were normalized with respect to the max values they can assume. The choice made in Equation (3.17) would satisfy the previous hypothesis:

$$\begin{cases} K_{q,vs} = \frac{K'_{q,vs}}{\frac{1}{2}\rho V_{max}^2} \geq 0, & V_{max} = V_{md} \\ K_n = \begin{cases} \frac{K'_n}{(n_1-1)} \geq 0, & for \quad n \geq 1 \Rightarrow K_n(n-1) \geq 0 \\ \frac{K'_n}{(n_2-1)} < 0, & for \quad n < 1 \Rightarrow K_n(n-1) \geq 0 \end{cases} \end{cases} \tag{3.17}$$

Furthermore, $K_{q,vs}$ and K_n can be interpreted as the strain the pilot must exert on the bar to produce a change in velocity or a change in the load factor during a maneuver. In literature [47], something similar to K_n is referred as *stick-force-per-g*.

V_{md} is the velocity maximum of design that was hypothesized to be the velocity to never exceed, V_{ne}, plus the 10% of the same. n_1 and n_2 are respectively the positive and negative maximum values of load factor of the aircraft.

As concerning K'_n and $K'_{q,vs}$, it could be interesting to find out the optimal values capable of minimizing a performance index. The first heuristic choice in this work was the value 0.5 for both. As long as the the constants are normalized with respect to the maximum values of the variable they weight (q and n), then the value 0.5 means that the *feel* in Equation (3.15) is made up by the changes in q for the 50%, by the changes in n for the remaining 50%. The quantity in squared parenthesis in Equation (3.16) will assume the value 1 at maximum. As said, the amount of the feedback force depends by K_f which scales the stiffness to the desired value. The Federal Aviation Regulation (FAR) of the Federal Aviation Administration (FAA) and in particulare the FAR 23 Sect.23.155 impose the strength limits necessary to control the elevator for certain values of the load factor, but the real amount of force to employ will depend at the end on the haptic device maximum output force.

The final expression of the haptic feedback force becomes then:

$$F_{CAAF,vs} = F_{SD,vs} \cdot + F_{WG,vs} \tag{3.18}$$

with $F_{SD,vs}$ and $F_{WG,vs}$ from Equations (3.16) and (3.15). Note that $delta_S$ and $\dot{\delta}_S$ of Equations (3.16) and (3.15) were replaced with the linear x_S and $\dot{x}_S$ in Equation 3.18 since the actual control device can only provide end-effector translations. The haptic feedback expression of Equation (3.18) was named Variable Stiffness Conventional (for mechanically-driven) Aircraft Artificial Feel (CAAF) by its aerodynamically inspired nature. This type of force feedback, in analogy to what found in the artificial feel literature [75], could be addressed as a *qn-feel* system since the force it generates is proportional to both dynamic pressure (q) and load factor (n). This force was tested through the CAAF Experiment (see Section 3.6.1).

3.3.2 Force Injection CAAF

The Force Injection CAAF of Equation (3.19) estimates the effect of wind gust as changes in the angle of attack α and of dynamic pressure q and produces an external force. The Force Injection CAAF focuses on the external force component as opposed to the former version (Section 3.3.1) that uses stick stiffness variations. Thus, as long as in the altitude regulation task (object of the experiments in Section 3.6) the velocity is close to the one of trim conditions (V_{trim}) and the load factor is close to the one of horizontal flight ($n = 1$), a constant value ($K_{S,fi}$) was chosen as stiffness and the external component, F_{WG}, as in Equation (3.14) was considered:

$$\begin{cases} F_{CAAF,fi} = F_{SD,fi} + F_{WG,fi} \\ F_{SD,fi} = K_{S,fi} \cdot \delta_S + K_{D,fi} \cdot \dot{\delta}_S \\ K_{S,fi} = K_{f,fi} \cdot K_{q,fi} \cdot q_{trim} \\ F_{WG,fi} = \eta_h S_e c_e G_e |C_{h,\alpha}| \cdot q(\alpha - \alpha_{trim})(1 - \frac{d\epsilon}{d\alpha}) \end{cases} \tag{3.19}$$

As previously, a damper component with damping constant $K_{D,fi}$ was added as well in order to provide some damping for the future implementation of the CAAF in an haptic device. q_{trim} is the dynamic pressure related to the trim velocity, V_{trim}.

$F_{CAAF,fi}$ represents the change in the stick force during a sudden vertical wind gust. The wind gust affects the angle of attack and move it away from the angle of attack in trim conditions, α_{trim}. δ_S and $\dot{\delta}_S$ are again the stick deflection and the stick deflection rate respectively.

$K_{q,fi}$ and $K_{f,fi}$ are respectively the weight of the dynamic pressure and a constant gain which determines the "amount" of force feedback.

As concerning the sign, the force the pilot feels on the stick during a vertical wind gust has the same sign as the deflection caused to the elevator by the wind gust. For example a downward wind gust will create a positive elevator deflection (trailing edge down), a fall in angle of attack ($\alpha - \alpha_{trim} < 0$) and so a positive stick deflection (i.e. towards). Thus, the force felt by the pilot is negative (the bar tends to move away from the pilot) for downward wing gusts, while it is positive (the bar tends to move closer to the pilot) for upward wind gusts. Thus, a positive value is needed as $K_{q,fi}$.

As concerning the dynamic pressure component, the goal is to make the pilot conscious about the change in the velocity of the UAV produced by the wind gust: a downward wind gust produces, as said, a diving maneuver and so a growing velocity and the haptic feel in Equation (3.19) would suggest that the aircraft is diving and a pilot input in the opposite direction (i.e. moving the bar toward the pilot) is needed in order to restore the previous trim condition value. The stronger is the gust, the bigger is the change in angle of attack and in the velocity produced, the bigger is the external force component and a stronger and clearer information about the presence of a wind gust will be given to the pilot. An improvement of the situational awareness about the external conditions of the aircraft will be produced. As said, the action requested to the pilot in order to restore the previous trim conditions is to counteract the haptic feel. This would be a natural reaction to the force for what Schmidt and Lee proved [77] (see Section 2.2).

The Equation (3.19) can be written as:

$$\begin{cases} F_{CAAF,fi} = F_{SD,fi} \cdot + F_{WG,IHA} \\ F_{WG,IHA} = K_{fWG,fi} \cdot [K_{q,\alpha} \cdot q(\alpha - \alpha_{trim})] \end{cases} \tag{3.20}$$

In order to assign meaningful values to the constants $K_{q,fi}$, $K_{q,\alpha}$, $K_{f,fi}$ and $K_{fWG,fi}$, the dynamic pressure and the product of dynamic pressure and the change in angle of attack $(\alpha - \alpha_{trim})$ were normalized with respect to the max values they can assume. The choice made in Equation (3.21) would satisfy the previous hypothesis:

$$\begin{cases} K_{q,fi} = \frac{K'_{q,fi}}{\frac{1}{2}\rho V_{max}^2} \\ K_{q,\alpha} = \frac{K'_{q,\alpha}}{\frac{1}{2}\rho V_{max}^2 \cdot (\alpha_{st} - \alpha_{trim})}, \end{cases} \tag{3.21}$$

Furthermore, $K_{q,fi}$ and $K_{q,\alpha}$ can be interpreted as the strain the pilot must exert on the bar to produce a change in velocity and a change in the angle of attack a maneuver.

$V_{max} = V_{md}$ which is defined in Section 3.3.1. α_{st} is the stall incidence of the aircraft.

As concerning $K'_{q,fi}$ and $K'_{q,\alpha}$, it could be interesting to find out the optimal values capable to minimize a performance indexes. The first heuristic choice in this work was the value 0.5 for both of them.

As long as the the constants are normalized with respect to the maximum values of the variable they weight (q and $q \cdot (\alpha_{st} - \alpha_{trim})$), then the value 0.5 means that the *feel* in Equation (3.19) is made up by the changes in q and $q \cdot (\alpha_{st} - \alpha_{trim})$ and it is the 50% of the maximum available values. The quantity in squared parenthesis in Equation (3.20) will assume both the value 0.5 at maximum. The amount of stiffeness and the amount of the external force depend by $K_{fS,fi}$ and $K_{fWG,fi}$ respectively. They scale the stiffness and the external force $F_{WG,fi}$ to the desired value. Their choice was made heuristically by taking into account the haptic device maximum output force.

The final expression of the haptic feedback force is represented by the Equation (3.20) and was named Force Injection Conventional (for mechanically-driven) Aircraft Artificial Feel (CAAF) by its aerodynamically inspired nature. This type of force feedback, in analogy to what found in the artificial feel literature [75], could be addressed as a *$q\alpha$-feel* system since the force it generates is proportional to both dynamic pressure (q) and angle of attack (α). This force was tested through the CAAF VS DHA Experiment (see Section 3.6.3).

Dickinson noted that "in particular we can take the opportunity of making control forces do what we desire them to do rather than having to accept the consequences of fundamental laws as hitherto" [75]. Thus from now on, the mentioned opportunity was taken by using heuristical stiffness, damping constants and external forces instead of using constants (as in Equations (3.17) and (3.21)) which depend from the particular aircraft under consideration. This would make the haptic force to be transportable because created on the human being feeling instead of the particular aircraft (remotely or not) piloted.

3.4 The Experimental Setup

In order to test the CAAF concepts exposed in Sections 3.3 and 3.5, a simulated flight experiment was set-up. A fully non linear aircraft simulator was used to provide a realistic aircraft response. An aircraft simulator was implemented using a Matlab/Simulink simulation. The selected aircraft model was a De Havilland Canada DHC-2 Beaver implemented using the Flight Dynamics and Control Toolbox [45].

The selected haptic device is the widely used Omega Device in Figure 3.2 (omega.3, Force Dimension, Switzerland) which was chosen in order to simulate a control column of a mechanically driven aircraft. It is a 3DOF high precision force feedback device which provides control stick simulated force up to *12 N* (See Section A for details).

Figure 3.2: The Omega Device reference frame.

A simulated Electronic Flight Instrument Display (Figure 3.3) was used during the experiments to produce the visual cues. It is a reproduction of a real one as it was designed to be as similar as possible to conventional aircraft head-down display (see Section A for details on the EFIS Display implementation). The display shows the relevant variables in the task (pitch, altitude, speed) and the variable to be regulated (altitude) with a magenta reference mark for the set point $300ft$ for altitude.

Figure 3.4 shows the experimental test bed comprising of a video display and the haptic device.

The only dynamics considered in this Chapter is the longitudinal one. In order to control the longitudinal dynamics, the pilot usually acts on the thrust and on the elevator. In the present work, the elevator deflection is, by hypothesis, the only input provided to the simulated aircraft. This is a reasonable choice as long as the present work is an artificial feel study. In fact, acting on thrust and on the elevator at the same time would be reasonable for an autopilot or a Stability Augmentation System (SAS) study. Acting on thrust and

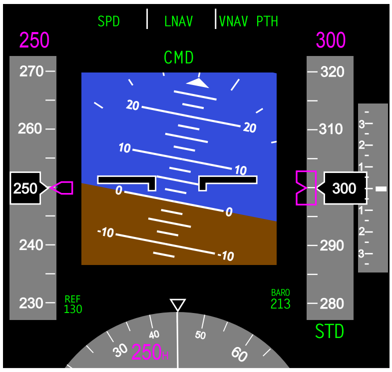

Figure 3.3: The Electronic Flight Instrument System Display.

on the elevator at the same time is also usually useless or undesirable, even on a real aircrafts (i.e. during the takeoff in which it occurs to pull-up the aircraft through the elevator with the maximum thrust). Furthermore, acting only on the elevator to pull-up the aircraft is a traditional piloting maneuver.

In this work, the elevator deflection is proportional to the displacement δ_S of Equations (3.15) and (3.15). δ_S is the input to the aircraft generated by the operator by moving the Haptic Device end-effector in the *x-direction* (see Figure 3.2).

An input on the elevator, starts the natural longitudinal aircraft modes: the Phugoid and the Short Period modes (see Section A.1.2). It causes a dynamic transient phase because of the exchanges between kinetic and potential energy and oscillations in the aircraft longitudinal variables (velocity, pitch angle, altitude, etc) around the center of gravity start. In Figure 3.5 the mentioned natural modes are shown (blue line).

In Figure 3.5 the Phugoid is the most visible oscillation, while the short period oscillation has, as the name suggests, a shorter period and, since it has usually a big damping constant, it disappears very soon. The Phugoid mode is characterized by complex and conjugate

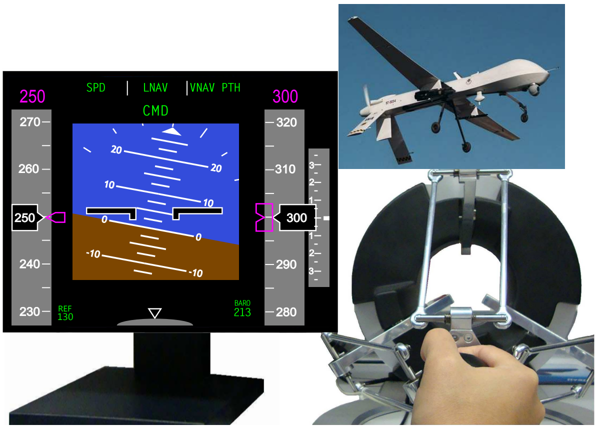

Figure 3.4: The wind gust rejection experimental setup.

poles that produce a lightly damped oscillation during which the dynamic pressure, the wing load factor and the aircraft angle of attack change because of the changes in the aerodynamic forces acting on the aircraft. The pilot (or the autopilot) is needed to extinguish them through the stick by holding the pitch angle through the use of the *artificial horizon*. Figure 3.5 shows as well (red line) a sample time history when a pilot acts on the stick to regulate it.

Since the subjects only controlled the longitudinal dynamics, the haptic aiding for the wind gust rejection task was only in the longitudinal axes of the control device that is the x axes of Figure 3.2.

The general force expression employed in both the just mentioned disturbance rejection experiments in give in Equation 3.22:

$$\begin{cases} F_{S,x} = F_{SD,x} + F_{WG,x} \\ F_{SD,x} = F_{SD} = F_{S,x} + F_{D,x} \\ F_{WG,x} = F_{WG} \end{cases} \tag{3.22}$$

In Equation (3.22), F_{SD} and F_{WG} indicate the Spring-Damper force and the external force of either the Equation (3.15) ($F_{SD,vs}$

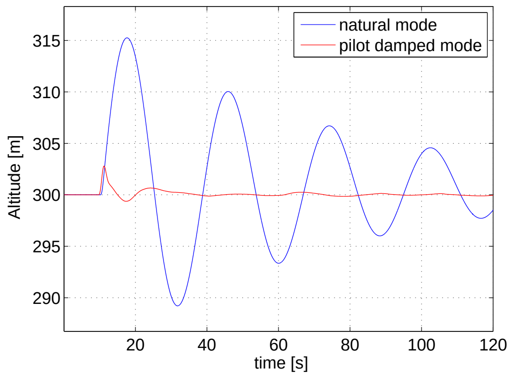

Figure 3.5: Response to elevator impulse input: Phugoid and Short Period natural aircraft modes (blue line) versus the typical aircraft response damped by a good pilot (red line).

and $F_{WG,vs}$) or the Equation (3.19) ($F_{SD,fi}$ and $F_{WG,fi}$).

$$F_x = K_{S,x} \cdot x_S + K_{D,x} \cdot \dot{x}_S + F_{WG} \tag{3.23}$$

Then, the force F_x felt by the operator during the wind rejection task (see Equation (3.22) and (3.23)) along the control device x axes (see Figure 3.2) is a combination of an elastic term, $F_{S,x}$ ($K_{S,x} \cdot x_S$), with constant stiffness $K_{S,x}$, a damping term, $F_{D,x}$ ($K_{D,x} \cdot \dot{x}_S$), with a damping constant $K_{D,x}$ (refer to the Table A.2 for the values used) and an external force component F_{WG}. x_S and $\dot{x}_S$ are the longitudinal displacement and displacement rate of the end-effector respectively.

3.5 Disturbance Rejection Experiments

Two experiments within the specific field of Remotely Piloted Vehicles control in a disturbance rejection task were run: the CAAF Experiment and the CAAF VS DHA Experiment.

The aim of the CAAF Experiment is to prove the effectiveness of the newly developed IHA-Variable Stiffness CAAF with respect to the absence of force feedback at all (only visual feedback and gravity compensation on the control device). See Section 3.6.1 for details.

The aim of the CAAF VS DHA Experiment is to compare three approaches: the newly developed and just described IHA-based Force Injection CAAF, the DHA force and a force which is only linked to the actual displacement of the control device, the NoEF. See Section 3.6.3 for details. Sections 3.5.2, 3.5.2 and 3.5.2 describe the simulators built in order to test the performance in the CAAF VS DHA Experiment.

3.5.1 The CAAF Experiment Simulators

NoF Simulator

Figure 3.6 shows the block diagram of the simulation system used to test the NoEF feedback. The altitude error (between desired altitude H_t and aircraft altitude H), e_H, is fed to the pilot P via the visual display showing the altitude error (see Figure 3.3). The pilot force input (F_h), is fed to the haptic device (OD block in Figure 3.8) to produce the stick deflection δ_S (which is used directly as aircraft elevator control by hypothesis). δ_{WG}, which represents the wind gust disturbance, is summed up to the stick deflection to produce the elevator input to the aircraft δ_e.

Under the NoF condition no haptic feedback is transmitted to the pilot (see Equation 3.24).

$$F_{NoF} = 0 \tag{3.24}$$

In fact, the NoF condition represents a condition in which neither the elastic or damping forces are fed-back to the pilot. Not even the gravity force is transmitted to the pilot as long as the gravity compensation is activated in the haptic device.

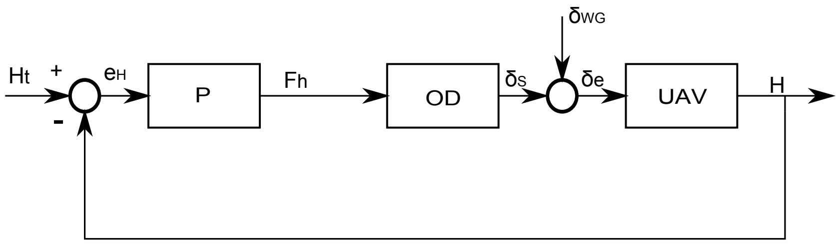

Figure 3.6: NoF simulator scheme.

Suppose a wind gust affects the aircraft: as long as $F_{SD,x}, F_{WG} = 0$ in the Equation (3.22), no force is directly linked either to the wind gust or to the actual end-effector displacement. Thus, the pilot will not feel through the sense of touch any haptic information about both the position of the control device end-effector and the presence of wind gust but he will just see the altitude changing through the visual display, an Integrated Flight Display (see Figure 3.3). The visual feedback is the same in all the conditions of the experiment.

IHA-Variable Stiffness CAAF Simulator

Figure 3.7 shows the block diagram of the simulation system used to test the IHA-Variable Stiffness CAAF feedback. The altitude error (between desired altitude H_t and aircraft altitude H), e_H, is fed to the pilot P via the visual display showing the altitude error (see Figure 3.3). The pilot force input (F_h), is fed to the haptic device (OD block in Figure 3.8) to produce the stick deflection δ_S (which is used directly as aircraft elevator control by hypothesis). δ_{WG}, which represents the wind gust disturbance, is summed up to the stick deflection to produce the elevator input to the aircraft δ_e.

Under the this condition the haptic feedback of Equation (3.18) is transmitted to the pilot.

Suppose a wind gust affects the aircraft: the pilot, while damping the phugoid mode, will feel a force feedback proportional to the

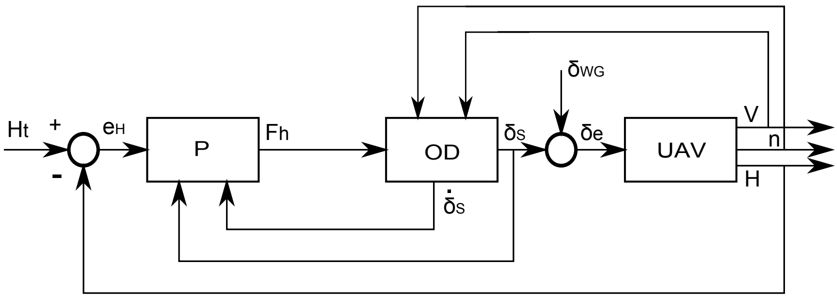

Figure 3.7: IHA-Variable Stiffness CAAF simulator scheme.

changes in the dynamic pressure and in the load factor according to the Equation (3.18) and will the same visual feedback as in the NoF condition.

3.5.2 The CAAF VS DHA Experiment Simulators

IHA-Force Injection CAAF Simulator

Figure 3.8 shows the block diagram of the simulation system used to test the IHA concept. The altitude error (between desired altitude H_t and aircraft altitude H), e_H, is fed to the pilot P via the visual display showing the aircraft speed and altitude (see Figure 3.3). The aircraft speed (V), used to compute the dynamic pressure, and the angle of attack (α) are fed to the Haptic device that implements the CAAF-IHA law and feeds-back the force (F_{WG}) as in Equations (3.19) and (3.20) which, together with the pilot force input (F_h), is fed to the haptic device (OD block in Figure 3.8) to produce the stick deflection δ_S (which is used directly as aircraft elevator control by hypothesis). δ_S and $\dot{\delta}_S$ indicate that pilots actually feels the elastic and damping haptic device response. δ_{WG}, which represents the wind gust disturbance, is summed up to the stick deflection to produce the elevator input to the aircraft δ_e.

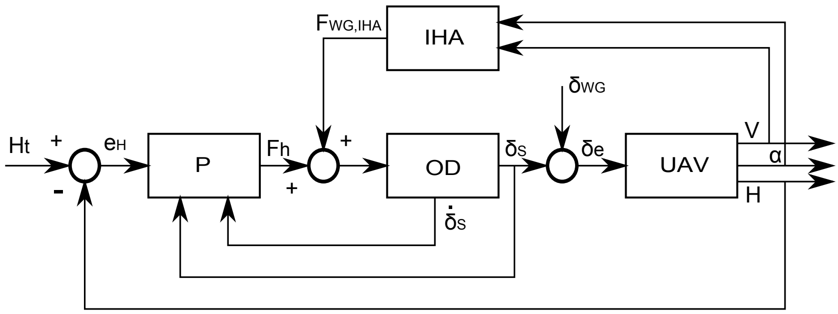

Figure 3.8: IHA-Force Injection CAAF simulator scheme.

Under this condition the haptic feedback of Equation (3.20) is transmitted to the pilot.

Suppose a downward wind gust affects the aircraft: the angle of attack of the aircraft decreases with respect to the trim condition, the dynamic pressure changes (possibly very lightly depending on the gust speed with respect to the aircraft speed) and the altitude tends to decrease. Within this condition, the CAAF-IHA law produces a negative force, F_{WG}, that would produce a positive stick deflection, δ_S, and thus induces the aircraft to dive even more. The force is immediately felt by the pilot who knows that something has changed. In this specific case the pilot feels a force that pulls the stick away from him, that is to dive, and he should react immediately, according to his experience, by opposing to the stick motion in order to keep the altitude constant. This type of force feedback, roughly speaking with opposite sign with respect to the actual maneuver to be taken, is in complete accordance with the IHA concept.

Figure 3.9 depicts an example of the variables history during a simulation trial.

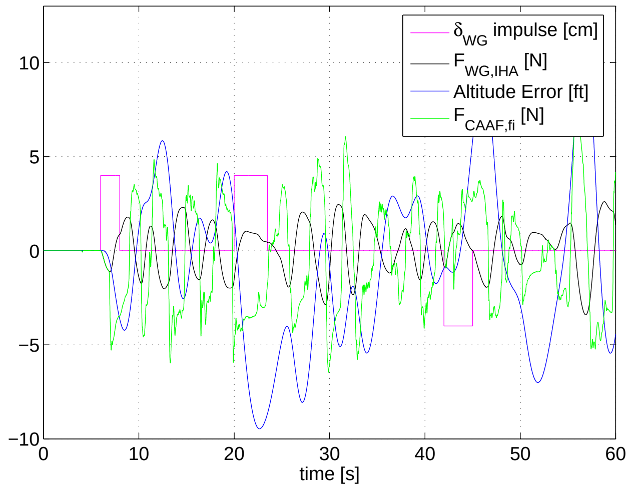

Figure 3.9: IHA-Force Injection CAAF simulation example.

NoEF Simulator

Figure 3.10 shows the block diagram of the simulation system used to test the NoEF feedback. The altitude error (between desired altitude H_t and aircraft altitude H), e_H, is fed to the pilot P via the visual display showing the aircraft speed and altitude (see Figure 3.3). The pilot force input (F_h), is fed to the haptic device (OD block in Figure 3.8) to produce the stick deflection δ_S (which is used directly as aircraft elevator control by hypothesis). δ_S and $\dot{\delta}_S$ indicate that pilots actually feels the elastic and damping haptic device response. δ_{WG}, which represents the wind gust disturbance, is summed up to the stick deflection to produce the elevator input to the aircraft δ_e.

The NoEF condition presents a constant stiffness stick ($K_{S,fi}$ in Table A.2 and simulates a fly-by-wire like situation. In the NoEF condition the force exerted by the haptic device is the same (i.e. the

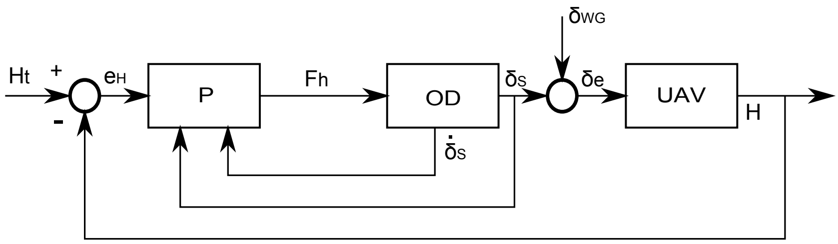

Figure 3.10: NoEF simulator scheme.

same Spring-Damper component) as in the Equation (3.19) except for $F_{WG,fi}$ which is set to zero in this condition. The pilot had an Integrated Flight Display as the only instrument showing the aircraft speed and altitude (see Figure 3.3). The visual feedback is the same in all the conditions of the experiment.

Under the NoEF condition, the haptic feedback of Equation 3.25 is transmitted to the pilot.

$$F_{NoEF} = F_{SD,x} \tag{3.25}$$

Suppose a wind gust affects the aircraft: as long as $F_{WG} = 0$ in the Equation (3.19), no force is directly linked to the wind gust. Thus, the pilot will not feel any haptic information about the presence of wind gust but he will just see the altitude changing through the visual display. The only haptic feedback felt by the pilot is proportional to δ_S and $\dot{\delta}_S$ produced only by the pilot input force F_h.

Figure 3.11 depicts an example of the variables history during a simulation trial.

Compensator-Based DHA Simulator

In order to compare the three approaches, a DHA-based simulator was designed. According to the DHA definition, a Direct Haptic Aiding system for wind gust rejection should produce a force or a change in stiffness that helps the pilot directly in achieving the task

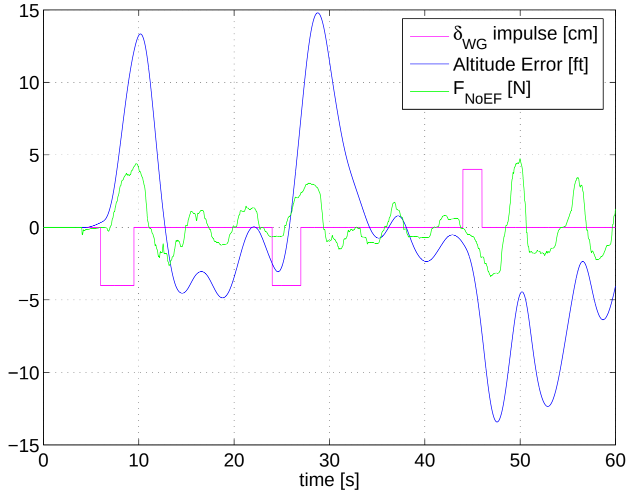

Figure 3.11: NoEF simulation example. F_{WG} (not shown) is null in this case.

that is in this case to reject the gust. Thus, a system that produces a force which pulls the stick in the same direction the pilot should do to reject the disturbance, seems appropriate for a DHA control. As a matter of fact, the obstacle avoidance system described in [1, 78] works exactly according to this principle. Stiffness variation, together with force feedback were investigated and found to be able to provide better results than single stiffness or force feedback [78]. Nevertheless, for the purposes of this comparison, we decided to investigate and compare force feedback only. A compensator was added to compute the external force to be felt by the pilot. The Haptic device was controlled as in Equation (3.19) to behave as a spring-damper system with an additional force F_{WG} which is generated by the DHA compensator (see later).

Figure 3.12 shows the block diagram of the simulation system used to test the DHA concept. The altitude error (between desired altitude H_t and aircraft altitude H), e_H, is fed to the pilot P via the visual display showing the aircraft speed and altitude (see Figure 3.3). The altitude error, e_H, is also fed to the DHA block that implements the DHA force and feeds-back the force (F_{WG}) which, together with the pilot force input (F_h), is fed to the haptic device (OD block in Figure 3.12) to produce the stick deflection δ_S (which is used directly as aircraft elevator control by hypothesis). δ_S and $\dot{\delta}_S$ indicate that pilots actually feels the elastic and damping haptic device response. δ_{WG}, which represents the wind gust disturbance, is summed up to the stick deflection to produce the elevator input to the aircraft δ_e.

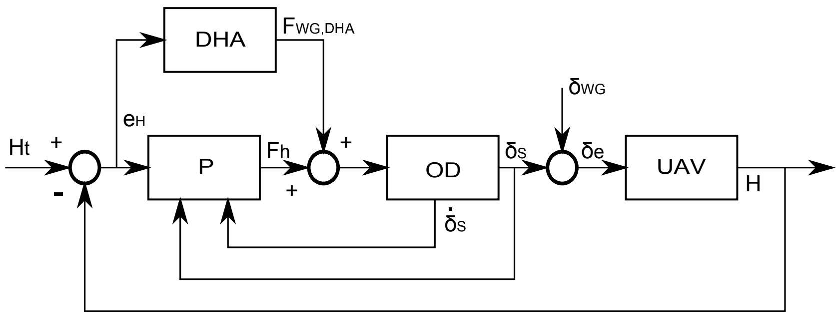

Figure 3.12: Compensator-Based DHA simulator scheme.

The DHA block in Figure 3.12 is a compensator represented by the transfer function of Equation (3.26) which calculates the DHA external force starting from the altitude error. It was designed in order to damp the Phugoid mode as a good pilot would do and cancel the Omega Device dynamics (see Section C.1). In order to design to DHA compensator, the Omega Device dynamics was identified (see Section B for details). The net result is that such compensator can damp effectively the Phugoid mode from altitude measurement by itself, without any pilot in the loop: the stick moves and the corresponding stick deflection is sufficient to control the aircraft. In order to leave the pilot with sufficient control authority, the gain of the compensator was reduced by 60%:

$$\frac{F_{WG,DHA}(s)}{e_H(s)} = \frac{(3687s^2 + 1477s) \cdot 0.4}{s^4 + 14.75s^3 + 209.5s^2 + 1089s + 13.04} \tag{3.26}$$

Thus, the force felt in DHA case is given from Equation (3.19) by considering $F_{WG,fi} = F_{WG,DHA}$ of the Equation (3.26):

$$F_{DHA} = F_{SD,x} + F_{WG,DHA} \tag{3.27}$$

Thus, the Spring-Damper component, $F_{SD,fi}$, is the same in each of the three force conditions (NoEF, IHA and DHA). Suppose a downward wind gust affects the aircraft: the altitude tends to decrease. Within this condition, the DHA compensator produces a positive force, F_{WG}, that would produce a negative stick deflection, δ_S, and thus induces the aircraft to climb back to the target altitude (the initial one). In this specific case the pilot feels a force that pulls the stick toward him, that is to climb, and he should be compliant with the force, by following and amplifying the stick motion, in order to keep altitude constant. This type of force feedback, roughly speaking with the same sign with respect to the actual maneuver to be taken, is in complete accordance with the DHA concept.

Figure 3.13 depicts an example of the variables history during a simulation trial.

The design of a DHA based augmentation scheme seems to be very task dependent; the compensator-based design approach described above was viable in our case since the task was specified as holding a reference altitude. This approach could not be used instead when the task cannot be specified as a reference signal to be tracked, or the pilot intention is not known; thus the design of a DHA augmentation scheme could be less straightforward than an IHA scheme.

The Section 3.6 present the experimental evaluation of the CAAF concepts.

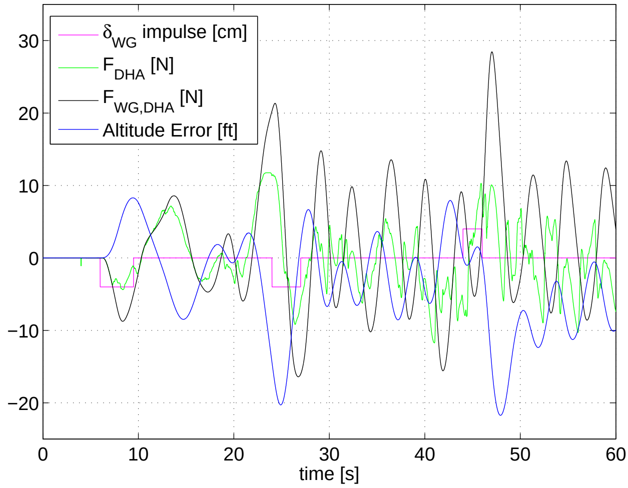

Figure 3.13: DHA simulation example.

3.6 CAAF Evaluation

This Section present the experimental evaluation of the concepts described in Sections 3.3 and 3.5. In particular, the Section 3.6.1 describes the CAAF experiment and results and the Section 3.6.3 describes the CAAF VS DHA experiment and results.

3.6.1 CAAF Experiment

In the CAAF Experiment, object of this section, a simple regulation task was prepared: the aircraft is initially flying leveled in trimmed condition (*300 ft* altitude) and at constant altitude; at a certain time, a disturbance (elevator impulse) is artificially injected, and the aircraft initiates a motion according to its Phugoid mode.

The pilot's task is to keep the aircraft leveled, non oscillating, to restore the initial altitude and to keep it as constant as possible.

During this task, the pitch and altitude oscillations of the Phugoid mode have to be damped by the pilot using the stick (as the red line in Figure 3.5).

The goal of these tests is to proof whether adding the Variable Stiffness CAAF kinesthetic (force) cue to the visual cue (a simulated cockpit) improves the control. In particular the goal is to assess as analytically as possible the differences in pilot performance in the two cases: with and without Variable Stiffness CAAF; the performance of the subjects (dependent variable) was measured through the IAE (Integral Absolute Error) between the current and desired altitude; a smaller IAE would indicate a better pilot performance in damping the Phugoid mode.

Eighteen naive subjects (aged 23 to 43, mean 30.7) participated to the experiment. All had normal or corrected-to-normal vision. They were paid, naive as to the purpose of the study, and gave their informed consent. The experiments were approved by the Ethics Committee of the University Clinic of Tübingen, and conformed with the 1964 Declaration of Helsinki. The experiment consisted of three different force conditions: No Force condition, with only compensation of gravity activated on the end-effector, Simple Force condition, the Variable Stiffness CAAF of Equation (3.15), and the Double Force condition, twice as much force as in the Simple Force condition, achieved by doubling the $K_{f,vs}$ gain. Each condition was run as a separate block, i.e., the experiment consisted of three successive blocks. The order of presentation of the blocks was counterbalanced (see Section D.2 for details).

In total, the experiment lasted from 60 to 90 minutes (including instructions and breaks between blocks).

3.6.2 CAAF Experimental Results

Mean IAE values were entered in a one-way repeated measures analysis of variance (ANOVA) [NoF, IHA-VS CAAF, IHA-Double VS

CAAF] (VS is for Variable Stiffness), which revealed a significant effect of the force factor

$$[F(2, 34) = 7.932, p < 0.01]$$

As shown in Figure 3.14, the participants were the least variable (performed best) when a simple force was applied, the most variable (performed worst) when no force was applied, whereas providing a double force gave rise to 'intermediate' results.

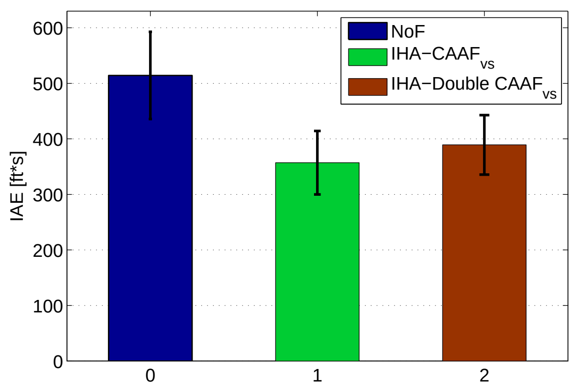

Figure 3.14: Performance (mean and standard error) for the three Force conditions (NoF, IHA-VS CAAF, IHA-Double VS CAAF).

Post-hoc tests using Bonferroni correction for multiple comparisons ($p < 0.05$) indicated that the performance with force (both Simple and Double) was significantly less variable than without force. In other words, providing Variable Stiffness CAAF force significantly improved piloting performance as it reduced the variability of the control. We also assessed the effect of the order of presentation of the blocks with a one-way repeated measures ANOVA [First Block, Second Block, Third Block], which revealed no significant main effect of the order of presentation. In other words, the variability of the performance was comparable irrespective of the order of presentation.

Our results clearly show that the Variable Stiffness CAAF facilitates control in this task. Indeed, participants' performance significantly improved when haptic cueing was available. As none of the participants had any experience with piloting, our results suggest that this type of aiding is rather 'natural', as beneficial effects can be observed without any previous learning. In line with these convincing initial results, could be interesting as future work to investigate the amount of additional information transferred to the operator via the CAAF variable stiffness haptic feedback as compared with other types of haptic aids (e.g., constant stiffness).

3.6.3 CAAF VS DHA Experiment

In the CAAF VS DHA Experiment, object of this section, a simple control task was prepared: the aircraft was initially flying leveled in trimmed condition at constant altitude (*300 ft*); three severe vertical wind gusts, which induce the aircraft to initiate a motion according to its Phugoid mode, are simulated by artificially injecting three control disturbances (elevator impulses) of randomized duration (2, 3 or 3.5 seconds), starting time and sign (upward or downward).

During this task, the pitch and altitude oscillations of the Phugoid mode have to be damped by the pilot through the use of the stick.

When a vertical wind gust disturbance affects a manned aircraft, the change in angle of attack and wing load are practically instantaneous. This has also an immediate effect on a mechanical-linkage based control stick. The altimeter on the GCS cockpit will though show the resulting change in altitude with a certain delay with respect to the actual disturbance time; as a matter of fact the aircraft dynamics has a low pass behavior and phase lag from angle of attack to altitude (in the simplest linear approximation it behaves as an integrator).

In order to focus on the haptic cueing we made the experiment more difficult for the pilots by setting the Artificial Horizon inoperable (zero pitch and roll); only altitude and speed readings were displayed.

The experiment consisted of three different external force conditions: No External Force condition (referred as *NoEF* condition) with only the spring-damper force on the end-effector, IHA condition (the Force Injection CAAF from Equation (3.19)) and DHA condition (see the Section 3.5.2 for details).

All the trials have been mixed and counter-balanced (see Section D.2 for details) and no instructions were given about the three different force conditions to test natural reaction of the pilots to the three different conditions.

A test campaign with a professional pilots was performed for the altitude regulation task. Seven professional pilots (from 50 to 700 hours of flight experience) participated to the experiment. The goal of these tests is to proof whether adding the IHA-Force Injection CAAF kinesthetic (force) cue or the DHA kinesthetic (force) to the visual cue (the simulated cockpit), improves the control with respect to a simple spring-damper behavior of the stick (NoEF). In particular the goal is to assess as analytically as possible the differences in pilot performance in three cases identified as NoEF, IHA-Force Injection CAAF, DHA. The performance of the subjects (dependent variable) was measured through the IAE (Integral Absolute Error) between the current and desired altitude; a smaller IAE would indicate a better pilot performance in damping the Phugoid mode.

All the trials (36 of 60 seconds each, 12 trials per condition) have been mixed and counter-balanced to test natural reaction of the pilots to the three different conditions. Before starting the experiment, every pilot was asked to run a 5 minutes trial where he/she had to perform a slightly different altitude regulation task; the goal of this initial trial, was to let the pilot acquire enough knowledge of aircraft dynamics to be able to pilot it confidently. During this trial a simple spring-damper behavior of the stick was employed. In total the experiment lasted 90 minutes. All pilots had normal or corrected-to-normal vision; they were paid and gave their informed consent. The experiments were approved by the Ethics Committee of the University Clinic of Tübingen, and conformed with the 1964 Declaration of Helsinki.

3.6.4 CAAF VS DHA Experimental Results

To summarize the forces felt by the pilots during the experiment an example is given: when a vertical wind gust (upwards for example) affects the aircraft, it will climb. The pilot should push over in order to reject the gust. So, to reject the gust the pilot should be compliant with the DHA Force and should oppose to the IHA Force.

As concerning the experimental results: mean IAE values for the three force conditions [NoEF, IHA, DHA] were entered in a one-way repeated measures analysis of variance (ANOVA). When all trials (12 trial for each condition) were considered, no main effect of the type of force was observed, i.e., the three types of force did not differ from one another. We then assessed whether all three types of force feedback were equally 'natural' for the subjects, i.e., whether the first exposure to the different types of feedback gave rise to comparable performance. Here, only the first two trials of each subject for each condition were considered, and the data were entered in the same one-way ANOVA (described above). This analysis revealed a main effect of the type of force feedback

$$[F(2, 12) = 12.943, p < 0.01]$$

As shown in Figure 3.15, the participants were the least variable in the NoEF and IHA conditions, and the most variable when the DHA force was applied, the variability being significantly worse in this last condition (post-hoc tests using Bonferroni correction for multiple comparisons, $p < 0.05$). In other words, when completely naive about the aiding schemes (in the first two trials), participants performed significantly better when either no force or the IHA aiding scheme was used than with the DHA aiding scheme.

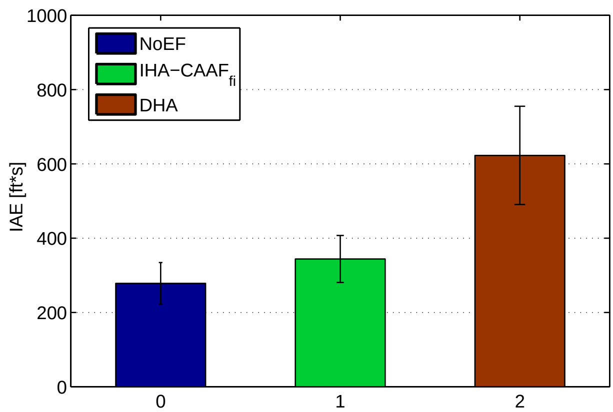

Figure 3.15: Performance (mean and standard error) for the 3 Force conditions of the first 2 trials.

Assuming that a certain degree of adaptation and learning of the pilots could have happened during the 12 trials, we also evaluated separately the last five trials of each condition. To test whether this was the case, the mean values of the last five trials were entered in the same one-way ANOVA. The analysis revealed a main effect of the type of force feedback

$$[F(2, 12) = 13.007, p < 0.001]$$

As shown in Figure 3.16, the participants were the least variable when the DHA force was applied, and the most variable when both NoEF and IHA forces were applied. Post-hoc comparisons using Bonferroni correction ($p < 0.05$) showed that this difference was significant. In other words, after some training, the DHA approach allowed the best results. It is worth noticing that, the pilot were not trained explicitly on the three force conditions, and that the trials consisted of a sequence of mixed conditions and not of a uniform batch of the same force condition; thus no explicit training was provided to the pilots on any of the three conditions, but the pilot were quickly capable to understand the DHA functionality and exploit it for improving their performance.

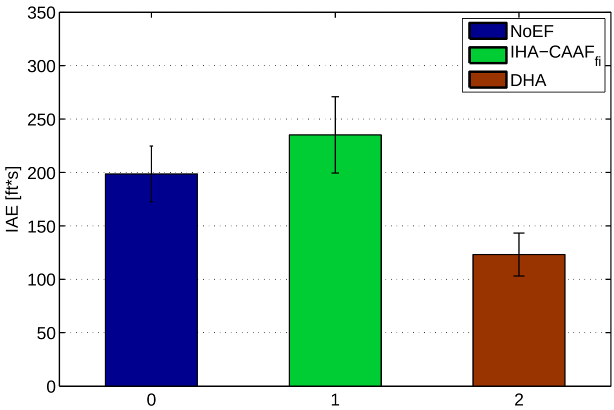

Figure 3.16: Performance (mean and standard error) for the 3 Force conditions of the last 5 trials.

After each experiment, pilots were interviewed separately; first of all the pilots were asked to describe their experience and identify the number of different types of sensations they felt during the experiment. All of them identified mainly two classes of force feedback: one which they called "natural", another which they called "autopilot" as they realized, after few tests (from 2 to 4), that in certain experiments the system was providing forces that where oriented in the direction of helping to perform the maneuver (autopilot case) and in other cases the forces were easier to associate with what they were expecting as the aircraft behavior (natural case). Only one pilot realized that some trials were run with the no force case in which the external disturbances give no sensation trough the stick.

Thus, in order to compare the results, each pilot was asked to fill in a questionnaire with 6 questions (Table 3.1). In each question he/she had to choose, accordingly to the classification of sensations described above, between two different force feedback cases: "Natural" and "Autopilot". According to the discussions with the pilots, we are confident that the Natural case can be mapped to the union of the NoEF and IHA cases, while the Autopilot case maps to the DHA condition. The 6 questions in the questionnaire are shown in the Table 3.1:

A.	*Which force condition was stronger?*
B.	*Which of the two conditions do you think was more helpful?*
C.	*Under which condition you think you had the best control on the aircraft?*
D.	*In which condition you think you had to produce the largest effort?*
E.	*In which of the condition you think you had the best performance?*
F.	*Which of the conditions did you prefer?*

Table 3.1: The wind gust rejection task questionnaire.

Figure 3.17 shows the corresponding pilot answers. Most pilots agree that the Autopilot case presented stronger forces and was more helpful (Questions A and B) with respect to the Natural case. Answers to question B and C show a controversial situation: although most pilots voted for the Autopilot as the most helpful, most pilots felt more like being actually piloting the aircraft (Question C) with the Natural case. Pilots' opinions about the workload (Question D) and about the evaluation of their own performance in the task (Question E) were divided. Finally, although it could appear that pilots were going to prefer the Autopilot case, most of them voted for the Natural case. With respect to the latter question, the pilot who voted "not sure" said that he would have voted for the Autopilot case but after a longer training.

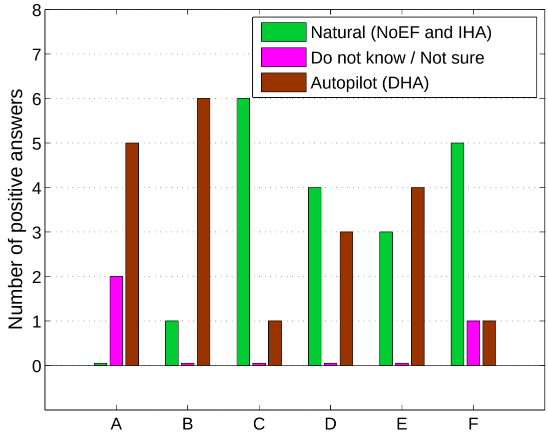

Figure 3.17: Pilot answers to questionnaire.

We can conclude that the NoEF and IHA case are the most natural forces to the pilots while after some training they can adapt to the DHA force feedback producing the best results even if the workload in this case results to be greater than in the previous cases.

Chapter 4

Obstacle Avoidance Feel

According to [10], the haptic feedback can compensate to some extent for the lack of sensory cues that will be presented to UAV operators (see Section 1.3), this means that a way improve the situational awareness of a remote UAV pilot and the efficiency of the teleoperation is the addiction of a haptic interface to the usually employed visual interface. It seems to be particularly necessary in cases of limited visual information. In the presence of foggy weather conditions, for example, or because of the employment of a limited FOV camera [1], the haptic feedback could provide information through the sense of touch, which can be applied directly on the control device.

In Section 2.2 a classification about the haptic aids of literature was given. The haptic aids were classified in DHA and IHA. Most of haptic literature is based on DHA concept. In particular, as concerning obstacle avoidance task every existing haptic aid seems to belong to the DHA class. Usually in this class, repulsive force is associated to the obstacles. Thus the pilot (or the teleoperator in general) has to be compliant with the force felt on the remote controller. In this Chapter, an attempt of designing a force feedback for the obstacle avoidance task which belongs to the IHA class was made. This will be shown to result more "natural" then the usually employed DHA-based approaches. This would confirm what Schmidt and Lee [77] (see Section 2.2).

The research resulted in an obstacle avoidance/detection force named *IHA-Obstacle Avoidance Feel* (IHA-OAF) and it is the object of the present Chapter. It will be shown to definitely improve the pilots' sensations and performance!

4.1 Simulation Environment

The present Section describes in details the simulation environment of the obstacle avoidance task.

Figure 4.1 shows the setup employed in the experiment. The virtual environment display produces the visual cue; a subjective view from the aircraft cockpit was simulated using a realistic virtual environment created using the DynaWORLDS software package [42] (see Section A.3 for details on the implementation). The environment was constituted by a non-Manhattan scenario (see Figure D.3) with a ground plane, the sky and buildings with regularly spaced windows to reproduce an appropriate perception of depth. As a matter of fact, the teleoperation of a vehicle in a opened area makes the simulation less problematic than the implementation of a constrained environment as long as, in the latter case, an accidental reduction of the visual feedback or small delays could bring to collisions. The obstacle avoidance task is a challenging problem in robotics.

To make the implementation of the experiment easier, the full non linear dynamics previously mentioned (DHC-2 Beaver [45]) was linearized around the trim conditions (horizontal flight at *300 ft* altitude). As concerning the obstacle avoidance task the aircraft dynamics was decoupled and only the lateral dynamic was considered. The Equation (3.5) shows how the elevator deflection through the changes of the lift coefficients modifies the aircraft lift and thus the longitudinal aircraft trajectory. It concerned the longitudinal dynamics. As concerning the lateral dynamics, something similar to

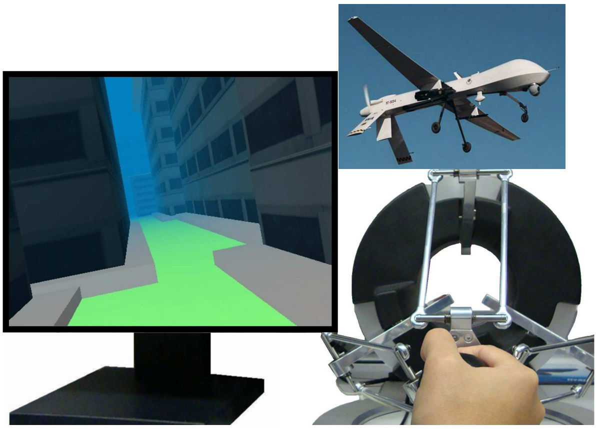

Figure 4.1: The obstacle avoidance teleoperation setup.

Equation (3.5) can be written.

In order to limit pilot workload and possible errors, only the aircraft lateral dynamics (i.e. roll and heading angles and lateral position) had to be controlled by the pilot. Equation (4.1) shows the lateral steady state equations of horizontal flight in Wind Axes (see Section 3.2.2 for the definition) [48]:

$$\begin{cases} 0 = C = C_C \cdot qS \\ 0 = l = C_l \cdot bqS \\ 0 = n = C_n \cdot bqS \end{cases} \tag{4.1}$$

where C, l and n are respectively the aircraft cross-wind force, the rolling and the yawing moments; C_C, C_l and C_n are respectively the aircraft cross-wind force, rolling and yawing moment coefficients. b is the wing span. Similarly to Equation (3.5), the coefficients present in Equation (4.1) can be re-written as proportional to the sideslip angle β, the angle between the aircraft direction of the motion (the relative speed) and the x-axis in the Body Reference Frame (see Section 3.2.1 for the definition), and to the aileron deflection δ_a (the rudder deflection δ_r and α are supposed to be fixed in the respective trim condition values). The only input to the lateral dynamics is the aileron deflection δ_a. The employed haptic device is again the Omega Device (see Section 3.4) and a lateral deflection, δ_A, of its end-effector was hypothesized to produce the aircraft lateral motion. See the following Section for details on the lateral linear dynamic model of the aircraft employed.

4.2 Aircraft Lateral Dynamics

Figure 4.2 shows the baseline scheme (i.e. no haptic aids) employed in the obstacle avoidance setup.

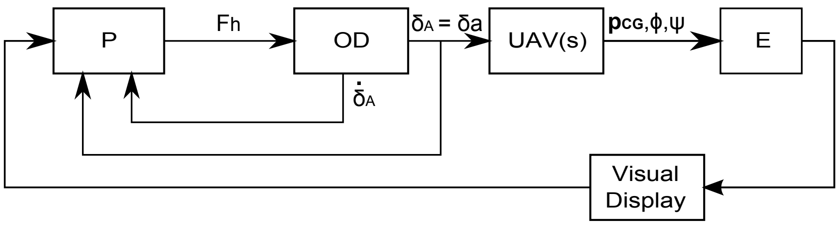

Figure 4.2: The obstacle avoidance simulation baseline scheme.

The input of the aircraft lateral dynamics $UAV(s)$ is the aileron deflection, δ_a, (in this Chapter coincident with the deflection δ_A of the haptic device represented by the OD block) and the outputs are the aircraft center of gravity position $\mathbf{p_{CG}}$ or (x_e, y_e), heading (ψ) and roll angle (ϕ) of the aircraft in the Earth Reference Frame (Earth-Centered, Earth-Fixed reference frame with origin in the center of the Earth, z_{OB} axis points North, x_{OB} and y_{OB} axes are on the equatorial plane). The block $UAV(s)$ in Figure 4.2 is shown in details in Figure 4.3.

In Figure 4.3 the transfer function $H_{UAV}(s)$ (4.2) (from aileron, δ_a, to roll rate, p or $\dot{\phi}$) was employed. It is obtained from linearization

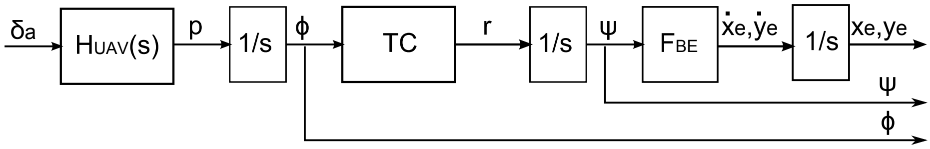

Figure 4.3: The aircraft lateral dynamics.

of the non linear Beaver DHC-2 of the *Flight Dynamics and Control Toolbox* [45]. The roll angle, ϕ, is obtained through integration and saturated to *50 degrees* to make the aircraft dynamics more realistic.

$$H_{UAV}(s) = \frac{-9s^4 + 9.8777s^3 + 10.413s^2 - 6.1385s + 0.018381}{s^4 + 8.1578s^3 + 10.2490s^2 + 11.8186s + 0.6961} \tag{4.2}$$

Then, by making the assumption of aircraft performing a coordinated turn [47] (*TC* block in Figure 4.3) (zero velocity in the lateral body axes) at constant speed V (about *50 m/s*), the heading rate r or $\dot{\psi}$ is calculated through the Equation (4.3):

$$\dot{\psi} = r = tan(\phi)\frac{g}{V} \tag{4.3}$$

where g is the gravity acceleration. The heading angle, ψ, is obtained by integration. $\dot{x_e}$ and $\dot{y_e}$ are calculated by a coordinates transformation (F_{BE} block) of Equation (4.4) from Body Reference Frame to Earth Reference Frame (see the Section 3.2.1 and above for the reference frames definitions).

$$\begin{bmatrix} \dot{x}_e \\ \dot{y}_e \end{bmatrix} = \begin{bmatrix} cos(\psi) \\ sin(\psi) \end{bmatrix} V \tag{4.4}$$

The coordinates of the aircraft center of gravity (x_e and y_e) are calculated from Equation (4.4) by integration. As shown in Figure 4.2, informations about the environmental constrains (contained in *E block*) are used to show through the *Visual Display* (see Figure

4.1) the virtual environment from the camera point of view which is represented by the aircraft center of gravity position and attitude.

4.3 The Stick Force

Since, as hypothesis, the only dynamics to control is the lateral one, the haptic aid for the obstacle avoidance task was applied only to the lateral axes of the control device that is the y axes in Figure 3.2.

Thus, the only force transmitted to the operator is along the y axis.

$$\begin{cases} F_y = F_{SD,y} + F_{OA,y} \\ F_{SD,y} = F_{SD} = F_{S,y} \cdot y_S + F_{D,y} \cdot \dot{y}_S \\ F_{OA,y} = F_{OA} \end{cases} \tag{4.5}$$

In Equation (4.5), F_{SD} is the Spring-Damper force. The lateral stiffness and damping components, $F_{S,y}$ and $F_{D,y}$, were chosen as in Table A.2. The lateral stiffness is a half of the longitudinal stiffness. As a matter of fact, as concerning the force and displacement characteristics, the sticks have usually stiffer gradients pitching commands (forward/backward arm movement) than for roll commands (left/right arm movements) [82] because of the differences in strength among the various arm muscles used for pitch and roll control. Similar difference exists between pulling movements (both longitudinal and lateral) towards the pilot body and pushing movements away from it [82] but in this work the stiffness is supposed to be constant for both longitudinal and lateral movements although the different values (smaller for lateral stick displacements).

The Spring-Damper term depends on the desired stick dynamics and it is present (same value) in all the conditions of the experiment, while the external force term for the obstacle avoidance, F_{OA}, depends on the experimental conditions. Three types of external force F_{OA} have been compared: DHA, IHA and a baseline force condition

(No External Force, NoEF) in which $F_{OA} = 0$ in order to test the operators performance in the obstacle avoidance task. To create Direct and Indirect external forces two simulators were prepared (see Section 4.4).

4.3.1 The haptic feedback

It is well known that an aircraft stick (even for modern fly-by-wire aircraft) should always offer a certain stiffness and damping to the pilot to mimic a real (mechanically driven) aircraft stick [47, 52]. In most teleoperation situations, it is common to try to make the haptic interface invisible to the human operator to achieve what is often defined as *transparency* of the teleoperation system. In this specific case though, we believe that the user must always feel a certain stiffness and damping of the interface even when not *feeling the presence* of the environment. The author also proved the importance of the spring-damper force (as shown in Chapter 3) in a previous paper [2].

Thus, for this particular application, we designed a system where the haptic interface appears as a stick with constant damping and stiffness with the addition of an external force which appears when needed (namely when close to obstacles). Then, the force F_y felt by the operator during the obstacle avoidance task (see Equation (4.5) and (4.6)) along the control device y axes (see Figure 3.2) is a combination of an elastic term, $F_{S,y}$ $(K_{S,y} \cdot y_S)$, with constant stiffness $K_{S,y}$, a damping term, $F_{D,y}$ $(K_{D,y} \cdot \dot{y_S})$, with a damping constant $K_{D,y}$ and an external force component F_{OA}. y_S and $\dot{y_S}$ are the lateral displacement and displacement rate of the end-effector respectively.

$$F_y = K_{S,y} \cdot y_S + K_{D,y} \cdot \dot{y_S} + F_{OA} \tag{4.6}$$

As said, the external force F_{OA} could belong either to the DHA class or to the IHA class. In the baseline force condition (No External

Force, NoEF) $F_{OA} = 0$. Section 4.4 presents DHA and IHA obstacle avoidance external forces.

4.3.2 The Obstacle Force Field

In order to produce some kind of haptic feedback on the stick with the goal of helping to avoid collisions with obstacles, we defined a force field around the obstacles (Equation 4.7). The force field starts in the center of each single obstacle and points away from the obstacles.

The intensity of the force field decreases with distance from the obstacle and becomes zero beyond a certain threshold distance. A haptic sensation will thus be produced proportional to this force field.

The total force $\mathbf{F_{OBS}}$ exerted by the environment at the position of aircraft center of gravity, in the obstacle reference frame (Equation (4.7)), the fixed Earth Reference Frame (see above for the definition) is the superposition of the repulsive forces produced by each obstacle.

$$\mathbf{F_{OBS}} = \begin{bmatrix} F_{OBS,x} \\ F_{OBS,y} \end{bmatrix} = \sum_{n=1}^{N} \mathbf{F_{OB}} \tag{4.7}$$

where N is the total number of obstacles. For both DHA and IHA approaches, the force field shows a maximum intensity on the obstacle boundary decreasing with distance from it. The force field is present inside the obstacle as well (see later).

By following this principle, a repulsive force field (Equation 4.8), similar to the one chosen by Melchiorri [4] and which represents the repulsive force field often used in literature, was associated to a collection of rectangular obstacles.

$$\mathbf{F_{OB}} = \begin{cases} -k_f \cdot (d(\mathbf{p_{OB}}, \mathbf{p_{CG}}) - r_e) \cdot \frac{\mathbf{p_{OB,C}} - \mathbf{p_{CG}}}{||\mathbf{p_{OB,C}} - \mathbf{p_{CG}}||}, & d(\mathbf{p_{OB}}, \mathbf{p_{CG}}) < r_e \\ 0, & \text{otherwise} \end{cases} \tag{4.8}$$

Let $\mathbf{p_{CG}}$, $\mathbf{p_{OB,C}}$ and $\mathbf{p_{OB}}$ to be respectively the position of the aircraft center of gravity (x_e,y_e), the position of the center of a single obstacle and the sides of the obstacle closer to the aircraft. In particular, the distance $d(\mathbf{p_{CG}} - \mathbf{p_{OB}})$ between the aircraft center of gravity and the obstacle depends from the position of the aircraft center of gravity with respect to the obstacle (see Figure 4.4). In particular, the aircraft can be positioned (see Figure 4.4) next to the obstacle sides (either A or B zone) or next to the obstacle vertices (C zone).

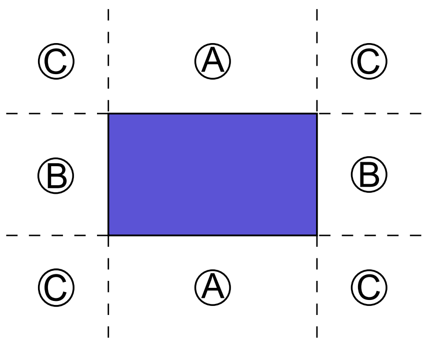

Figure 4.4: Definition of the distance between the aircraft center of gravity and the obstacle.

Depending on this, the distance between the aircraft center of gravity and the obstacle is defined as:

CASE A: the vertical distance between $\mathbf{p_{CG}}$ and the closer horizontal obstacle side;

CASE B: the horizontal distance between $\mathbf{p_{CG}}$ and the closer vertical obstacle side;

CASE C: the euclidean sum of the previous ones;

The term $\frac{\mathbf{p_{OB,C}}-\mathbf{p_{CG}}}{||\mathbf{p_{OB,C}}-\mathbf{p_{CG}}||}$ indicate the force field versor given by the congiunction between the aircraft center of gravity and the center of the obstacle.

The force field at the position $\mathbf{p_{CG}}$ is aligned with the versor $\frac{\mathbf{p_{OB,C}}-\mathbf{p_{CG}}}{||\mathbf{p_{OB,C}}-\mathbf{p_{CG}}||}$ and the intensity is selected to be linearly decreasing with the distance $d(\mathbf{p_{OB}}, \mathbf{p_{CG}})$ of the point $\mathbf{p_{CG}}$ from the nearest point of the obstacle boundary.

The constant k_f is an appropriately selected constant and can be thought as the stiffness of the virtual environment. When the distance $d(\mathbf{p_{OB}}, \mathbf{p_{CG}})$ is less than r_e (which was set to *50 m*, the maximum distance of influence, a repulsive force is used to generate the Haptic Aid in order to help the aircraft pilot to avoid the obstacle.

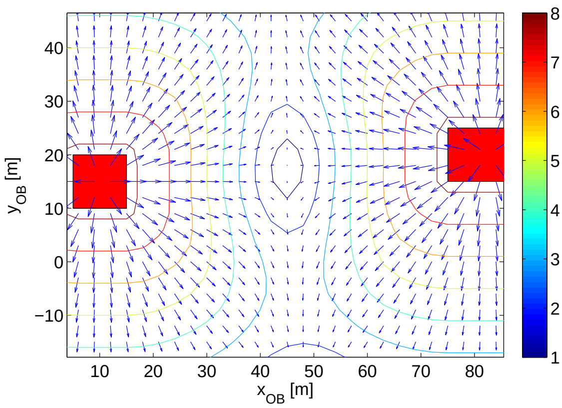

Figure 4.5: Example of the obstacle repulsive force field.

Figure 4.5 shows an example of the force field with force vectors and ISO-force contour lines that is produced by the obstacles. The value and direction of the force field at the current position of the aircraft are used in the simulator to generate the haptic sensation.

An example of the mentioned non-Manhattan scenario generated force field is depicted in Figure 4.6 in which also the contour lines are shown.

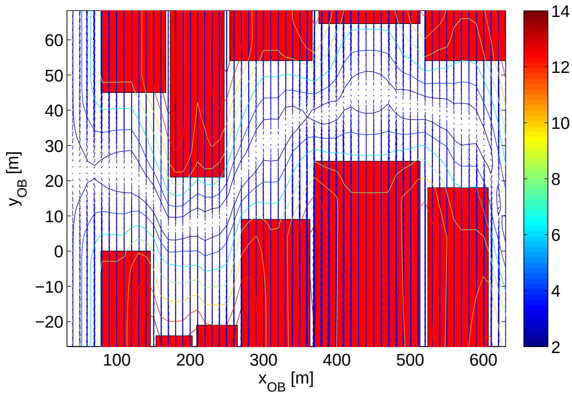

Figure 4.6: Example of non-Manhattan scenario repulsive force field with contour lines.

Figure 4.6 clearly shows a low amplitude force field in the virtual corridor created in the middle of the street and the maximum force (about $10N$) at the obstacles sides.

As mentioned, the total force exerted by the obstacles (Equation 4.7) is expressed in the fixed Earth Reference Frame. A change in the aircraft Body Reference Frame (see Section 4.2 for the definition) is necessary to appropriately select the force component that lies on the lateral axis of the current aircraft direction:

$$\begin{bmatrix} F_{B,x} \\ F_{B,y} \end{bmatrix} = \begin{bmatrix} cos(\psi) & sin(\psi) \\ -sin(\psi) & cos(\psi) \end{bmatrix} \cdot \begin{bmatrix} F_{OBS,x} \\ F_{OBS,y} \end{bmatrix} \tag{4.9}$$

In Equation (4.9), $F_{B,x}$ and $F_{B,y}$ are the force component in the aircraft Body Reference Frame. ψ is the heading angle of the aircraft.

The haptic force will be function of $F_{B,y}$ only. From now on, the force produced by the environment, F_{AO} of Equation 4.5, will be considered to coincide with the y component of the one in Equation (4.9), i.e. $F_{OA} = F_{B,y}$.

4.4 The OAF VS DHA Experiment Simulators

In order to test the IHA-Obstacle Avoidance concept, three simulators were created. The first one is the NoEF Simulator (see Section 4.4.1); the second one, the DHA Simulator (see Section 4.4.2), belongs to the DHA class; the third one, the IHA-OAF Simulator (see Section 4.4.3), belongs the IHA class.

As preliminary assessment of the techniques and for tuning of the IHA and DHA simulators, a simple experiment with an isolated obstacle was run (Section 4.4.4). A more complex scenario (the mentioned non-Manhattan scenario) was used instead for a deep test campaign (see Section 4.5).

4.4.1 NoEF Simulator

Figure 4.2 shows the block diagram of the simulation system used to test the NoEF feedback force that is the baseline scheme (no haptic cues related to the obstacles).

Let $\mathbf{p_{OBS}}$ to represent the position of the obstacles and $\mathbf{p_{CG}}$ the position of the aircraft center of gravity. The pilot may perceive the distance from the obstacles using the visual display (see Figure 4.1). The pilot force input (F_h), is fed to the haptic device (OD block in Figure 4.2) to produce the stick deflection δ_A (which in this Chapter is used directly as aircraft elevator control δ_a). δ_A and $\dot{\delta}_A$ indicate that the pilot actually feels the elastic and damping haptic device response.

This case represents just a visual aid as long as the haptic feedback is only related to the actual stick displacement and to its rate and it is not related to the environmental constraints.

The NoEF condition presents a constant stiffness stick (to simulate a fly-by-wire like situation). In the NoEF condition the force exerted by the haptic device is the same as in the Equation (4.6) except for F_{OA} which is set to zero in this condition. The pilot had the mentioned virtual scenario as the only instrument showing the virtual buildings from the aircraft center of gravity point of view (see Figure 4.1). The visual feedback is the same in all the conditions of the experiment.

Thus, the force felt in NoEF case is given from Equation (4.10):

$$F_{NoEF} = F_{SD,y} \tag{4.10}$$

Suppose the aircraft is close to an obstacle: as long as $F_{OA} = 0$ in the Equation (4.5), no force is directly linked to the the obstacle. Thus, the pilot will not feel any haptic information about the presence of the obstacle but he/she will just see it through the visual display (only in good visibility conditions, i.e. no foggy weather) while approaching. The only haptic feedback felt by the pilot is proportional to δ_A and $\dot{\delta}_A$ produced only from the pilot input force F_h.

Figure 4.7 depicts an example of the variables' history during a simulation trial.

4.4.2 DHA Simulator

According to the DHA concept, a Direct Haptic Aiding system for obstacle avoidance should produce a force or a change in stiffness that helps the pilot directly in achieving the task that, in this case, is to avoid collisions with the obstacles. Thus, a system that produces a force which pulls the stick in the same direction the pilot

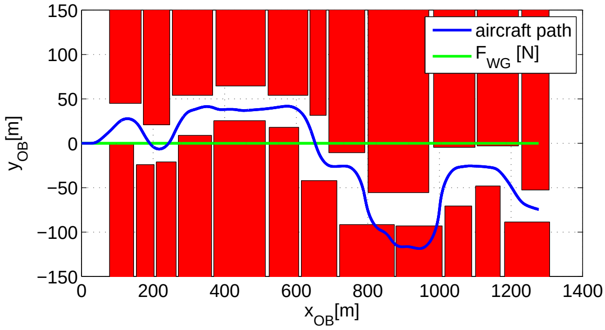

Figure 4.7: NoEF simulation example.

should do to avoid the collision, seems appropriate for a DHA control. As a matter of fact, the obstacle avoidance system described in [1, 78] works exactly according to this principle. Stiffness variation, together with force feedback were investigated and found to be able to provide better results than single stiffness or force feedback [78]. Nevertheless, for the purposes of this comparison, we decided to investigate and compare force feedback only. A compensator (DHA block in Figure 4.8) was added to compute the external force to be felt by the pilot. The Haptic device was controlled as in Equation (4.6) to behave as a spring-damper system with an additional force F_{OA} from the y component of Equation 4.9 (remember in fact that $F_{OA} = F_{B,y}$).

Figure 4.8 shows the block diagram of the simulation system used to test the DHA concept.

The pilot may perceive the distance from the obstacles using the visual display (see Figure 4.1). The same distance is also perceived via a haptic display through the DHA block that implements the DHA force and feeds-back the force (F_{WG}) which, together with the pilot force input (F_h), is fed to the haptic device (OD block in Figure 4.8) to produce the stick deflection δ_A. δ_A and $\dot{\delta}_A$ indicate that pilots actually feels the elastic and damping haptic device response.

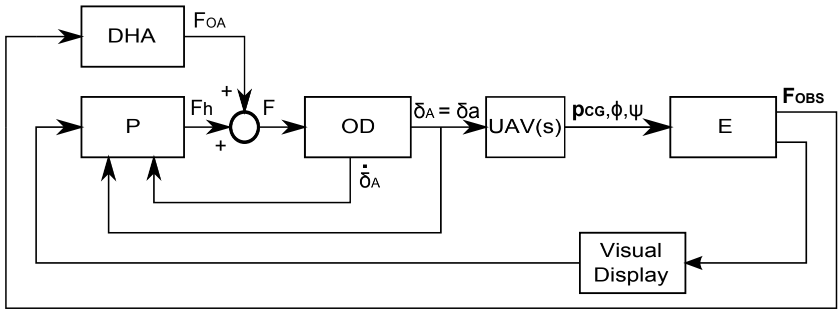

Figure 4.8: DHA-based obstacle avoidance simulator scheme. The haptic force F_{OA} deflects the stick inducing a helpful change of the aircraft trajectory.

Thus, the force felt in DHA case is given from Equation (4.11) by considering $F_{OA,DHA} = F_{B,y}$ of the Equation (4.9):

$$F_{DHA} = F_{SD,y} + F_{OA,DHA} \tag{4.11}$$

Suppose the aircraft is close to an obstacle: as long as $F_{OA} = F_{B,y}$ in the Equations (4.5) and (4.6), the repulsive force F_{OA} generates a stick motion that deviates, at least partially, the aircraft trajectory away from the obstacle, thus the pilot has to follow it (being compliant) in order to avoid the collisions. Thus, the pilot will feel a haptic information about the presence of the obstacle and he/she will see it through the visual display (when the visibility conditions are good enough) while approaching. A haptic feedback proportional to δ_A and $\dot{\delta}_A$ produced from both the pilot input force F_h and from the obstacle force F_{OA} is present as well.

Figure 4.9 depicts an example of the variables' history during a simulation trial.

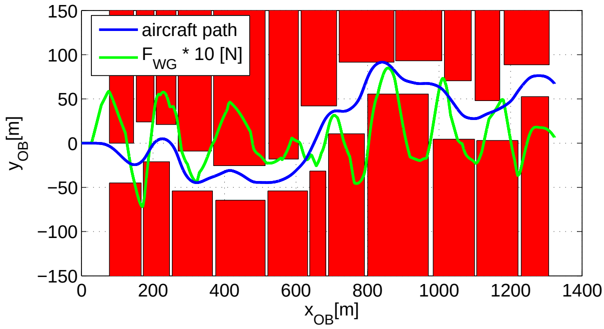

Figure 4.9: DHA simulation example.

4.4.3 IHA-OAF Simulator

The design of a IHA-inspired obstacle avoidance aid appears complex since no force sensation is "naturally" generated by coming close to an obstacle. But, in order to follow the concept that already was proven to be successful in the gust rejection task, that opposition to haptic stimuli is a "more natural" pilot reaction with respect to compliance to stick motion (see Section 2.2), a haptic aid of opposite sign with respect to the DHA one was designed. This type of aid would result in a tendency of the aircraft to fly toward the obstacle instead of flying away from it as in DHA. Thus, in order not to penalize too much the IHA system and to make it safe, the indirect force feedback (the same as the direct force feedback of Equations (4.7)-(4.9) but opposite in sign) was transformed in a shift of the neutral point of the stick.

This means that only the stick, de facto, would move towards the obstacle without producing the aircraft to fly against it. For example, if an obstacle is on the right side, the stick would move to the right but, if the pilot is not in the loop, the UAV will continue to fly straight. What happens if the pilot is in the loop? In the same direction of what Schmidt and Lee think [77], the idea is that when the stick moves on one direction, it would be more natural for the pilot to move it in the opposite side. Going back to the example: with the obstacle on the right, the neutral point of the stick shifts to the right, the pilot would feel this movement and perhaps he naturally would oppose it by moving the stick toward the left (that is simply moving the stick a little back to the center) performing a turn on the left that is, in the example, the maneuver to perform to fly away from the obstacle.

The vanishing of the haptic cue informs the pilot that the obstacle is far away and not dangerous anymore.

Figure 4.10 shows the block diagram of the simulation system used to test the IHA concept.

The distance between the obstacles and aircraft center of gravity may be perceived by the pilot P via the visual display (see Figure 4.1). The same distance is also perceived via haptic display through the IHA block that implements the IHA force and feeds-back the force F_{OA} which, together with the pilot force input (F_h), is fed to the haptic device (OD block in Figure 4.10) to produce the stick deflection δ_A. The block OD_i takes care of producing the effect of shifting the neutral point of the stick and will be detailed later. δ_A and $\dot{\delta}_A$ indicate that pilots actually feels the elastic and damping haptic device response.

Thus, the force felt in IHA case is given from Equation (4.12) by considering $F_{OA,IHA} = -F_{B,y}$ of the Equation (4.9):

$$F_{IHA} = F_{SD,y} + F_{OA,IHA} \tag{4.12}$$

Suppose the aircraft is close to an obstacle: as long as in this case $F_{OA} = -F_{B,y}$ of the Equations (4.5) and (4.6), a force which attract the stick neutral point is directly linked to the the obstacles and the pilot has to oppose it in order to avoid the collisions. In fact, the shifting of the stick (neutral point) towards the obstacle makes the pilot to think that he is flying against the obstacle. The force is immediately felt by the pilot who knows that something has

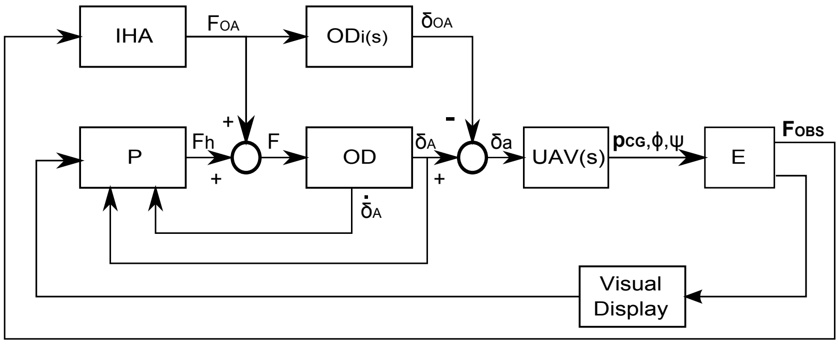

Figure 4.10: IHA-OAF simulator scheme. The haptic force F_{OA} deflects the stick without producing any change to the aircraft trajectory thanks to the effect of the compensating signal δ_{OA}.

changed. The pilot should react immediately by opposing to the stick motion in order to fly away from a possible collision.

Thus, the pilot will feel a haptic information about the presence of the obstacle and he/she will see it through the visual display (when the visibility conditions are good enough, i.e. no foggy weather) while approaching. A haptic feedback proportional to δ_A and $\dot{\delta}_A$, produced from both the pilot input force F_h and from the obstacle force F_{OA}, is present as well.

Figure 4.11 depicts an example of the variables' history during a simulation trial.

In other words, the IHA-OAF follows the general IHA concept described before: it provides to the pilot the information about the presence of the obstacle on a side of the aircraft but it does not effect in any way the commands actually sent to the aircraft; this helps the pilot indirectly by improving his/her SA, that is to let him/her know that in the remote environment a collision is going to happen, and leaving him/her the full authority to take control decisions by changing the direction of the motion of the vehicle.

A mathematical proof of the neutral point shift concept described

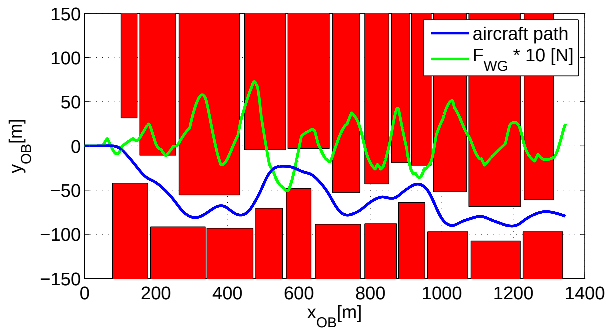

Figure 4.11: IHA-Obstacle Avoidance Feel simulation example.

above is presented in the Subsection 4.4.3.

IHA-OAF Implementation Proof

In order to modify the neutral point so that the haptic force F_{OA} would produce no actual change of the aircraft trajectory (i.e. the aircraft continues to fly straight if the pilot takes no command actions), the same external force, F_{OA}, is sent to both the real Haptic Device (actually tha Omega 3DOF Device, Force Dimension, Switzerland) and an identified model of it. The output of the identified haptic device model is subtracted from the total displacement of the end-effector of the real device in a way that the effect of F_{OA} will not be an input command to the aircraft but just a change in the neutral position of the stick.

Let $OD(s)$ to be the transfer function of the real Omega Device (by supposing that the real Omega Device has a linear behavior and representing it through a transfer function is possible) and with $OD_i(s)$ the transfer function of the identified model of it. Let the displacement of the real Omega Device end-effector and the displacement of the identified model of it be respectively δ_{OA} and $\delta_{OA,i}$. Let us to suppose that by giving the same input, F_{OA}, to the Omega

Device and to its identified model the output, the produced displacement, is the same in both cases: $\delta_{OA} = \delta_{OA,i}$ (i.e. the identified model is exact); the net result is that the operator moves the end-effector by δ_A through the application of the force F_h. As a matter of fact, from the Figure 4.10:

$$\begin{cases} F_h + F_{OA} = F \\ \delta_A - \delta_{OA} = \delta_a \end{cases} \tag{4.13}$$

$$\begin{cases} \delta_{OA} = OD(s) \cdot F_{OA} = OD_i(s) \cdot F_{OA} = \delta_{OA,i} \\ \delta_A = OD(s) \cdot F = OD(s) \cdot (F_h + F_{OA}) = OD(s) \cdot F_h + \delta_{OA} \end{cases} \tag{4.14}$$

From the second of the Equation 4.13 and the second of the Equation 4.14:

$$\delta_A = OD(s) \cdot F_h \tag{4.15}$$

The final result is that the F_{OA} changes just the neutral point of the Omega Device by δ_{OA} and the only input to the aircraft dynamics is given by the pilot command F_h (Equation (4.15)). The transfer function $OD_i(s)$ of the actual Haptic device used in the experiments was identified by using frequency sweeps (from 0.0262 to 10 Hz) and the Empirical Transfer Function Estimate (ETFE) technique (Ljung, 1999) (something similar to what explained while talking of the longitudinal dynamics which details could be found in Appendix B).

4.4.4 Isolated Obstacle Scenario

In order to test the beneficial anticipatory effect of the haptic feedback several experiments were run using a scenario with an isolated obstacle placed along the path of the aircraft; the task of the participant was to fly straight. The participant sees the obstacle from different distances, according to the three visibility conditions described above. The most relevant test performed had a very low visibility condition (i.e. foggy weather condition): the participant was not able to detect the presence of the obstacle early enough to maneuver the aircraft without the haptic feedback; as can be noted in Figure 4.12, while in the DHA and the IHA cases no collisions occurred, in the NoEF case a collision occurred confirming, at least according to this preliminary results, the importance to have a haptic feedback in addition to visual feedback to improve the flight safety. The reaction delay in the NoEF case, with respect to DHA and IHA, appears clearly from the stick forces plots (blue lines).

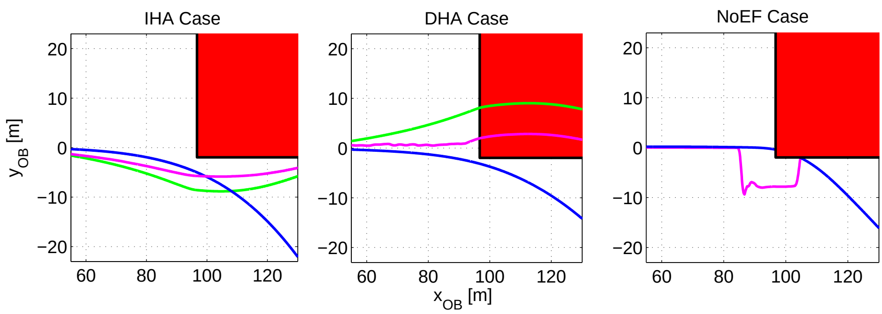

Figure 4.12: Isolated obstacle scenario: IHA, DHA and NoEF experiments in the Maximum Fog visibility condition. The obstacle is drawn in red. The lines represent: the aircraft trajectory (blue) starting from the left, the force F_{WG} (green when present) and the total force F_y (magenta).

4.5 IHA-OAF Evaluation

In order to test the IHA-Obstacle Avoidance concept, several experiments about an obstacle avoidance task were run.

The experiments were run under three different visibility conditions: a) *Minimum Fog*; b) *Medium Fog*; c) *Maximum Fog* (see Figure 4.13) and under three different force condition: DHA, IHA and NoEF.

Figure 4.13: Out of the window view from the same viewpoint while the same obstacle, in the left side, is approaching under the three different visibility conditions: a) *Minimum Fog*; b) *Medium Fog*; c) *Maximum Fog*.

In Figure 4.13c the fog is so thick that the only information the pilot can rely on is the haptic cue only. Under the third visual condition, in fact, when an obstacle placed along the path of the aircraft, the pilot sees it from different distances and the available time to react to avoid the collision is different. The most relevant test performed had the Maximum Fog visibility condition; in this case the pilot was not able to detect the presence of the obstacle early enough to maneuver the aircraft without the haptic feedback.

A simple control task was prepared: the aircraft had to be flown in an urban canyon with buildings placed irregularly (non Manhattan-like) along the desired path; thus, the buildings constituted a narrow street with buildings in both sides. The task of the experiment was to get the end of the street by avoiding the collisions with them. Five different scenarios (i.e. position of the N obstacles) were used to avoid the effect of learning in test subjects (see Figure D.3 for an example about one of the 5 employed scenarios). To test the natural response to the different types of force no instructions were given to the participants about the force they were going to feel on the stick.

The error metric is the number of collisions.

The goal of these tests is to prove whether the IHA-OAF kinesthetic (force) cue to the visual cue (a simulated cockpit) improves the control with respect to the other two conditions. In particular the goal is to assess as analytically as possible the differences in pilot performance in the three cases. Thus, the performance of the subjects (dependent variable) was measured through the number of collisions in the flight across a constrained environment.

Ten naive subjects participated to the experiment. All had normal or corrected-to-normal vision. They were paid, naive as to the purpose of the study, and gave their informed consent. The experiments were approved by the Ethics Committee of the University Clinic of Tübingen, and conformed with the 1964 Declaration of Helsinki.

The experiment consisted of three different force conditions: NoEF, DHA and IHA-OAF.

All the trials (see Section D.3 for details) have been mixed and counter-balanced and no instructions were given about the three different force conditions to test natural reaction of the subjects to the three different conditions.

Each fog condition was run as a separate block, i.e., the experiment consisted of three successive blocks.

The participants in the experiment had to run 45 trials of about 2 minute each. The first 15 under the Minimum Fog condition, the second 15 under the Medium For condition, the last 15 under the Maximum Fog condition.

In total, the experiment lasted about 120 minutes (including instructions and breaks between blocks).

As concerning the instructions to the subjects: they were informed about the presence of three different force conditions. One in which only the stick was felt as a normal joystick (if they left it, it would come back to the center neutral position) named Spring Force. The other two conditions were said to produce a force which would tried to move the stick itself named A Force and B Force. They were asked to try to recognize the type of forces trying to classify it according to what they felt. After each trial they were asked what kind of force they felt.

4.5.1 Experimental Results

Mean number values of collisions for the three force conditions [NoEF, IHA-OAF, DHA] were entered in a one-way repeated measures analysis of variance (ANOVA). See the results in Figure 4.14.

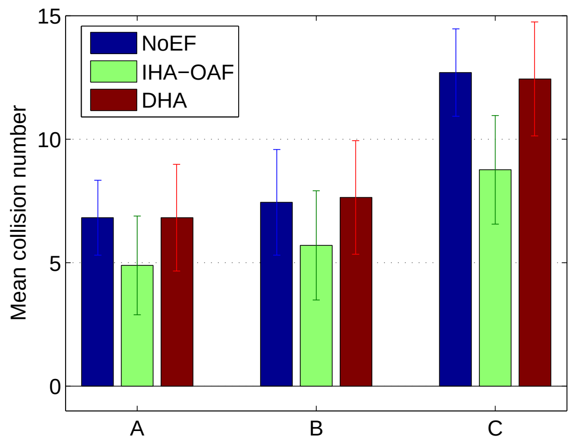

Figure 4.14: Performance (mean and standard deviation) for the 3 Force conditions (DHA, IHA-OAF, NoEF) and for the 3 visibility conditions (A, B, C).

A main effect of the fog condition was found:

$$F(2, 9) = 18.366, p < 0.001$$

Post-hoc tests using Bonferroni correction for multiple comparisons, $p < 0.05$ confirmed that the subjects performed significantly worse in the Maximum Fog condition than in the Minimum and in the Medium ones.

A main effect of the force condition was found as well:

$$F(2, 9) = 6.427, p < 0.01$$

Post-hoc tests using Bonferroni correction for multiple comparisons, $p < 0.05$ confirmed that the subjects performed significantly better when the IHA-OAF haptic cue was provided in the haptic device than when both DHA and NoEF were provided.

No interaction was found between the two variables.

In other words, the just introduced IHA-Obstacle Avoidance Feel was proved to provide the best results in the obstacles avoidance task irrespective of the fog condition. Thus, the subjects collided less times aided by the IHA-OAF than both the DHA and the NoEF cases.

This is a pretty surprising result as long as it was expected that NoEF case would have produced the best results in presence of Minimum Fog condition. While, according to the present results, the employment of IHA-OAF improves the performance with all the visibility conditions.

Furthermore, better performance of the DHA than the NoEF was expected in presence of both Minimum and Maximum Fog conditions. This seems to be against previous results [51]. A possible explanation is that under both the DHA and the IHA conditions a haptic help (not given in the NoEF case) was given in finding again the main street once lost right after a collision. This is due to the presence of the non null force field inside the obstacle in case of both DHA and IHA. Thus, while in NoEF case was not possible to find again the main street once collided, with both DHA and IHA cases it was easier; even if, to be precise, the best help in finding again the main street is given by the DHA which gives the clearest suggestion about where to go to get out from the collided building because being compliant already helps a lot. A second possible explanation is the different type of baseline condition employed: a difference in the stiffness constant chosen (*120 N/m* of the present work, in Table A.2, against about *200 N/m* of the previous one). A third possible explanation is that the DHA force in the present work could be weaker than the one employed in previous works and this would make easier to fly close to the obstacles with not too much effort.

After each trial the subjects were asked what kind of force they felt to check if they could recognize the type of forces trying to classify them.

Most of them were very able to distinguish between the Spring Force condition (see Section 4.5) and the force feedback conditions (both A Force and B Force). It was, in general, more difficult to classify and distinguish the A and the B Forces.

Some of them correctly noticed and reported the difference between A and B in terms of cue direction with respect to the obstacles (force pushing away from or towards the obstacles). Other participants were only able to identify the difference in strength (actually not present because the amplitude of the force in the two force conditions was exactly the same for the same distance between the aircraft and the obstacles). Someone's classification was really poor (till the end of the 45 trials they still were not able to classify and recognize the force conditions).

Three participants of 10 were not able to recognize more than the 40% of the forces during the 45 trials.

Only 6 participants of 10 were able to recognize more than the 60% of the trial forces. Only 3 of them were able to recognize more than about 75% of the same.

After the 45 trials, pilots were interviewed separately. In order to compare the results, each pilot was asked to fill in a questionnaire with 6 questions which is the same as in the CAAF VS DHA Experiment (see Table 3.1 of Section 3.6.4):

The answers to the questionnaire of the 3 only subjects who recognized more than about the 75% of the forces step by step during the 45 trials, are for sure more meaningful than the others (see Figure 4.15).

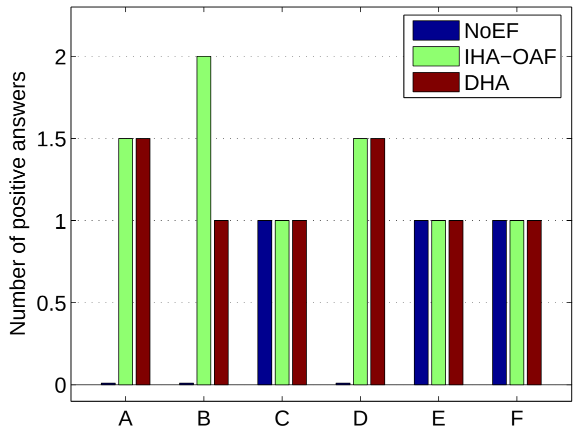

Figure 4.15: Answers to the questionnaire for the 3 participants who recognized $\geq 75\%$ of the trial forces.

Figure 4.16 shows instead the answers of the 6 participants able to recognize only the 60% of the trial forces.

It seems that the haptic cues in general (both DHA and IHA-OAF) were retained to be the stronger forces (Questions A) and the forces which produced the most efforts (Questions D) with respect to the NoEF. But DHA and IHA-OAF were also considered as the most helpful forces (Questions B). Similarly, the NoEF condition was thought to produce no efforts, softer forces but without proving a useful haptic cue (i.e. not helping at all).

About the evaluation of their own performance in the task (Question E), about the condition which gave them the best control on the aircraft (Questions C) and about their own preference between

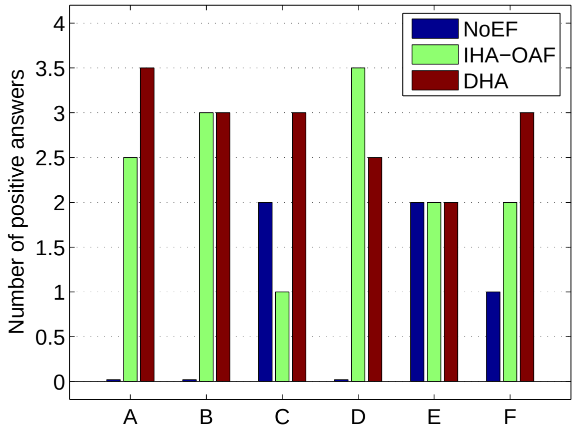

Figure 4.16: Participants answers to questionnaire for the 6 participants who recognized $\geq 60\%$ of the trial forces.

the forces (Questions F) they were more or less divided.

By concluding, it was shown that Indirect Haptic Aid could provide better help for subjects than the Direct Haptic Aid and a baseline case (NoEF case, i.e. visual feedback and only the elastic component of the force) in an obstacle avoidance task with a simulated aircraft, confirming the importance to have a haptic feedback in addition to visual feedback to improve the flight security in case of (tele-)operated systems even in pretty good visibility conditions.

From the answers to the questionnaire, it seems that the degree of helpfulness of the haptic cues (both DHA and IHA-OAF) has to be paid through strongest forces feelings and the addiction of some effort. This seems to be a good compromise to get the best performance!

Chapter 5

The Mixed CAAF/OAF

This Chapter extends the previously described haptic aid systems by merging them into a system capable of aiding a pilot involved in an obstacle avoidance task in presence of lateral wind gusts.

The simulation environment is the same that is described in Section 4.1 with the addiction of sudden lateral wind gusts.

The remote piloted flight with the presence of environmental constrains is already a dangerous task as long as a crash of a UAV during teleoperation will not only lead to possible damage to the local environment, but could also lead to the loss of the vehicle followed by the failure of the mission.

Usually UAV missions happen in outdoor environments, thus the UAV is very often subject to adverse weather conditions. The most dangerous windy condition is represented by the sudden wind gusts that, if not appropriately and suddenly compensated, for example in a constrained mission environment (e.g., a urban canyon) could bring to a fatal collision. As a matter of fact, the buildings of an urban canyon can disturb the airflow creating strong vortices and eddies, tunnel and wake effects, which happen in the horizontal plane, (see Figure 5.1) among other things. In the narrow street "canyons" the wind speed is significantly increased at street corners where lateral streets across the main street and the *tunnel effect* takes place.

a)
b)
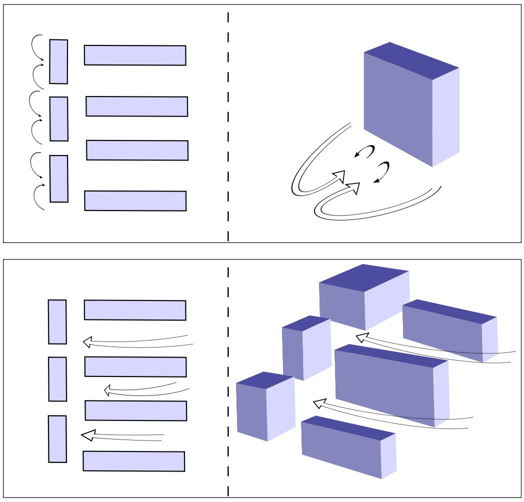

Figure 5.1: The interaction between the wind and the urban canyon: a) the wake effect, b) the tunnel effect.

Two possibilities of CAAF haptic aids implementation capable of helping to compensate for lateral wind gusts preventing the mission failure will be presented in the first part of this Chapter. It will be shown that designing a new IHA implementation appears straightforward. Designing a DHA system instead can be very complex, especially if the aircraft trajectory is not pre-defined.

After designing both the IHA and DHA to help the pilot in the lateral wind gust rejection, the same force feedback employed in the Chapter 4 will be added to the wind gust haptic aid in order to help the remote pilot in a doubled task: an obstacle avoidance task in a windy environment.

The resulting IHA-based haptic aid was named *Mixed Conventional Aircraft Artificial Feel/Obstacle Avoidance Feel* and referred as Mixed-CAAF/OAF. It will be shown to definitely improve the pilots' performance with respect to the other approaches (see later) improving the safety of the teleoperation by keeping higher the attention of the pilot in the task.

5.1 CAAF for lateral dynamics

As concerning, the IHA-based feel for lateral dynamics, is very easy to think about and design a force expression. Two examples in the next Subsections are presented: Section 5.1.2 presents the first feedback type that relies on changes of the sideslip angle (it is analogous with what seen in Section 3.3.2) and Section 5.1.3 presents a different approach based on the lateral acceleration produced by the wind gust on the aircraft dynamics.

The Section 5.1.1 explains how the lateral wind gust is simulated.

5.1.1 The Wind Gust Simulation

By hypothesis, only the wind tunnel effect of Figure 5.1 takes place during the simulation. The present Section describes how the tunnel effect is simulated.

As in Chapter 4, the aircraft dynamics was decoupled and only the lateral dynamic was considered (see Section 4.2). The only difference is represented by the addiction of the lateral wind gusts that affect the aircraft lateral dynamics.

In both IHA and DHA cases, the lateral wind gust is simulated using a triangular velocity profile for the wind disturbance: the lateral gust starts at the position $x_{OB} = x_1$ and ends at the position $x_{OB} = x_2 = x_1 + \sim 20m$ (20 meters is the width of the lateral streets) as it happens in the presence of lateral wind tunnels (see Figure 5.1) that cross the main street where the aircraft is flying. The maximum magnitude, in our experiment set to *40 knt*, of the wind gust is reached at the position $x_{OB} = (x_1 + x_2)/2$.

The above described wind gust is then fed to a second order filter which output, v_W, is summed to the lateral velocity of the aircraft in Earth Reference Frame, $\dot{y}_e$:

$$\dot{y}'_e = \dot{y}_e + v_W \tag{5.1}$$

In Equation (5.1), v_W is the filtered lateral wind gust in Earth Reference Frame, while $\dot{y}_e$ and $\dot{y}'_e$ are the lateral aircraft center of gravity velocity in Earth Reference Frame respectively before and after the lateral wind gust.

Afterwards, the roll angle ϕ, the yaw angle ψ and the aircraft center of gravity velocities in Earth Reference Frame after the wind gust, $\dot{x}_e$ and $\dot{y}'_e$, are employed to calculate the aircraft center of gravity velocities in Body Reference Frame $\dot{x}_B$ and $\dot{y}_B$ through the Equation 5.2:

$$\begin{bmatrix} \dot{x}_B \\ \dot{y}_B \end{bmatrix} = \begin{bmatrix} cos(\psi) & sin(\psi) \\ -sin(\psi)cos(\phi) & cos(\psi)cos(phi) \end{bmatrix} \begin{bmatrix} \dot{x}_e \\ \dot{y}'_e \end{bmatrix} \tag{5.2}$$

Figure 5.2 depicts what just explained.

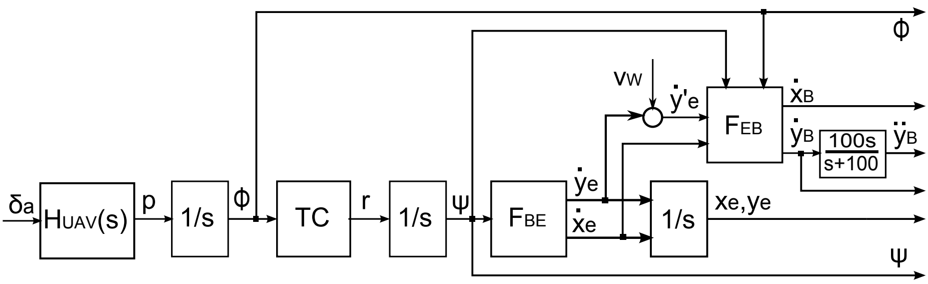

Figure 5.2: The wind gust implementation in the aircraft dynamics.

Equation (5.2) is implemented in the F_{EB} block, and the lateral velocity in Body Reference Frame output ($\dot{y}_B$) is fed through the causal filter $100s/s + 100$ to produce the lateral acceleration $\dot{y}_B$ as noiseless as possible.

5.1.2 β-CAAF

As already discussed, UAVs pilots often are manned aircrafts pilots as well, thus they expect in the presence of external disturbances such as wind gusts or turbulences, a cue which is similar to the one they would feel by piloting the aircraft on board. Again, in order to inform the remote pilot about the external disturbances, an attempt to reproduce, through the haptic feedback, a feeling which mimics the real one was made. The lateral wind gust haptic feedback would produce an immediate effect on the pedals because it affects the rudder which is mechanically commanded through the pedals and this would make the pilot to reject the gust as soon as possible avoiding the consequent changing in the yaw angle which, if not adequately addressed, could bring to dangerous collisions with the environmental constrains.

As in Chapter 4, the rudder deflection δ_r and α (see Section A.1) are supposed to be fixed in the respective trim condition values thus, the only input to the lateral aircraft dynamics (the only one present in this Chapter) is represented by the ailerons which again are commanded through the lateral motion of the haptic device end-effector. This seems to be a reasonable hypothesis as long as an aileron deflection produces first a roll rate and afterwards a yaw rate and vice versa, the lateral wind gust produces a yaw rate and a roll rate as well. Finally, the hypothesis of only the ailerons as lateral input is justified by the lateral coupling between the rolling and the yawing moments, both created by both an aileron and a rudder deflection.

The lateral wind gust affects above all the sideslip angle β. Due to the previous considerations and given the analogy with the longitudinal dynamics, the force felt on the stick associated to the wind gust in this case is approximately proportional to both the dynamic pressure, q, and to the change of the sideslip angle, β, with respect to its value in trim conditions (see Equation (5.3)) by analogy with the simplified longitudinal force in Equation 3.3.

$$F_{WG,y} \propto q_{trim} \cdot (\beta - \beta_{trim}) \tag{5.3}$$

By following the same considerations made in Section 3.3.2, the lateral proportionality constants are chosen as the longitudinal proportionality constants were chosen by considering the constrain that a half of the total haptic feedback (heuristically set to *10 N*) has to be given by the wind gust aid and the other half by the obstacle avoidance haptic aid. The same maximum velocity as in Section 3.3.2 and a maximum value of *40 deg* for the sideslip angle were used.

Equation (5.4) shows how the sideslip angle was computed:

$$\beta = \arctan\left(\frac{\dot{y}_B}{\sqrt{\dot{x}_B^2 + \dot{z}_B^2}}\right) \tag{5.4}$$

Note that, as for the hypothesis, the motion is in the horizontal plane only, thus $\dot{z}_B = 0$.

5.1.3 Lateral Acceleration-CAAF

This alternative method to implement the IHA-based lateral wind gust rejection was born in order to more easily compare IHA and DHA since it was difficult to find the DHA correspondence of the sideslip-based haptic aid signal.

The signal chosen to be given to the pilot through the control device was the lateral acceleration in Body Reference Frame calculated as shown in Figure 5.2.

The obtained lateral acceleration in Body Reference Frame, $\ddot{y}_B$, multiplied by a heuristically chosen constant (in order to obtain a force of about *5 N*, that is the 50% of the total haptic aid) creates the feedback for the pilot to inform him/her about the presence of the lateral wind gust.

Thus, in this case:

$$F_{WG,y} \propto \ddot{y}_B \tag{5.5}$$

5.2 Lateral Acceleration-DHA

For comparison purposes, a DHA system was designed using lateral acceleration; the same lateral acceleration of Section 5.1.3, $\ddot{y}_B$, is employed in this case. The lateral acceleration is compared with the zero value and the result is fed through a compensator, in Equation (5.6), which job is to null the lateral acceleration $\ddot{y}_B$, that is to reject the lateral wind gust. The compensator gain is scaled (of about 80%) in order to get a maximum haptic feedback value of about *5 N*, as in the IHA case, and to require the need of pilot action.

$$C_{WG}(s) = \frac{F_{WG,y}(s)}{e_{acc}(s)} = \frac{102.0894s + 0.4717}{s + 0.0048} \tag{5.6}$$

where e_{acc} is the error between the current lateral acceleration and the zero value. See Appendix C for details about the compensator of Equation (5.6) design.

5.3 Obstacle Avoidance Force Field

The obstacle avoidance force field for both IHA and DHA simulators is the same as in the Section 4.3.2 with the only difference that here the magnitude is scaled to get an amount of about *5 N*.

5.4 Haptic cueing for lateral dynamics

Since, as hypothesis, the only dynamics to control is the lateral one, the haptic aid for the obstacle avoidance in windy condition task was applied only to the lateral axes of the control device that is the

y axes in Figure 3.2, which is thus, the only direction of the force transmitted to the operator.

The total haptic aid $F_{S,y}$ needed to run the experiments concerning the obstacle avoidance in windy conditions is shown in Equation 5.7.

$$\begin{cases} F_{S,y} = F_{SD,y} + F_{OA,y} + F_{WG,y} \\ F_{SD,y} = F_{S,y} + F_{D,y} \end{cases} \tag{5.7}$$

where $F_{S,y}$, $F_{D,y}$ are exactly the same as in Chapter 4.

The obstacle avoidance force term, $F_{OA,y}$, depends on the experimental conditions. Three types of external force $F_{OA,y}$ were compared: DHA, IHA and a baseline force condition (see later). The value of $F_{OA,y}$ in both IHA and DHA cases is taken from the Chapter 4 but scaled in magnitude.

The wind gust rejection aid term, $F_{WG,y}$, depends from the experimental conditions as well. The IHA condition value is given in the Equation (5.5) while the DHA condition value is given in the Equation (5.6).

The conditions compared through this experiment were three: DHA (both obstacle avoidance and wind gust rejection aids from DHA case), IHA (both obstacle avoidance and wind gust rejection aids from IHA case) and a baseline force condition in which both $F_{OA,y}$ and $F_{WG,y}$ in Equation (5.7) were set to zero.

To create the Direct and Indirect haptic aids two simulators were prepared (see Section 5.5).

The Mixed-CAAF/OAF was compared to the DHA approach through the evaluation experiment of Section 5.6.

5.5 The Windy Obstacle Avoidance Simulators

In order to test the IHA-Mixed CAAF/OAF concept, three simulators were created. The first one is the NoEF Simulator, the second one is the DHA Simulator and the third one is the Mixed-CAAF/OAF Simulator.

Subsections 5.5.1, 5.5.2 and 5.5.3 describe the simulators built in order to test the performance in the obstacle avoidance task in the presence of lateral wind gusts object of this Chapter.

5.5.1 NoEF Simulator

Figure 5.3 shows the baseline scheme (i.e. no haptic aids) employed in the obstacle avoidance with wind gusts setup.

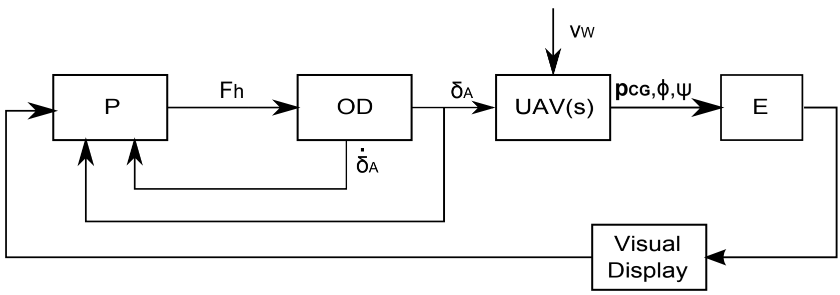

Figure 5.3: The obstacle avoidance with lateral wind gusts simulation baseline scheme.

It is possible to note that the only difference between the present Chapter simulation and the Chapter 4 simulation is represented by the adding of the lateral wind gusts in Figure 5.3 through the v_W signal that represents the gusts in y-axes of the Earth Reference Frame.

The aircraft lateral dynamics employed in this Chapter is exactly the same as in Chapter 4.2 and the same hypothesis (such as coordinated turn) are employed here as well.

This case represents just a visual aid as long as the haptic feedback is only related to the actual stick displacement and to its rate (as in a fly-by-wire like system).

In fact, in this case (see Equation 5.7) $F_{OA,y}$ and $F_{WG,y}$ are set to zero, $F_{SD,y}$ is the same as in the OAF VS DHA Experiment (see Section 4.4), while $F_{WG,y}$ is taken from the Equation 5.6.

The pilot had the same virtual scenario employed in Chapter 4 as the only cueing of the virtual buildings as seen from the aircraft center of gravity (see Figure 4.1).

Thus, when the wind gusts affects the aircraft, in the case of NoEF feedback, the gust is perceived through the visual feedback only because of the sudden variation in the aircraft attitude caused by the lateral wind gust.

The visual feedback is the same in all the conditions of the experiment.

The only haptic feedback felt by the pilot is proportional to δ_A and $\dot{\delta}_A$ produced only from the pilot input force F_h.

Figure 5.4 depicts an example aircraft trajectory during a simulation trial.

5.5.2 DHA Simulator

Figure 5.5 shows the block diagram of the simulation system used to test the DHA concept.

As concerning the visual feedback (the same as in NoEF Simulator), the pilot may perceive the distance from the obstacles through the visual display (see Figure 4.1).

While as concerning the haptic feedback, the haptic device was controlled as in Equation (5.7) to behave as a spring-damper system with two additional forces: $F_{OA,y}$ and $F_{WG,y}$. $F_{SD,y}$ and $F_{OA,y}$ are

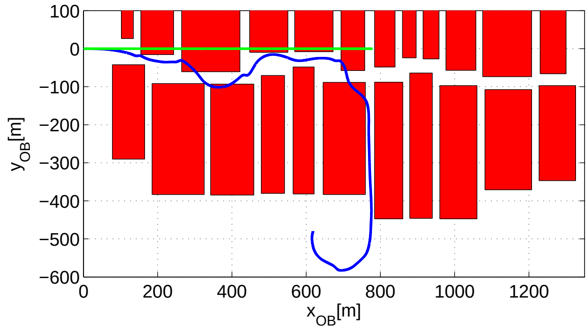

Figure 5.4: NoEF simulation example. The blue, the green and the magenta lines (the last two are superimposed and constantly null) represent respectively the aircraft trajectory, the obstacle avoidance force (F_{OA}) and the wind gust rejection force (F_{WG}).

the same as in the OAF VS OAF Experiment (see Section 4.4)

Thus, a force made up of two components is given to the pilot through the haptic device: the total force exerted by the obstacles $\mathbf{F_{OBS}}$ (the same as in Section 4.3.2) which is fed into the DHA_{AO} block to output the obstacle avoidance DHA haptic aid $F_{AO,y}$ and the wind gust rejection aiding force $F_{WG,y}$ produced by the compensator represented by the DHA_{WG} block (see Figure 5.5) as explained in Section 5.4.

This compensator was added to help the pilot in rejecting the lateral wind gust. As a matter of fact, it was designed in order to cancel the lateral acceleration $\ddot{y}_B$ produced by the lateral wind gusts.

Both the haptic cues, $F_{OA,y}$ and $F_{WG,y}$ (F_{OA} and F_{WG} in Figure), together with the pilot force input F_h, are fed through the haptic device (OD block in Figure 5.5) to produce the stick deflection δ_A. The δ_A and $\dot{\delta}_A$ feedback indicate the proprioceptive feedback.

The obstacle avoidance feel, part of the current haptic feedback, works exactly as the one of Chapter 4: again, $F_{OA} = F_{B,y}$ in the Equation (4.6).

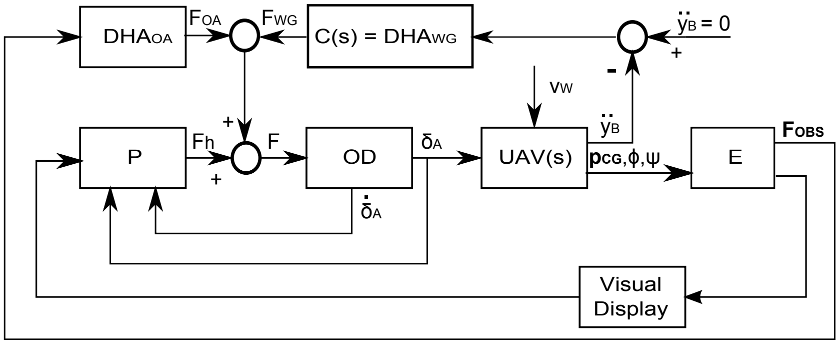

Figure 5.5: DHA-based obstacle avoidance in the presence of lateral wind gusts simulator scheme. The haptic forces F_{OA} and F_{WG} deflect the stick inducing a helpful change of the aircraft trajectory.

Suppose the aircraft is affected by a lateral wind gust, a lateral acceleration in Body Reference Frame rises, the compensator detects it and produces a force which would, at least partially, make it null. In fact, the pilot should follow and amplify it (remember that the gain of the compensator is scaled by the 80%) in order to make the lateral acceleration null, that is to fully reject the lateral wind gust.

Figure 5.6 depicts an example of the aircraft trajectory during a simulation trial.

5.5.3 IHA-Mixed CAAF/OAF Simulator

By following the same principle as in all the previously described IHA-based haptic feedbacks, the Mixed-CAAF/OAF should produce a force sensation "naturally" generated when both an obstacle is approaching (see Chapter 4) and a lateral wind gust is affecting the aircraft.

For example, if the wind gust comes from the right side of the aircraft, the lateral acceleration of the aircraft will increase towards the left and also the stick would move towards the left. Again, the

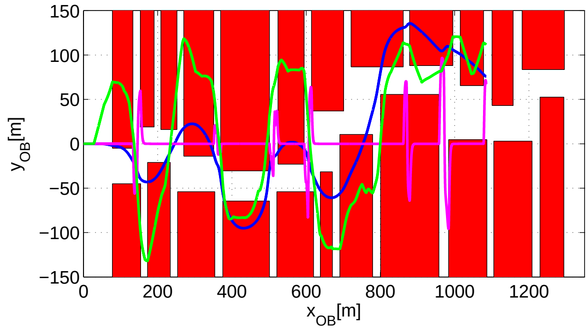

Figure 5.6: DHA simulation example. The blue, the green and the magenta lines represent respectively the aircraft trajectory, the obstacle avoidance force (F_{OA}) and the wind gust rejection force (F_{WG}).

pilot would naturally oppose this movement by rolling towards the right (stick on the right), that is in the direction needed to reduce the lateral acceleration generated by the gust.

And again, the stick moves through a shifting of the stick neutral point.

The vanishing of the haptic cue informs the pilot that no gusts are present anymore.

As concerning the visual feedback (the same as in both NoEF and DHA Simulators), the pilot may perceive the distance from the obstacles through the visual display (see Figure 4.1).

Regarding the haptic feedback, the haptic device was controlled as in Equation (5.7) to behave as a spring-damper system with two additional forces: $F_{OA,y}$ and $F_{WG,y}$ (F_{OA} and F_{WG} in Figure 5.7) as explained in Section 5.4.

Thus, a force with two components is given to the pilot through the haptic device: the total force exerted by the obstacles $\mathbf{F_{OBS}}$ (the same as in Section 4.3.2) which is fed through the HA_{AO} block to output the obstacle avoidance DHA haptic aid $F_{AO,y}$ and the wind gust rejection aiding force $F_{WG,y}$ produced by the IHA_{WG} block (see Figure 5.7). This force just transmits to the pilot the lateral acceleration produceded by the lateral wind gust.

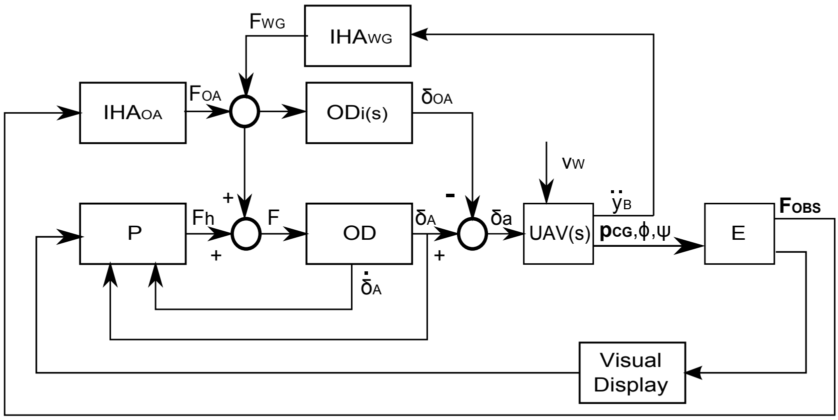

Figure 5.7: IHA-Mixed CAAF/OAF simulator scheme. The haptic forces F_{OA} and F_{WG} deflect the stick without producing any change to the aircraft trajectory thanks to the effect of the compensating signal δ_{OA}.

As concerning the wind gust rejection feel in Mixed-CAAF/OAF case, an example is given: suppose the aircraft is affected by a lateral wind gust, a lateral acceleration in Body Reference Frame arises, the pilot would naturally oppose it by rejecting the wind gust and, as a consequence, will hopefully avoid a potential collision that might occur in case the wind gust is not readily and suddenly rejected.

Thus, the pilot will feel a haptic information about both the presence of the obstacle and the presence of a lateral wind gust and he/she will see it through the visual display (when the visibility condition is good enough, i.e. no foggy weather).

Figure 5.8 depicts an example of the aircraft trajectory during a simulation trial.

In other words, the IHA-Mixed CAAF/OAF follows the general IHA concept described before: it provides to the pilot the informa-

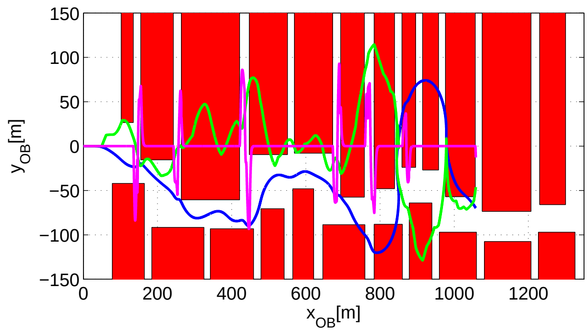

Figure 5.8: IHA-Mixed CAAF/OAF simulation example. The blue, the green and the magenta lines (the last two are superimposed and constantly null) represents respectively the aircraft trajectory, the obstacle avoidance force (F_{OA}) and the wind gust rejection force (F_{WG}).

tion about the presence of the obstacle on a side of the aircraft and about a lateral wind gust but it does not effect in any way the commands actually sent to the aircraft; this helps the pilot indirectly by improving his/her SA, that is to let him/her know that in the remote environment a collision is going to happen and/or a lateral wind gust affected the aircraft and leaving him/her the full authority to take control decisions by changing the direction of the motion of the vehicle.

The mathematical proof of the concepts described above is similar to the one presented in the Subsection 4.4.3 with the final result that F_{OA} and F_{WG} change just the neutral point of the Omega Device by δ_{OA} and the only input to the aircraft dynamics is given by the pilot command F_h (Equation 4.15).

5.6 Mixed CAAF/OAF Evaluation

In order to test the three haptic aiding systems, several experiments of obstacle avoidance in the presence of sudden lateral wind gusts were run.

The present task is even more difficult with respect to the one in Chapter 4 because not only the street is a bit tighter but also 8 lateral wind gusts (4 toward left, 4 toward right), which exact position was strategically set in each of the five employed scenarios (the same as in previous Chapter), were added.

An attempt to make the experiment as realistic as possible was made, in the sense that the gusts were added where some of the lateral smaller streets cross the main street. The lateral street which was the ideal candidate to host the lateral wind gust is a street in which the physical characteristic might bring to tight turns very close to the buildings to avoid, making the potential collision very likely to happen.

The experiments were run under two different windy conditions: i) No Wind (*NW*) and j) Wind (*W*), two different visibility conditions: a) *Minimum Fog* (same as the first fog condition in the previous Chapter) and b) *Maximum Fog* (same as the worse fog condition in the previous Chapter) and under three different force condition: DHA, IHA and NoEF. In total the condition were twelve.

Note that the worse visibility condition, shown in Figure 4.13c, is even more dangerous in windy conditions than it was in the previous Chapter.

Thus, a even stronger effect about the performance was expected (again the number of collision was chosen as metric).

The experimental task is the same as in the previous Chapter: to get the end of the street by avoiding the collisions with them although the presence of 8 lateral wind gusts. Again, to test the natural response to the different types of force no instructions were given to the participants about the force they were going to feel on the stick.

The goal of these tests is to prove whether the Mixed-CAAF/OAF kinesthetic (force) cue to the visual cue improves the control with respect to the other two conditions. In particular the goal is to assess as analytically as possible the differences in pilot performance in the three cases (NoEF, IHA and DHA). Thus, the performance of the subjects (dependent variable) was measured through the number of collisions in the flight across a constrained environment and in the presence of lateral wind gusts.

Seven naive subjects participated to the experiment. All had normal or corrected-to-normal vision. They were paid, naive as to the purpose of the study, and gave their informed consent. The experiments were approved by the Ethics Committee of the University Clinic of Tübingen, and conformed with the 1964 Declaration of Helsinki.

The experiment consisted of two different wind conditions: No Wind and Wind, two different for conditions: Minimum and Maximum Fog and three different force conditions: NoEF, DHA and IHA-Mixed CAAF/OAF.

All the trials (see Appendix D for details) have been mixed and counter-balanced and no instructions were given about the three different force conditions to test natural reaction of the subjects to the different twelve conditions.

Each fog condition was run as a separate block and counterbalanced as well.

The participants had to run 60 trials of about 2 minute each.

In total, the experiment lasted about 150 minutes (including instructions and breaks between blocks).

As concerning the instructions to the subjects: they were informed about the presence of three different force conditions. One in which only the stick was felt as a normal joystick (if they left it, it would come back to the center neutral position) named Spring Force. The other two conditions were said to produce a force which would tried to move the stick itself named A Force and B Force. They were asked to try to recognize the type of forces trying to classify it according to what they felt. After each trial they were asked what kind of force they felt.

After each of the 4 blocks (Wind plus Maximum Fog, Wind plus Minimum Fog, No Wind with Maximum Fog, No Wind with Minimum Fog) and after the whole experiment they were interviewed separately. In order to compare the results, each pilot was asked to fill in a questionnaire with 6 questions (the same questionnaire as in the previous experiments, see the Table 3.1).

5.6.1 Experimental Results

Mean number values of collisions for each of the twelve conditions were entered in a one-way repeated measures analysis of variance (ANOVA). See the results in Figure 5.9.

A main effect of the wind condition was found:

$$F(1,6) = 6.6365, p < 0.05$$

Post-hoc tests using Bonferroni correction for multiple comparisons, $p < 0.01$ confirmed that the subjects performed significantly worse in the Wind condition than in the No Wind.

A main effect of the fog condition was found:

$$F(1,6) = 19.252, p < 0.01$$

Post-hoc tests using Bonferroni correction for multiple comparisons, $p < 0.001$ confirmed that the subjects performed significantly worse in the Maximum Fog condition than in the Minimum one.

A main effect of the force condition was found as well:

$$F(2,12) = 16.928, p < 0.001$$

Post-hoc tests using Bonferroni correction for multiple comparisons, $p < 0.05$ confirmed that the subjects performed significantly better

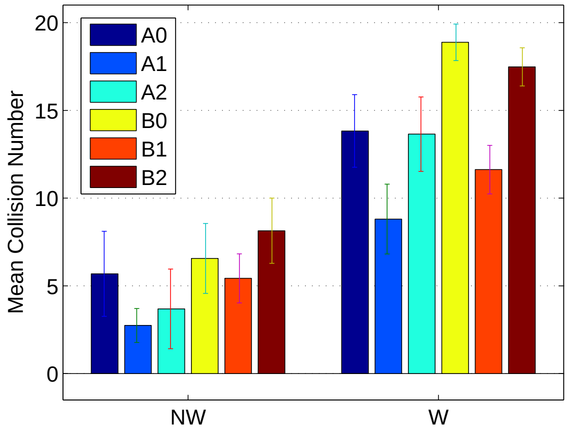

Figure 5.9: Performance (mean and standard error) for the two Wind conditions (No Wind and Wind), for the 3 Force conditions (DHA=2, IHA-Mixed CAAF/OAF=1, NoEF=0) and for the 2 visibility conditions (A, B).

when the IHA-Mixed CAAF/OAF haptic cue was provided in the haptic device than when both DHA and NoEF were provided.

No interaction was found between the two variables.

In other words, the just introduced IHA-based Mixed-CAAF/OAF was proved to provide the best results in the obstacles avoidance in windy conditions task irrespective of the fog condition and of the wind conditions. Thus, the subjects collided less times aided by the IHA-based Mixed-CAAF/OAF than both the DHA and the NoEF cases. It is possible to conclude that the employment of IHA-based Mixed-CAAF/OAF improves the performance in obstacle avoidance in all the visibility conditions with and without wind.

Once again, the same observations as in Section 4.5.1 can be made here about the surprising results and the possible explanations.

In particular, Figure 5.4 clearly shows what does getting lost after a collision mean and how in NoEF case was not easy to find again the main street once collided which was instead easier with both DHA and IHA cases.

After each trial the subjects were asked what kind of force they felt to check if they could recognize the type of forces trying to classify them.

Most of them were very able to distinguish between the Spring Force condition and the force feedback conditions (both A Force and B Force). It was, in general, more difficult to classify and distinguish the A and the B Forces.

Some of them correctly noticed and reported the difference between A and B in terms of cue direction with respect to the obstacles (force pushing away from or towards the obstacles).

Other subjects were only able to identify the difference in strength (actually not present because the amplitude of the force in the two force conditions was exactly the same for the same distance between the aircraft and the obstacles). Someone's classification was really poor (till the end of the 60 trials they still were not able to classify and recognize the force conditions).

Only 4 subjects over 7 were able to recognize more than the 60% of the trial forces. Only 2 of them were able to recognize more than about 70% of the same.

After the 60 trials, pilots were interviewed separately. In order to compare the results, each pilot was asked to fill in a questionnaire (the same as in the previous experiments in Table 3.1).

The answers to the questionnaire of the 2 only subjects who recognized more than about the 70% of the forces step by step during the 60 trials, are for sure more meaningful than the others (see Figure 5.10).

Figure 5.11 shows instead the answers of the 4 subjects able to recognize only the 60% of the trial forces.

It seems that the IHA-Mixed CAAF/OAF in general was retained to be the strongest force (Questions A) and the forces which

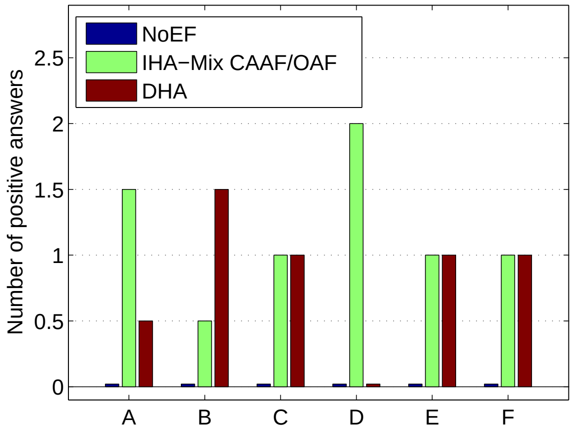

Figure 5.10: Answers to questionnaire for the 2 participants who recognized $\geq 70\%$ of the trial forces.

produced the most efforts (Questions D) with respect to both the DHA and the NoEF conditions. The DHA was considered as the most helpful force (Questions B). As concerning the NoEF condition, it was thought to produce no efforts, weaker forces but without proving a useful haptic cue (i.e. not helping at all).

About the evaluation of their own performance in the task (Question E), about the condition which gave them the best control on the aircraft (Questions C) and about their own preference between the forces (Questions F) they were more or less divided between IHA and DHA forces.

What just mentioned are the general results, e.i. the results coming from the final questionnaire regarding all the wind and fog conditions. They are more or less representative of the results which come from the questionnaire after each of the four blocks (No Wind-Minimum Fog, No Wind-Maximum Fog, Wind-Minimum Fog, Wind-Maximum Fog), but an exception has to be reported: when the

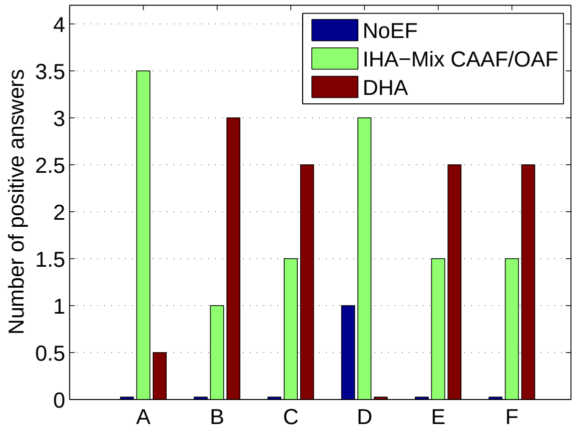

Figure 5.11: Answers to questionnaire for the 4 participants who recognized $\geq 60\%$ of the trial forces.

experimental condition got worse (No Wind-Maximum Fog, Wind-Minimum Fog, Wind-Maximum Fog), the NoEF condition was the conditions the most subjects preferred; in fact, they classified it as most helpful, they felt to have the best control on the aircraft and they thought they obtained with it the best results. This is due maybe to the fact that the worse are the visibility and the windy conditions, the less the participants trusted in the haptic cues (both DHA and IHA) maybe because not enough trained on it.

By concluding, the aim of the obstacle avoidance in windy conditions haptic cues evaluation experiment was to test whether the employment of a newly developed IHA-Mixed CAAF/OAF (Obstacle Avoidance Feel) would produce some improvement with respect to other approaches present in literature. It was shown that Indirect Haptic Aid could provide better help for subjects than the Direct Haptic Aid and a baseline case (NoEF case, i.e. visual feedback and only the elastic and damping components of the force) in an obstacle avoidance task in windy conditions with a simulated aircraft, confirming the importance to have a haptic feedback in addition to visual feedback to improve the flight safety in case of (tele-)operated systems even in pretty good visibility conditions.

It seems, finally, that the degree of helpfulness of the haptic cue IHA-Mixed CAAF/OAF has to be paid through strongest forces feelings and the addiction of some effort. This seems to be a good compromise to get the best performance!

Chapter 6

Delayed Bilateral Teleoperation

A teleoperation system in presence of force feedback is often referred to as a bilateral system. In such systems, the human operator controls a remotely located teleoperator.

In the particular case of UAV bilateral teleoperation, the remote pilot is responsible for the UAV at all times, it is crucial that he/she at all times can understand the state of the airborne UAV.

The introduction of a haptic feedback in the UAV's CGS, seems to improve the SA of the remote pilot. The improvement of the SA could also bring an improvement of the teleoperator performance.

The introduction of a haptic feedback also introduces an additional control loop which acts directly on the pilot control device. The further addition of communication time delays could easily bring the system to instability.

Furthermore, the time delay in the communication channel could also degrade the SA of the remote pilot.

All these troubles could have an affect on system performance and overall safety.

A lot of remedies exist in literature to solve the instability problems in a delayed bilateral teleoperation system (see Section 2.4).

A widely employed method to overcome such instability problems is the scattering theory through the wave variables approach [29, 30, 31]. Such implementation does not seem to be suitable in the present work implementation (see Section 6.3).

A less employed method is represented by the admittance control [43, 14]. This method was shown to improve the stability characteristics of the delayed bilateral teleoperation system at the cost of transparency [43]. Usually a good transparency/virtual presence is needed when the real/virtual environment is asked to be scanned in details (e.g. exploration, manipulation of objects, etc). In the present work, a good transparency property it is not really requested; on the contrary the stick dynamics has to be felt by the pilots to obtain good performance as the author shown (see Chapter 3) and published [2].

This reason brought to the implementation of the admittance controller in the delayed teleoperation system object of this Chapter.

The admittance controller needs a force sensor in the implementation. This problem was overcome with the design of an observer for the human force. It is shown to work pretty good in simulation. The implementation of the admittance controller plus the observer of the human force improves the stability properties of the system under consideration.

The only type of force feedback employed in this Chapter is the DHA-based one (see Chapter 4).

6.1 System Setup

This Chapter presents a bilateral teleoperation system in which a human operator, a pilot, controls a remotely located UAV, the slave, via a man-machine interface, the master device, while receiving haptic feedback of the interaction between the UAV and the remote environment, see Figure 6.1.

Figure 6.1: The teleoperation system (picture from http://www.flickr.com). The red arrow represents the force feedback on the control device.

In details:

Master: the master device was chosen in order to simulate a control stick through the use of a high precision force feedback device (omega.3, Force Dimension, Switzerland) (see Section A.2 for details).

Slave: the slave system is constituted by the dynamics of the aircraft under control; in order to maximize the pilot attention on its task, only the lateral aircraft dynamics was considered: thus the slave input is the aileron deflection and its output is the lateral position.

Environment: a virtual environment was displayed during the experiments to produce the visual cues; a subjective view from the aircraft cockpit was simulated using a realistic virtual environment created using the DynaWORLDS software package [42]. The environment is the same as in Chapters 4 and 5 (see Section A.3 for details). Figure 4.1 depicts the employed setup.

All the just mentioned component of the setup are described in details in section 6.2.

The control task is the same as in Chapter 4 (narrow street scenario) with the addiction of time delays in the communication link. In the design phase, for the purpose of a more straightforward understanding of the system behavior in presence of time delay a simple scenario with two long obstacles was prepared representing a straight narrow street, namely a corridor. The aircraft had to be flown in this corridor getting to the end of the street by avoiding the collisions with the virtual buildings. A repulsive force field is associated to the obstacles and it is sent back to the operator through the communication link.

As anticipated, only the DHA approach was tested in the teleoperation environment. Since the DHA approach must produce stick motions that induce beneficial trajectory variations of the aircraft, the DHA system was designed as it would be done with a compensator: a control system that regulates the distance from the obstacles, or equivalently, brings the aircraft to the minimum of the repulsive force field. The total compensator effect was assumed to substitute both human pilot and haptic augmentation system. In order to design it and evaluate its performance, simulations with the pilot out of the loop were performed first (only the DHA compensator was moving the stick) with the simplified simple corridor scenario, then the system was tested with pilots and with the narrow street scenario of Chapter 4.

As concerning the baseline bilateral scheme implemented in this Chapter, the scheme of Figure 4.8 was thus modified by employing a compensator in place of the human pilot and by implementing a local controller in the slave side. Section 6.2 explains in details the just mentioned scheme.

6.2 F-P scheme

For the purposes of this work a two-channel architecture [37] was employed and two physical signals were exchanged between master and slave: a position command (stick position that encodes the yaw rate command) is sent from the master side to the slave side and a force signal is sent from the slave side to the master side. This scheme is known as Force-Position architecture [37].

The teleoperation scheme considered in this Chapter is schematically illustrated in Figure 6.2.

The classical teleoperation schemes employ a local controller both the master and the slave side. In analogy to this, a yaw rate command is used as input for the slave side and a local controller was employed to regulate the actual aircraft yaw rate signal to the desired one (see below).

As concerning the master side, since the haptic device used for the experiments (the Omega Device) does not possess a force sensor, an open-loop force control was adopted in the master side and a local controller $C_s(s)$ was instead employed in the slave side.

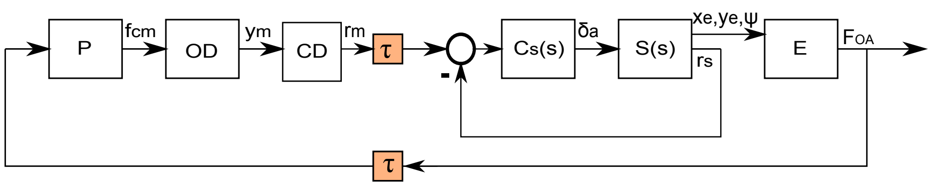

Figure 6.2: The baseline Force-Position scheme.

In Figure 6.2, OD is the Omega Device (the master haptic device); $S(s)$ and $C_s(s)$ are the aircraft dynamics and its local controller. The P block represents the real pilot who produce the force f_{cm} to directly act on the Omega Device producing the displacement, y_m, of the end-effector. This displacement is then converted (through the car-driving metaphor [46] (see later), CD block) to a heading rate command used as a reference command, r_m, for the aircraft heading rate, r_s. In order to simulate the system with the real pilot out of the loop a compensator $C(s)$ was designed. In Figure 6.2, the compensator *C(s)* would take the place of the pilot P. This architecture was chosen with the possibility in mind of future splitting the compensator action in two components as will be detailed and better described later (Section 6.2.6). The local controller $C_s(s)$ was designed for the slave side in order to regulate r_s to r_m. The aircraft position (x_e,y_e) and its heading (ψ) are used by the environment block, E, to calculate the force F_{OA}, based on the relative distance between the aircraft and the obstacles, to generate the haptic force for the master side. τ is the time delay when present. The compensator *C(s)* was designed by making use of the identified model of the Omega Device (Equation B.2 in Subsection B) to take the feedback force F_{OA} as input and to produce the force input for the Haptic Interface, f_{cm}.

This will be considered as the baseline scheme of this Chapter.

The slave dynamics together with its input and output will be explained in the next section.

The compensator of Equation (6.1) was designed in the linear domain using the Evans' Root Locus tool, in order to have a reasonable response time (about $4s$), a well damped behavior (damping factor of about 0.5) and a limited force for the Omega Device (about $4N$).

$$C(s) = \frac{2.799s + 0.8748}{s + 10} \tag{6.1}$$

The compensator $C(s)$ produces a force on the stick that acts as the sum of the human operator force and the haptic aiding itself.

Figure 6.3 shows the root locus used for the design. In blue you can see the open loop poles, in red the compensator roots, in magenta the closed loop poles.

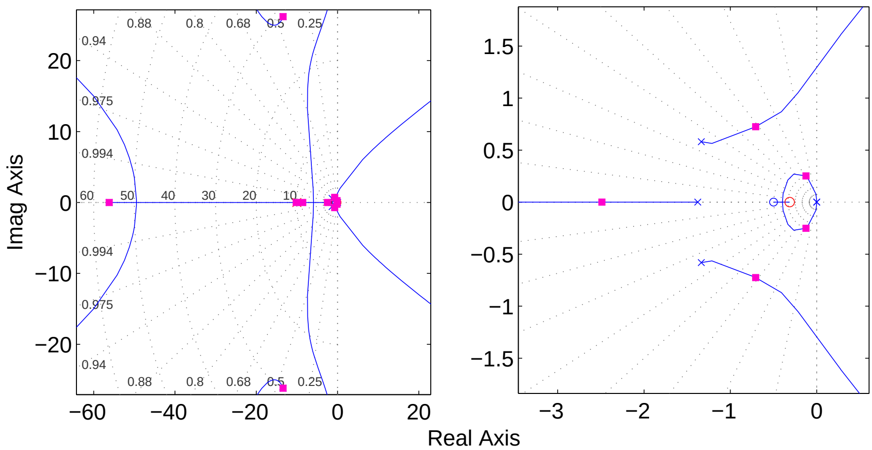

Figure 6.3: The system root locus to design the compensator $C(s)$. On the right side is shown a zoom around origin.

6.2.1 The Car-Driving Metaphor

A car-driving metaphor [46, 55, 57] for direct control of the UAV was employed. According to it the operator uses the end-effector of the haptic device to designate the desired speed and rate of turn. A logical point (x, y) (obtained by projecting the 3D haptic end-effector location to a xy-plane) is mapped to motion parameters such as speed and turning rate as in Figure 6.4.

A constant longitudinal velocity was chosen for the UAV (see Section 4.2), then only the lateral motion of the end-effector was considered and was converted into a heading rate command (in rad) used as a reference command, r_m, for the aircraft heading rate, r_s. Equation 6.2 shows the equation implemented inside the CD block of Figure 6.2.

$$r_m = CD(y_m) = 4.380 \cdot y_m \tag{6.2}$$

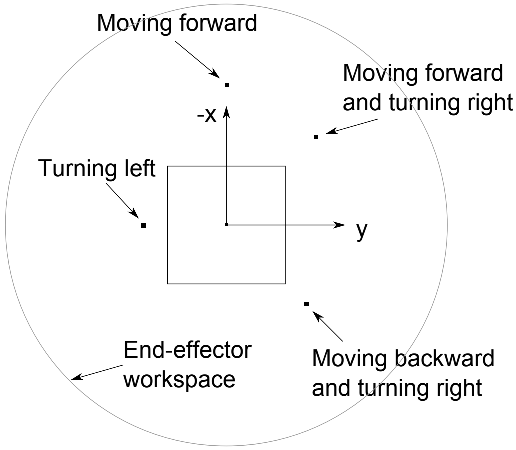

Figure 6.4: Car-driving metaphor: mapping a logical point (x, y) to motion parameters (speed rate, turning rate).

6.2.2 The slave dynamics

The input of the aircraft system $S(s)$ is the aileron deflection, δ_a, (that is the output of the $C_s(s)$ controller (see Figure 6.2) and the outputs are yaw rate (r_s), position (x_e and y_e) and heading (ψ) of the aircraft. The block $S(s)$ of Figure 6.2 is shown in details in Figure 6.5.

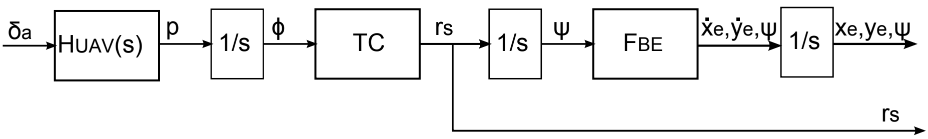

Figure 6.5: The aircraft lateral dynamics.

In Figure 6.5 the transfer function $H_{UAV}(s)$ (6.3) (from aileron, δ_a, to roll rate, p or $\dot{\phi}$) was employed. It is obtained from linearization and dominant poles approximation of the non linear Beaver DHC-2 of the *Flight Dynamics and Control Toolbox* [45]. The roll angle, ϕ, is obtained through integration.

$$H_{UAV}(s) = \frac{-3.7972}{s^2 + 6.9828s + 0.4297} \tag{6.3}$$

As in Chapters 4 and 5, the assumption of the aircraft performing coordinated turns [47] was made (see Equation 6.4) (TC block in Figure 6.5) (zero velocity in the lateral body axes) at constant speed (V), the heading rate r_s or $\dot{\psi}$ is calculated through the equation (6.4):

$$r_s = tan(\phi)\frac{g}{V} \tag{6.4}$$

The rest (i.e. calculation of the heading angle, ψ, and of the aircraft center of gravity coordinates in Earth Reference Frame) is the same as in Section 4.2.

As seen in Figure 6.2, the roll rate r_s is used to calculate the error for the slave controller, while position and its heading are used by the environment block, E, to calculate the force F_{OA}, based on the relative distance between the aircraft and the obstacles, to send back to the master side (see section 6.2.4).

6.2.3 The slave controller

The slave controller (6.5) was designed in the linear domain using the Evans' Root Locus tool. The controller was designed in order to have a reasonable response time (1.2sec), a well damped behavior (damping factor of about 0.9) and a limited motion for the aileron surfaces (less than 50% of maximum aileron dfelection).

$$C_s(s) = \frac{-7,2672s - 3,6336}{0,17s + 1} \tag{6.5}$$

Figure 6.6 shows the Root Locus plot used for the design. In blue you can see the open loop poles, in red the compensator roots and in magenta the closed loop poles.

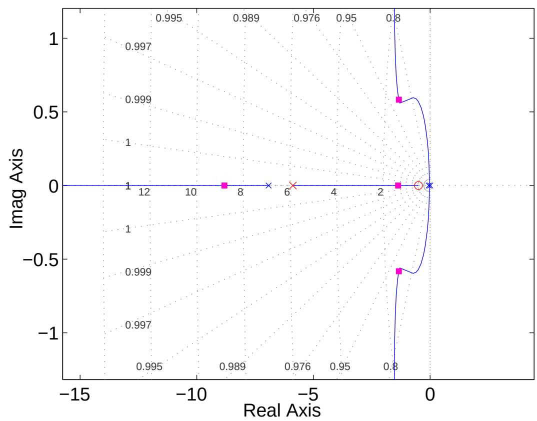

Figure 6.6: The slave root locus used to design the compensator $C_s(s)$.

6.2.4 The haptic feedback

As in Chapters 4 and 5, the only aircraft dynamics to be controlled is the lateral one and the haptic aid for the obstacle avoidance task will be only in the lateral axes of the stick (actually the Omega Device), that is the y axes in Figure 3.2.

A system where the haptic interface appears as a stick with constant damping and stiffness with the addition of an external force which appears when needed (namely when near obstacles) was designed. Then, the force $F_{S,y}$ felt by the operator during the obstacle avoidance task is the same as in Equation 4.6.

The force field around the obstacles (again in the fixed Earth Reference Frame) is the same as in Equation 4.7 of Section 4.3.2.

As concerning the force field generated by a single obstacle a small difference is now introduced: in order to simplify the force field in which the aircraft flies, a different versor than the one used in Equation 4.8 was chosen.

In fact, the unity vector $\frac{\mathbf{p_{OB}}-\mathbf{p_{CG}}}{||\mathbf{p_{OB}}-\mathbf{p_{CG}}||}$ is now employed. The meaning of the symbols is the same as in Section 4.3.2. The force field is aligned with the vector distance between the aircraft center of gravity and the obstacle; thus, the force field is always perpendicular to the obstacles' walls (in the obstacles' vertices it is radial but here it is not relevant as long as the simulations take place along the obstacles' sides as in the corridor scenario) (see later).

Figure 6.7 shows an example of the force field produced by the obstacles. The value and direction of the force field at the current position of the aircraft are used in the simulator to generate the haptic sensation.

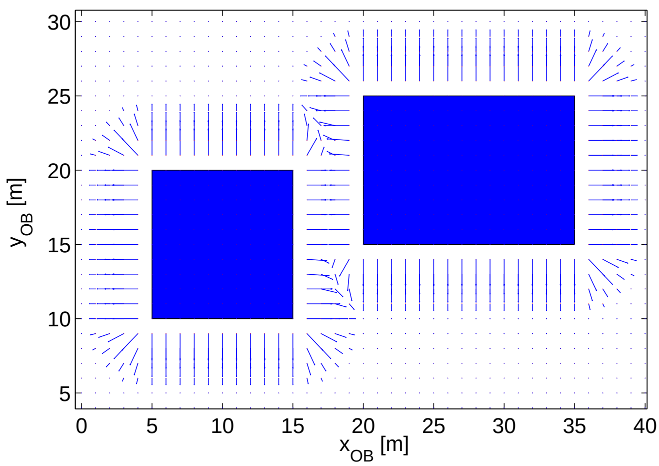

Figure 6.7: Example of the obstacle repulsive force field.

As in Section 4.3.2, the total force exerted by the obstacles (Equation 4.7) is expressed in the fixed Earth Reference Frame and a change in the aircraft Body Reference Frame is necessary (see Equation 4.9).

The distance between the obstacles was set to $2r_e$ (see Section 4.3.2), then the force field has a V shape with null force in the middle of the corridor and the maximum force (about $8N$) at the obstacles sides. It is possible to observe that the haptic force F_{OA} is proportional to the distance of the aircraft from the middle of the corridor. Assuming that the reference frame where the position of the aircraft is defined has its $\mathbf{x_B}$ axis aligned with the corridor and its origin in the middle of the corridor, the force field can be hypothesized:

$$F_{OA} \cong k_f \cdot y_{OA} \tag{6.6}$$

and y_{OA} assumes zero value, thus producing zero force, in the middle of the corridor. The corridor generated force field is depicted in Figure 6.8 in which also the contour lines are shown.

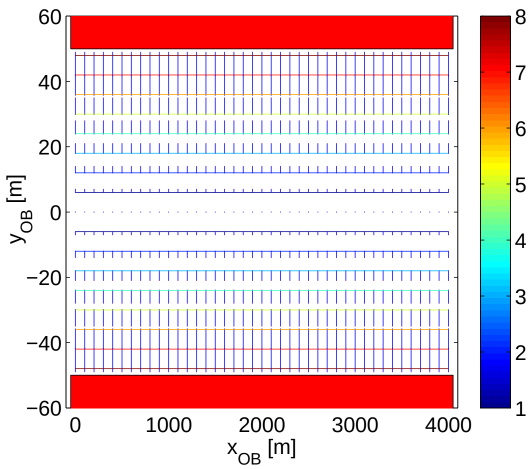

Figure 6.8: Corridor repulsive force field with contour lines.

6.2.5 Omega Device dynamic model

Haptic devices are usually modeled as a simple mass (M), thus their transfer function is usually:

$$\frac{1}{Ms^2}$$

As anticipated above, a system where the haptic interface appears as a stick with constant damping and stiffness with the addition of an external force was designed. Thus, the stick transfer function would be:

$$\frac{1}{Ms^2 + Bs + K}$$

Due to its non-idealities (friction, actuator dynamics etc.) the Omega Device actual behavior, with the added stiffness and damping, had to be identified (see Section B for details).

The transfer function $OD_y(s)$ obtained is shown in equation (B.2)

6.2.6 Compensator Splitting and Pilot Simulation

As anticipated (Section 6.1), the compensator, which replaces the human behavior, was designed with the feedback force F_{OA} as input as depicted in Figure 6.2. As long as Equation (6.6) is valid, the force F_{OA} and the aircraft distance from the corridor center line y_{OA} are linearly related. Thus the compensator, which has a pole and a zero, similarly to a proper Proportional Derivative Controller, produces, roughly speaking, a control action that is proportional to distance form the center line and to its derivative. The human operator, for any regulation task of this kind, shows a proportional-derivative behavior in the sense that his/her command is proportional to the error (the distance from the center of the street) and to the derivative of the error (the center-line approach speed) as a kind of prediction of future error.

This allows to split the compensator into two actions: the haptic aid and the pilot action. Figure 6.9 depicts this concept.

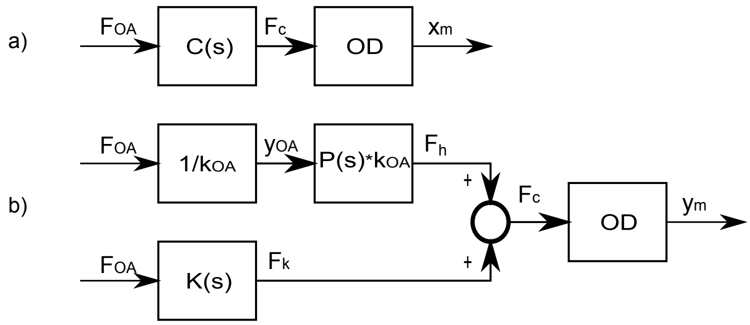

Figure 6.9: Compensator splitting.

The force F_h can be thought as the output of a pilot ($P(s)$ in Figure 6.9) that is summed up with the force F_k that gets out from the latter part of the compensator ($K(s)$). Given the linear relationship between F_{OA} and y_{OA}, the pilot's input becomes the distance from the center-line (y_{OA}) as he/she would receive from a visual feedback. Thus the pilot transfer function $P(s)$, which was designed to regulate the force F_{OA} to zero, has the same effect of regulating the distance from the center-line to zero. Thus the upper part of the Figure 6.9b can be thought as visual feedback, while the bottom part of Figure 6.9b can be thought as haptic feedback.

As you can see in the Figure 6.9, $P(s)$ and $K(s)$ are designed in respect of Equation (6.7).

$$C(s) = P(s) + K(s) \tag{6.7}$$

In order to define the values of the two components in Equation (6.7) of the compensator, the possibility of providing a static haptic aiding system ($K(s) = const$) was evaluated first, thus starting from the results of a typical simulation of the system (see later the Figure 6.14a) it was realized that the spatial period of the first oscillation

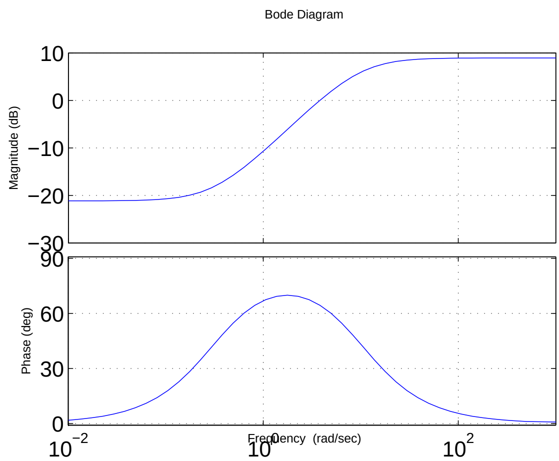

Figure 6.10: Bode plot of the compensator $C(s)$.

(the most significant) is about *500 m*. As long as the velocity is constant (about *50 m/s*), the corresponding time period is *10 s*. Then, the frequency is *0.1 Hz* which corresponds to *0.63 rad/s*. The compensator gain at this frequency is (see Figure 6.10) about *-14 dB* that corresponds to *0.2*. Thus our first choice was of $K(s) = 0.2$. $P(s)$ was easily found from Equation (6.7). A simulation of the scheme resulting from the splitting shows (see Figure 6.11) that there is a big difference between F_h and F_k and, in particular this means that, in the first instants of the simulation, the haptic component (F_k) is not that relevant.

Then, different choices for $K(s)$ were evaluated; Figure 6.12 shows the comparison between F_h and F_k for 3 different values of $K(s)$ (i.e. 0.1, 0.5, 0.9). $P(s)$ is still calculated according to the Equation (6.7).

As you can see in Figure 6.12, F_h and F_k are opposite in sign for the most part of the simulation time, then it would not be good for the pilot to have the haptic force always in opposition. Accord-

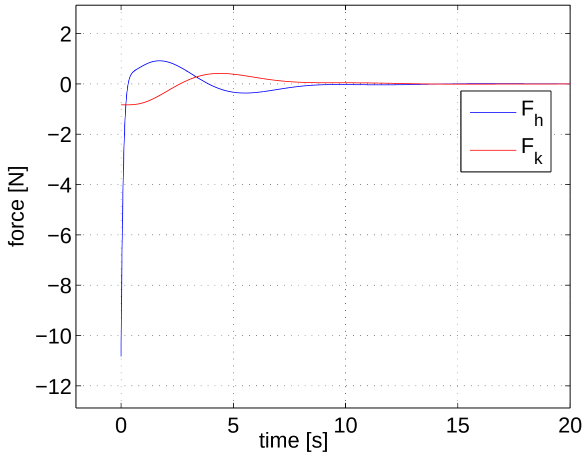

Figure 6.11: F_h and F_k time response when $K(s) = 0.2$.

ing to this, maybe a relevant anticipatory effect or phase lead (as the derivative effect of standard industrial controllers) was needed also in $K(s)$; otherwise the pilot would have to produce the whole anticipatory effect by him/herself. Then the choice of $K(s)$ as a percentage of $C(s)$ (see Equation 6.8) was made.

$$\begin{cases} K(s) = \gamma \cdot C(s) \\ P(s) = (1-\gamma) \cdot C(s) \end{cases} \tag{6.8}$$

$\gamma = 0.5$ was chosen as to divide the feedback exactly in two halves: a half the visual one, a half the haptic one. Figure 6.13 shows the new values for F_h and F_k.

The final transfer functions chosen for $K(s)$ and $P(s)$ are shown in Equation (6.9).

$$K(s) = P(s) = \frac{1.4s + 0.4374}{s + 10} \tag{6.9}$$

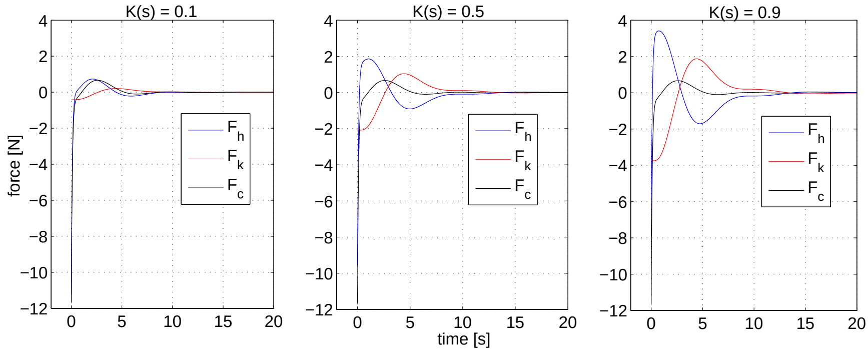

Figure 6.12: F_h and F_k time response when $K(s) = 0.1, 0.5, 0.9$ respectively.

6.2.7 F-P scheme: simulations

The capability of the designed haptic aiding force with respect to keeping the straight flight in the mentioned symmetric scenario (the long straight corridor between two buildings) was first tested. A simulation was run with the pilot out of the loop (i.e. the Omega Device end-effector moves by itself flying the aircraft into the corridor).

To initially perturb the state of the aircraft a non zero initial condition $y_e = 5m$) was set for the system.

Figure 6.14a shows a sample simulation of scheme 6.2 obtained using the identified transfer function of the Omega Device instead of the real device; the system shows a very fast and satisfactory response in the absence of delay, and the *200 ms Delay* curve shows that the presence of the delay induces larger oscillations that anticipate instability with larger delays.

The same simulation was performed using the real Omega Device (without Pilot because his/her action was substituted completely by $P(s)$). Figure 6.14b shows an evident limit cycle that is due to the non linearities that are present in the real Omega Device and that are not captured by its linear identified model. According to our

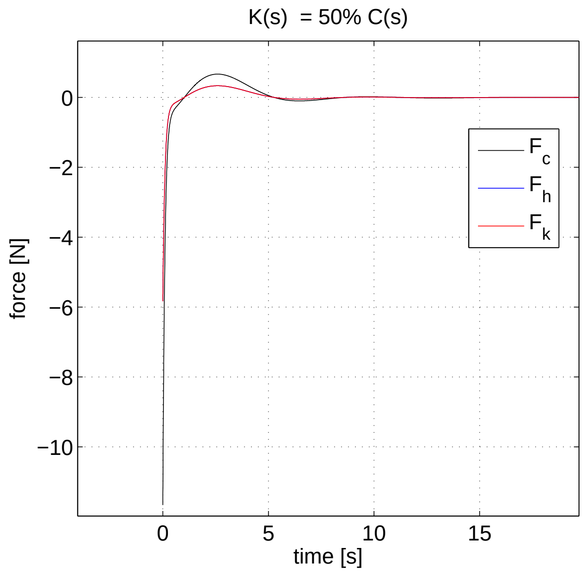

Figure 6.13: F_h and F_k time response when $K(s) = 50\% C(s)$.

experience the limit cycle vanishes when the pilot holds the stick very likely because his/her arm provides additional inertia and damping. As a matter of fact, let us to consider the same simulations run with the real Omega Device but with the human operator in the loop. Figure 6.15a represents a simulation with and without time delay in which $F_{OA} = 0$ with the operator in the loop. These simulations show that the pilot does not produce a good trajectory (he comes too close to the obstacles) without the haptic aiding.

Conversely Figure 6.15b represents a simulation with and without time delay with $F_{OA} \neq 0$ with the operator in the loop (in this case the output F_h of the block $P(s)$ in the scheme 6.9b is disconnected).

By comparing the Figure 6.15a with the Figure 6.15b, it is possible to note how important is for the human operator the presence of the haptic feedback F_k which helps him to stay in the middle of the corridor. Clearly the presence of delay makes the task harder and

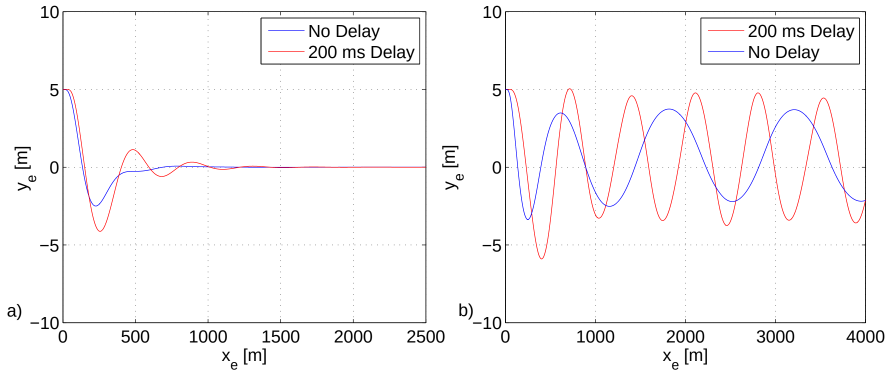

Figure 6.14: Path comparison (Figure 6.2 scheme) with and without time delay by using: a) the Omega Device model; b) the real Omega Device and the pilot out of the loop.

produces more oscillations around the condition where the haptic force is zero (the middle of the street).

6.3 The Wave Variables Approach

Often stability problems induced by delays are tackled in teleoperation systems using wave variables.

The typical Force-Position scheme with wave variables is shown in Figure 6.16.

The wave variables are calculated starting from the power variables, velocity and force, through the equations depicted in the blocks "wave transformation master/slave" of Figure [29] were τ is the communication delay; the subscripts "h", "e", "m" and "s" represent respectively the human operator, the environment, the master and the slave variables. The wave variables technique is based on the concept of energy and on the concept of passivity. Intuitively, a system is passive if it absorbs more energy than it produces. In fact, the

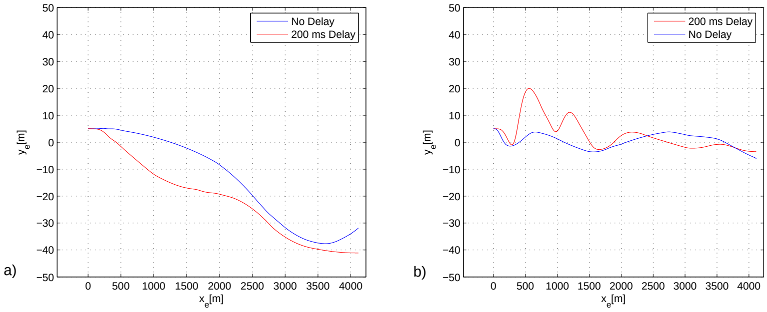

Figure 6.15: Path comparison (Figure 6.2) with and without time delay and the human operator in the loop. a) $F_{OA} = 0$; b) $F_{OA} \neq 0$.

power in the communication link is defined through the difference between the power input (velocity and force from the master/slave side) and the power output (velocity and force from the slave side). If a system is passive than it is stable. The delays in the communication link may destroy the stability of the system by producing energy; in fact, the communication delays shift the signals and the product between the just mentioned power variables may change may bring to the production of energy in the communication link. The wave variable were shown to produce always a positive energy (the input energy is bigger than the output energy); thus, passivity and stability are theoretically ensured. For details on this technique refer to [29, 30, 31].

In this work, a preliminary evaluation of the effect of the wave variables transformation was performed.

Figure 6.17a shows a simulation with and without time delay with the operator out of the loop and the real Omega Device.

Figure 6.17b shows the path comparison with and without time delay of the scheme obtained by employing the Omega Device transfer function (i.e. a simulated haptic device) instead of the real Omega Device.

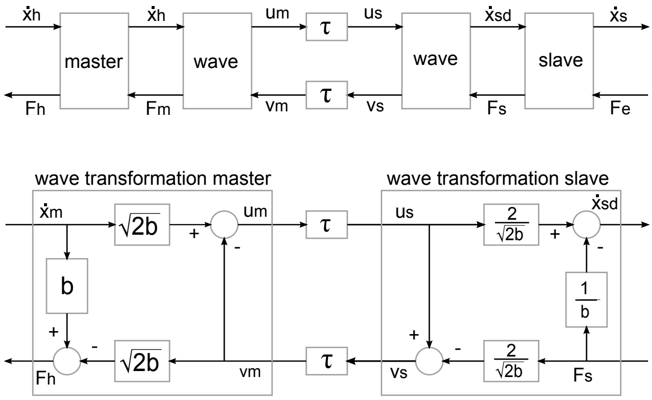

Figure 6.16: The typical wave variable scheme [29].

It is pretty evident that the addition of wave variables do not add a significant improvement in the present implementation, then, a different scheme should be employed to mitigate the effect of the delay over the aircraft trajectory.

6.4 Fa-P scheme

In order to mitigate the effect of the delay over the aircraft trajectory that were pointed in the previous section, an admittance-based teleoperation scheme was setup. The compensator splitting described in Section 6.2.6 was employed. Figure 6.18 shows the employed Fa-P admittance scheme. It was designed with the help of Ref. [43].

The force F_h can be thought as the pilot force that is summed up with f_{mc} (the local master compensator, $C_m(s)$, output) and with F_k. The pilot transfer function $P(s)$ acts in a way that makes the force F_{OA} to be zero (i.e. in the middle of the street where $y_{OA} = 0$). The force F_c can be fed through an admittance block, $Adm(s)$, to produce a reference signal for the master side, $y_{m,des}$, to help the human operator in the obstacle avoidance task. Clearly, the F_h

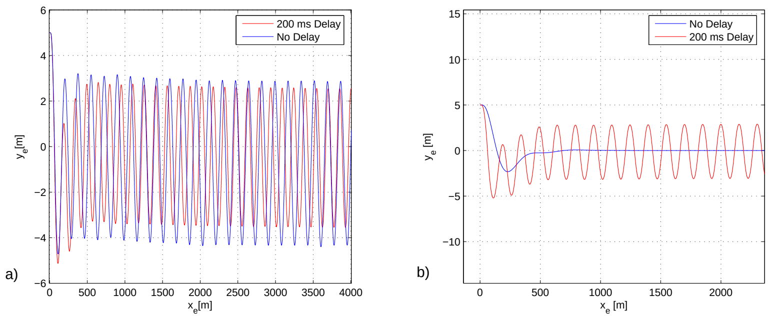

Figure 6.17: The wave variable simulation without time delay by using: the real Omega Device and the operator out of the loop (a); the Omega Device transfer function (b).

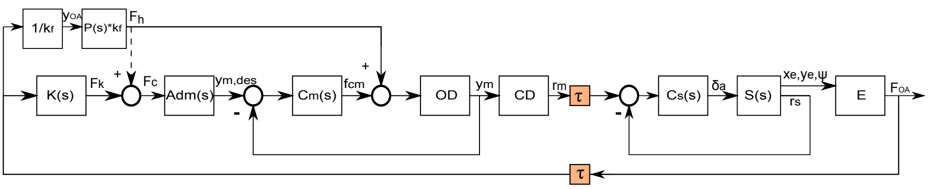

Figure 6.18: The admittance scheme Fa-P.

signal can be feed-forwarded through the admittance block only in simulation (i.e. using the Pilot model $P(s)$, and with real device only if a force sensor is available on the stick).

6.4.1 Admittance and local master controller

Equation (6.10) shows the admittance transfer function employed in the $Adm(s)$ block in Figure 6.18.

$$y_{m,des}(s) = \frac{F_k(s)}{M_d s^2 + B_d s + K_d} = \frac{F_k(s)}{0.1s^2 + 1s + 200} \tag{6.10}$$

In the Equation (6.10) the values of the desired mass M_d, desired damping B_d and desired stiffness K_d are chosen in order to obtain good stability properties of the system with the operator out of the loop. The bigger they are, the more prone to instability is the system.

Equation (6.11) shows the local master controller transfer function which was employed.

$$C_m(s) = \frac{37.56s + 981.1}{s} \tag{6.11}$$

It was designed in the linear domain using the Evans' Root Locus tool in order to have a good response time (about $0.6s$). Figure 6.19 shows the root locus used for the design. In blue you can see the open loop poles, in red the compensator roots, in magenta the closed loop poles. In order to design the compensator $C_m(s)$ (6.11), the identified model of the Omega Device (B.2) was employed.

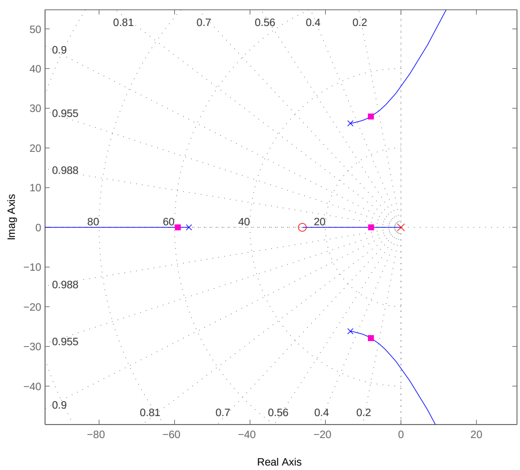

Figure 6.19: The master root locus to design the compensator $C_m(s)$.

6.4.2 Fa-P scheme: simulations

Figure 6.20a shows the aircraft trajectory between the buildings in a simulation with and without time delay when the dotted line F_h to the admittance block is employed (see Figure 6.18).

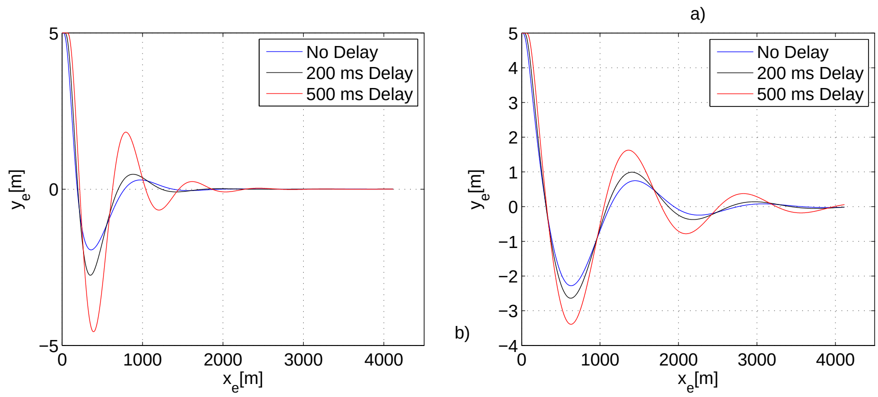

Figure 6.20: Admittance scheme (Figure 6.18) simulations with and without time delay when the dotted line is: a) employed; b) cut.

Figure 6.20b shows the aircraft trajectory between the buildings in a simulation with and without time delay when the dotted line F_h to the admittance block is cut (see Figure 6.18).

By comparing Figure 6.20a and Figure 6.20b, you can see that summing up F_h to F_k, that is having a force sensor on the stick, provides better transient properties to the system.

In Figure 6.21 you can see a simulation with the human operator in the loop (then $P(s) = 0$ in Figure 6.18) with and without time delay.

By comparing the Figure 6.21 with the Figure 6.20a and the Figure 6.20b, it is possible to think that maybe it would be better to sum up the force of the human operator to the haptic feedback F_k as in Figure 6.18. Unfortunately the Omega Device employed for the experiments did not have a force sensor, thus an observer

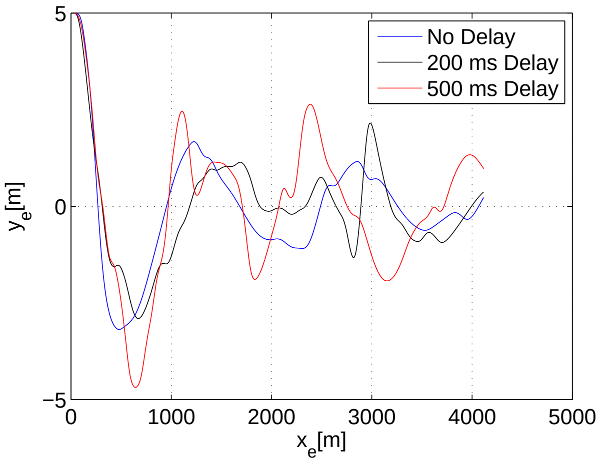

Figure 6.21: Admittance scheme (Figure 6.18) simulations with and without time delay with the real Omega Device and the human operator in the loop.

(see Subsection 6.4.3) for the human force was designed in order to implement something similar to the scheme of Figure 6.18.

6.4.3 The human force observer

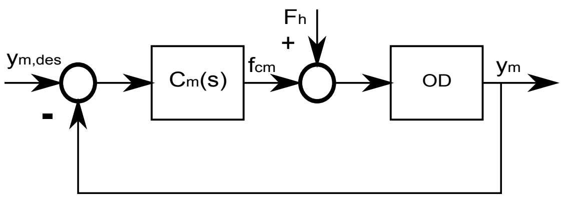

Figure 6.22: Scheme employed to build the human force observer.

Figure 6.22 shows the inner part of the Master control loop, where the human force acts as unknown input, the system OD_i (the identified model of the Omega Device) is known with a certain approximation, the system $C_m(s)$ (the master admittance controller) is known exactly, the signal $y_{m,des}$ is internally generated and then known exactly, and the signal y_m is measured by the haptic device sensors, then it is known with approximations. Equation (6.12) shows the transfer function from $y_{m,des}$ to y_m in Figure 6.22.

$$y_m(s) = \frac{C_m(s) \cdot OD_i(s)}{1 + C_m(s) \cdot OD_i(s)} \cdot y_{m,des} + \frac{OD_i(s)}{1 + C_m(s) \cdot OD_i(s)} \cdot F_h \quad (6.12)$$

Solving for F_h, it is possible to define the final expression of the observer transfer function, $O(s)$ as in equation (6.13):

$$O(s) = \hat{F}_h = \frac{1 + C_m(s) \cdot OD_i(s)}{OD_i(s)} \cdot y_m - C_m(s) \cdot y_{m,des} \qquad (6.13)$$

where $\hat{F}_h$ is the observed F_h.

Figure 6.23 shows the scheme employed for the implementation of the observer (Equation 6.13).

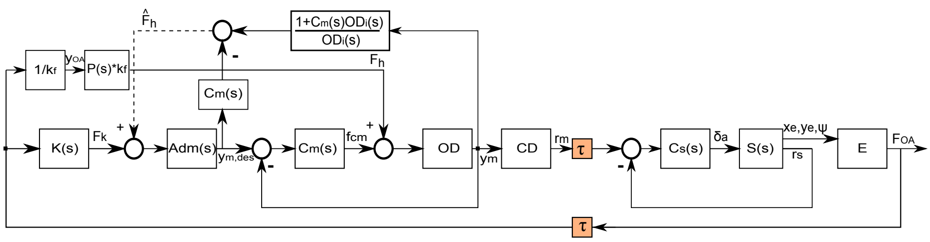

Figure 6.23: The observer scheme.

Figure 6.24 shows the observer scheme in which also the visual feedback (delayed by τ seconds) is shown explicitly.

Since the first component of Equation (6.13) is an improper transfer function, through the addition of two high frequency poles it was

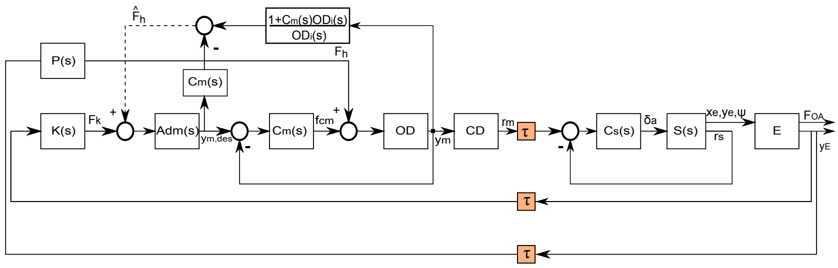

Figure 6.24: The observer scheme with visual feedback.

made proper in order to be able to implement it (see later the Figure 6.26 for the Bode plot). Figure 6.25 shows the comparison between F_h and $\hat{F}_h$ during a sample simulation.

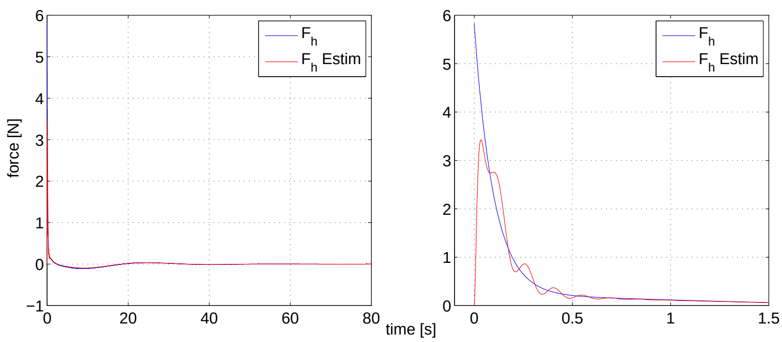

Figure 6.25: Observer validation (Figure 6.23) by employing the Omega Device model. Comparison between F_h and $\hat{F}_h$. On the right, zoom around the origin.

In order to implement the observer with the real Omega Device in the loop, which provides the signal y_m as a discrete signal, a discretized of the observer dynamics is needed. The Tustin approximation which is preferred for filter approximation was employed. Figure 6.26 shows both the effect of making the observer transfer function proper, and the quality of the discrete approximation.

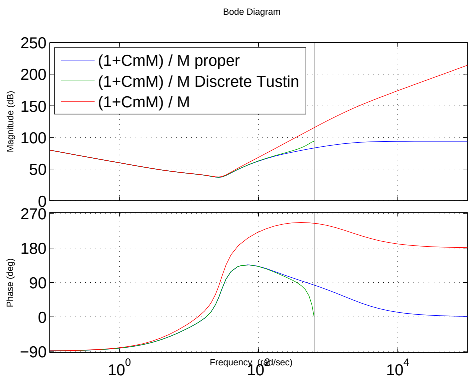

Figure 6.26: Bode plot comparison of the first term of the equation (6.13). In red, blue and green respectively the improper, the proper and the discrete transfer functions.

In order to evaluate the observer performance, since no force sensor is available to compare with, two simulated human operator force scenarios were defined. In the first one F_h was set to be a constant force ($2N$ magnitude). The red line is obtained with the identified model of the Omega Device, the magenta line is obtained with the real Omega Device in the loop. You can see the result in Figure 6.27a and note that the observer produces a signal which mean value is very similar to F_h. In the second test the observer was asked to estimate a sinusoidal force which magnitude (about $2N$) and frequency (about $25s$) are similar to the oscillating forces produced during a simulation with the aircraft. You can see the result in Figure 6.27b. Then, the observer works pretty well even if some spike is present; these are caused by the noisy signal y_m, the output displacement of the real Omega Device.

Figure 6.28 shows two simulations where the system output (lateral position of the aircraft) is compared when using the real F_h and the observed $\hat{F}_h$; it appears that the results achieved in both cases

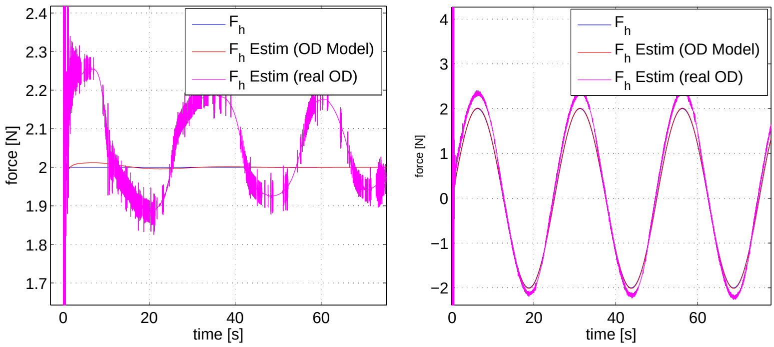

Figure 6.27: Observer validation (Figure 6.23) by employing both the Omega Device model and the real one. Comparison between F_h and $\hat{F}_h$. Zoom around the origin. In the legend *OD* is for Omega Device. Instead of the human operator a forcing function is employed: a) $2N$ constant force; b) $2N$ amplitude and 25 seconds period sinusoidal force.

are very similar.

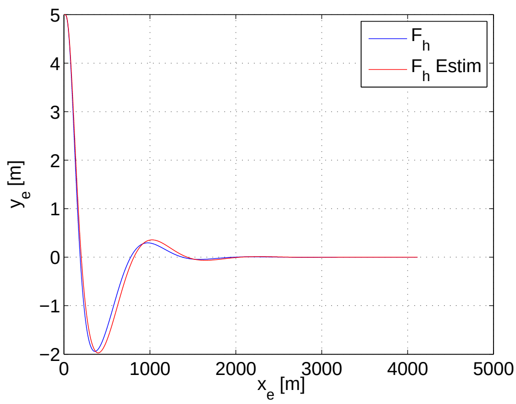

Figure 6.28: Simulation comparison (Figure 6.23) by using F_h and $\hat{F}_h$.

Figure 6.29a shows three simulations obtained using the observer (scheme of Figure 6.23). Figure 6.29b compares the results obtained by running the simulation of Figure 6.23 with and without the dotted line $\hat{F}_h$, and with a time delay of 500 ms. It appears clearly, also by direct comparison with figures 6.20a and 6.20b, which present the same simulations achieved with the exact knowledge of the human force, that the addition of the observer has a beneficial effect in terms of transient response of the system.

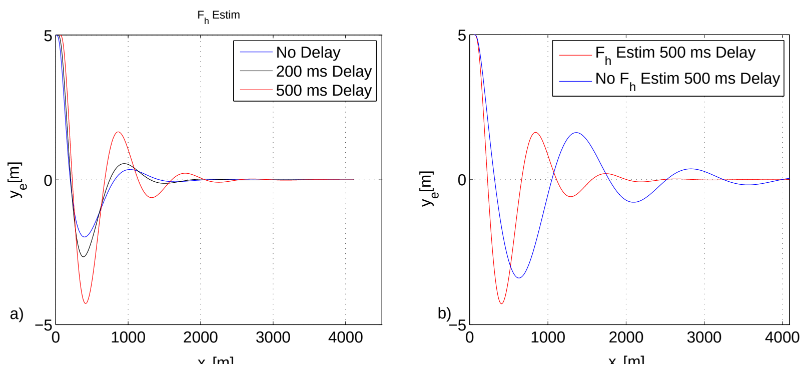

Figure 6.29: Observer scheme (Figure 6.24) simulation by employing the Omega Device model: a) the dotted line is employed (0,200ms,500ms delay); b) 500 ms delay comparison with and without the dotted line.

Figure 6.30 shows the improved system stability under 500 ms delay with the employment of the admittance controller and the observer with respect to the baseline scheme (FP teleoperation). The same Figure compares the simulation outputs using both the real F_h and the observed $\hat{F}_h$; it appears clearly that the observer works pretty well and that the degradation of the transient performance when using the observer is minimal.

Finally, Figure 6.31 shows three trials with the human operator in the loop. By direct comparison between figures 6.31 and 6.21, even though a throughout analysis with a relevant number of trials

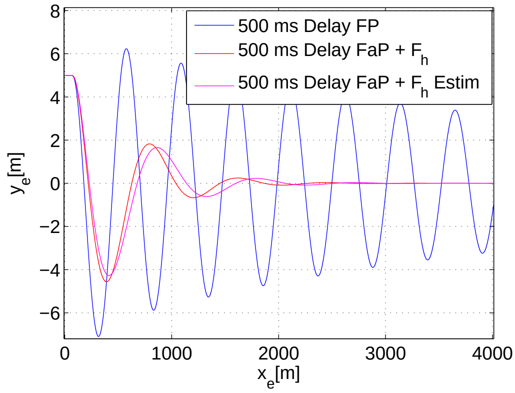

Figure 6.30: FP and FaP (Figures 6.2 and 6.23) simulation comparison under 500 ms delay by employing the Omega Device model.

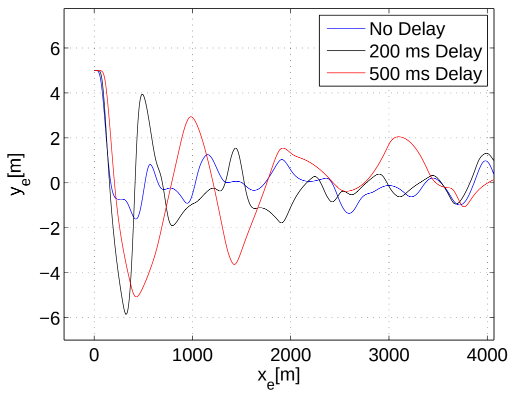

Figure 6.31: Admittance scheme (Figure 6.24) simulations with and without time delay with the human operator in the loop.

and test pilots would be needed, it appears that transient performance improves with the adoption of the observer, and that the transient performance achievable with the FaP admittance scheme outperforms those of the FP scheme.

In order to evaluate the performance of the system over a more complex environment, four trials were run within the obstacle environment designed in Chapter 4. The simulations were performed using the scheme described in Figure 6.24 (dotted line included) with the real Omega Device and the pilot in the loop. Figure 6.32 shows two trials in which $F_{OA} = 0$ (i.e. no Haptic aiding). Figure 6.33 shows two trials in which $F_{OA} \neq 0$ (i.e. the haptic aiding is active).

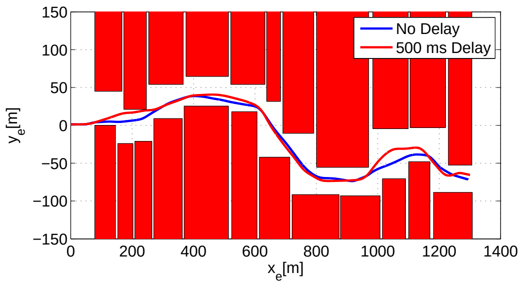

Figure 6.32: Simulation (Figure 6.24) with pilot in the loop with $F_{OA} = 0$.

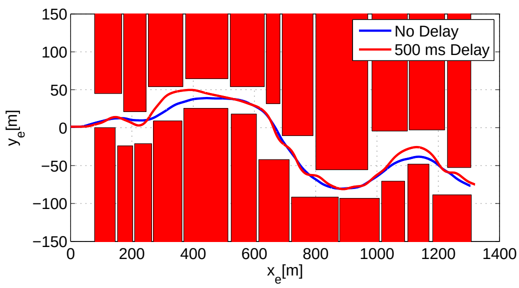

Figure 6.33: Simulation (Figure 6.24) with pilot in the loop with $F_{OA} \neq 0$.

By comparing Figure 6.32 with Figure 6.33 you can see that there are no important differences in pilot performance (i.e. number of collisions). Then, in order to make the task more difficult, some fog in the visual display was; the resulting visibility became thus extremely low and the pilot, de facto, had to rely much more on the haptic cues. Figure 6.34 shows two trials in which $F_{OA} = 0$. Figure 6.35 shows two trials in which $F_{OA} \neq 0$.

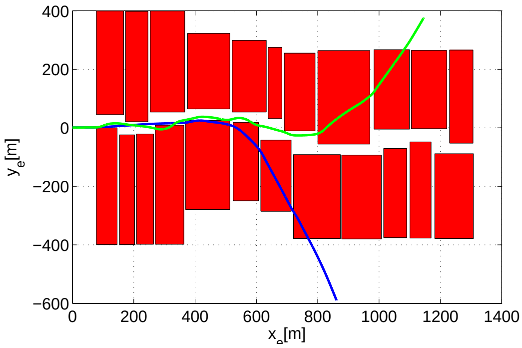

Figure 6.34: Simulation (Figure 6.24) with pilot in the loop with $F_{OA} = 0$ in fog conditions. The blue line shows the *No Delay* trial. The green line shows the *500 ms Delay* trial.

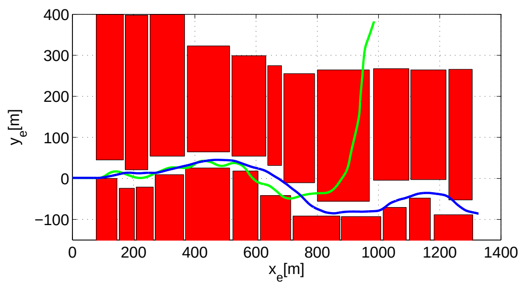

Figure 6.35: Simulation (Figure 6.24) with pilot in the loop with $F_{OA} \neq 0$ in fog conditions. The blue line shows the *No Delay* trial. The green line shows the *500 ms Delay* trial.

By comparing Figure 6.34 with Figure 6.35 you can see that, at least for the *No Delay* trajectory, the haptic feedback is very important in improving the pilot performance. The *500 ms Delay* trajectory in Figure 6.35 appears a little better than the corresponding without haptic feedback, but suggests at the same time that an improvement in the haptic feedback is probably needed.

Chapter 7

Conclusions

Both Fly-By-Wire systems for manned aircraft (which the present study could be applied as well, see Section 3.1) and remote piloting systems for Unmanned Aerial Vehicles do not transfer to the pilot important information or cues regarding the state of the aircraft and the loads which are being imposed by the pilot's control actions. These cues have been shown to be highly responsible for pilot situational awareness.

Thus, the opportunity of artificially reintroducing them in the pilot control input arose and brought to the necessity of designing an artificial feel in the control device [75].

Furthermore, the bandwidths of modern flight control systems approach the pilot's own sensing and actuation systems and this could bring to unwanted effects like pilot-induced-oscillations (PIO).

It has been shown in the past [18] that, since Situational Awareness is created through the perception of the situation (SA First Level), the quality of SA is very dependent on how the person directs attention and how attention to information is prioritized based on its perceived importance. Thus, it is necessary to increase the knowledge of human-machine challenges among system developers and users [10].

Furthermore, blaming crashes and mishaps on human error is usual in UAV teleoperation field this wrong assumption, that humans cause most errors, brings many people to believe that errors can be avoided by removing the human and by employing full automation [11]. On the contrary, several UAVs incidents and crashes have been attributed to automation errors or loss of situational awareness because the human has been "automated out of the loop" (Human System Interface deficiencies) [10].

There has been little research on UAV "cockpit" design and its impact on the human operator. A lot of research is still required in evaluating different designs of UAV interfaces that optimize operator performance abilities. Human and automation teamwork, when efficient, could achieve levels of performance and safety beyond that of the human or automatic systems. Automation entities are not flexible as humans are. The high rates of mishaps and crashes we have today in the UAVs field would have been significantly lower if human-machine teamwork would have been given more attention in the design evolution of UAVs control laws [10].

The automation should be designed differently to better support human performance, reduce the workload and support the decision making. Thus, investing in a human machine interface design tailored on the human needs would improve the operator situational awareness and maybe the performance.

All the previous considerations suggest in particular that the force-feel system design is still an important issue; now that the performance capabilities of modern aircraft have increased exponentially and these are the reasons for which **the force feel are now to be considered as part of the vehicle**!

Thus a question arises: which are the specifications and the behavior of the "ideal" artificial force-feel system?

The maximum forces a human can exert is an example of how important is to tailor the artificial feel directly on the human.

Due to the previous consideration, it appears that taking into consideration the human operator natural behavior in the design of new generation aiding system might be a winning point. In the present work, to better address the haptic aid design a review and a classification of the haptic aids present in literature was made. Two haptic aids classes were defined and were given the name of Direct and Indirect Haptic Aid. Afterwards, the idea to consider the human operator natural behavior in the haptic feedback design, was made through the introduction of the Indirect Haptic Aid for disturbance rejection and/or obstacle avoidance tasks. Thus, an artificial feel system, that drew its inspiration in the mechanical force-feel systems for fixed-wing aircraft in which important informations are felt by the pilot through the control device, was employed and developed in this work.

Although haptic feedback is used in various areas (included UAV teleoperation) and with different goals, application of haptic feedback in UAV teleoperation for both collision avoidance and path following in low airspace in the presence of external disturbances such as wind gusts was not investigated so far. The haptic information should not only map the environmental constraints or location goals but also the external wind conditions because the gusts (vertical or lateral) in presence of obstacles could be very dangerous for the structural safety of the UAV. Thus, the haptic feedback should be needed for both natural and environmental constrains.

Particularly, when the visual information is hinder or limited (e.g. obstacles outside of the field of view or foggy weather conditions), the haptic feedback might compensate for the lack of visual information also in the presence of external disturbances as wind gusts.

As a matter of fact, when the UAV is approaching the obstacle in the presence of fog, for example, a sudden maneuver is needed in order to avoid the obstacle. In the presence of fog, in fact, the distance at which the obstacle is seen is shorter than the same distance in case of good visibility condition; then, the presence of fog reduces the useful time for avoiding the obstacle. By employing the haptic canal of information in addiction to the visual canal, the remote pilot would feel the obstacle approaching faster through the haptic feedback than through the visual one.

This would increase the Situational Awareness and the safety of teleoperation.

All the Indirect Haptic Aids introduced in this work (Conventional Aircraft Artificial Feel, Obstacle Avoidance Feel and Mixed-CAAF/OAF) are an attempt of readily inform the remote pilot about the presence of a potential danger which could bring to the mission failure.

In fact, the main goal of the IHA-based approaches developed here was to improve the situational awareness about the state of the drone hopefully showing that a performance improvement would also come as a consequence. As a matter of fact, The CAAF would inform the pilot about an external disturbance affecting the UAV; OAF would inform the pilot about the environmental constraints and Mixed-CAAF/OAF would inform the pilot about both the environmental constraints and about the external disturbances affecting the UAV.

Furthermore, the present work shows an improvement of IHA-based approach as well:

- the Variable Stiffness CAAF was tested and it was shown to increase the performance with respect to the absence of haptic feedback at all;
- Force Injection CAAF was shown to increase the performance in terms of instinctive response to a stimulus in pilots without any previous training on the experiment with respect to the conventional haptic aids.
- OAF and Mixed-CAAF/OAF were shown to increase the performance in terms of collisions avoidance with and without the presence of wind gusts with respect to the conventional haptic aids.

Such performance improvements were compared to those available with the other commonly used, and published in the scientific literature, approaches which fall in the DHA category.

The goal of the DHA simulators employed in this work was not to obtain state-of-the-art performance, but to serve only as a comparison term for the IHA simulators.

During the implementation of the DHA simulators for comparison with the IHA approach, we found out that the design of a DHA based augmentation scheme is very task dependent.

In the CAAF VS DHA Experiment, for example, a reference altitude had to be chosen and the a compensator capable of holding it was designed. The compensator gain was then reduced in order to give the pilot some authority of control: the aim of this work is aiding teleoperation and not designing an automatic control system. Reducing the gain of the DHA-compensator would make the pilot useful.

In the OAF VS DHA Experiment an attempt to design the DHA compensator to be a little more task-independent was made. As a matter of fact, the pilot was given a certain freedom in choosing the path. In this experiment, what made the performance difference between the IHA and the DHA concepts was probably the fact that DHA forced the operators to fly at a distance from obstacles in which the force field was not too strong and, for this reason, more comfortable; while with the IHA force the pilot was free to fly very close to the obstacles because there was no force trying to avoid it.

In the MIXED CAAF/OAF VS DHA Experiment, the DHA was designed in order to make the aircraft lateral acceleration null; this behavior would efficiently reject the lateral wind gust as a standalone compensator but it was shown not to be safe in terms of number of collision. Furthermore, this approach would fail or, at least, show an undesirable behavior in the case the pilot's intention was to perform a maneuver that creates a lateral acceleration as, for example, in the sideslip maneuver.

All the previous considerations make the DHA-approach very likely to be an "almost automatic system" having almost the same drawbacks of autonomous systems: its design is very task-dependent and it would try to leave the pilot out in the decision making process. While, the IHA-based approach would focus on the pilot leaving him/her full authority in the decision making process and, as long as it is very important that the pilot run and at least supervise the whole mission, it would keep higher the attention of the pilot on the task and, as a consequence, all the UAVs mishaps causes would hopefully be reduced and an improved safety would be reached. The IHA-based approach would leave space to the pilot in case its intention is not known and very independent from anything but only on his/her last moment decisions reached through some unknown cognitive process.

It might appear singular to compare two Haptic Aiding schemes, which produce force sensations which have opposite sign, for the same task. In fact the experiments conducted so far shown that the participants to the experiments (both professional pilots and naive subjects) can control the aircraft within both DHA and IHA approaches without a-priori instructions or training but the IHA-based ones produced better results. IHA systems appeared to be more intuitive to be handled.

In general, human responses to external stimuli are highly conditioned by the required processing operations. In line with this, some motor responses are more 'automatic' (less affected by cognitive factors) and occur with shorter latency. For instance, saccades are more 'natural' than antisaccades [3]. The stretch reflex, which is a reflex contraction of a muscle in response to passive longitudinal stretching, is an highly automatic motor response that is believed to be the spinal reflex with the shortest latency [77]. Application of the IHA concept to both the disturbance rejection and the obstacle avoidance problems, which is subject of this thesis, produced a force stimulus to which the operator must, in general, oppose.

Several other examples could be built following the IHA concept and would lead to similar results: a stimulus to be counterbalanced and overtaken. Thus, the IHA concept, which requires a reaction in opposition to stimuli rather than compliance, might therefore be more 'natural' for the system because it very likely exploits the highly automatic and fast stretch response [83, 84]. These preliminary analysis of the psychophysical implications of this research suggests that the type of motion task required by the IHA concept could be thought like being composed by a stretch reflex in response to initial force peak (caused by the gust and/or obstacle edge), together with a higher-level response caused by the experience in rejecting wind gust disturbances and by the visual cues. Would this be true, we could conclude that, at least for certain types of applications, an Haptic feedback which operates accordingly to the IHA concept (i.e which produces stimuli to be opposed) would result more natural to be understood and followed by the operator, and possibly would provide better task performance, than a similar system built according to the DHA concept.

The teleoperation object of this thesis was also tested in the presence of time delay in the communication link. The employed setup resulted in a "non-classical" teleoperation scheme, since the feedback is related to the distance from obstacles and not to the force that results from the interaction with the environment. This is the reason for which the results obtained in literature when applying classical teleoperation architectures [43, 14, 29, 30, 31]needed an adaptation to be ported to this application.

Since, no force sensors were available in the actual control device, an observer was designed and proven capable to estimate the human force (at least simulated human force injected into the actual haptic device in software). The resulting admittance scheme plus the human force observer shown to be able to provide good transient performance both in simulations and with the human operator in the loop.

Ackowledgements

The present work was mainly conducted at the Max Planck Institute (MPI) for Biological Cybernetics of Tübingen which is under the direction of the Professor Heinrich H. Büelthoff. The first persons I have to thank are the Professor Heinrich H. Büelthoff and my supervisor, the Professor Lorenzo Pollini. Professor Heinrich H. Büelthoff not only gave me the financial support and provided me with the MPI facilities but also gave me really important advices on my work in which he was really interested and his constant presence proves it. I have also to thank my supervisor, the Professor Lorenzo Pollini, and the University of Pisa for the sponsorship and for giving me the chance to start a beautiful work period in Tübingen. Although Lorenzo was in Pisa, his Skype-presence and his problem solving characteristic were very important for my work. I also have to thank Professor Alfredo Magazzú for being my only reference point on the aircraft aerodynamics, always ready to answer to my questions and happy to help me with his always useful and outstanding advices. The Tübingen experience started one day when Lorenzo asked me if I would have liked to spend some time in an excellent research institute and after my "why not?!", a flight ticket and a presentation of my research proposal, a period which I am sure I will never forget both in terms of research and relationships quality started. In fact, the MPI of Tübingen does not only offer an amazing amount of very good devices and some of the best researchers I have never known but only a really nice and friendly

environment. I will never forget the amazing time spent with my MPI colleagues and, above all, friends: Florian, Stephan, Paolo RG, Betty, Joachim, Paolina and Carlo gave me, since I was just arrived, the most beautiful way of spending my spare time. I will also never forget the meals at the MPI canteen were Florian, Paolo P and Alessandro supported me for all the time by making less hard a really busy period. I will never forget the beautiful time spent with them talking about the sad Italian politics. I really enjoyed my lunch times! My flatmates Alejandro, Gilberto, Linda and Katharina gave me a lot of good memories as well: from the astrophysics speeches together with Alex and the economics and politics informations exchanged in the nice common room. In that house I could breath a good air and I will never forget that nice wooden house in the middle of downtown. Very nice spending of my spare time at the swimming pool and in the evenings together with Barbara, Izabela, Lilia, Antonio and Paolo. God bless Skype also for all the time spent with Alessia which I could feel the presence literally night and day; the really funny, and not only, speeches about whatever. Her sleeplessness time and my night working time were always framed by her presence. What to say about my parents, Salvatore and Concetta, and my sisters, Giuseppina and Giovanna, my brothers in law, Marco and Guglielmo, and my beloved nefhews, Alberto and the little Andrea? The calls with them through the Internet and the Skype gave me the family support I needed to have a very nice break from my work. The always present and precious love and encouragement of my parents and my sisters and my funny calls with Alberto always asking "when do you come here?". And finally the strongest support ever known by Marika, always sustaining me in my hardest periods although my often present agitation about deadlines and whatever. The constant video calls which helped me to feel always with her and Ciccio, the most adorable dog ever. Her presence made my work and my life the best ever and gave me everything I needed and the most precious things imaginable.

Finally, thank you to everyone, colleagues and friends (Sara, Donatella, Marta, who supported me a lot till the deadline for the thesis submission, and a lot of other friends which there would not be enough space to mention), who made my time nicer. Although this period was very hard and tiring, I actually enjoyed my years as a researcher and I am happy having done it.

Appendix A

Experiments Setup

The present work was mainly conducted at the Max Planck Institute for Biological Cybernetics of Tübingen under the sponsorship of the director Professor Heinrich H. Bülthoff and of the University of Pisa and the supervision of the Professor Lorenzo Pollini.

All the experiments were conducted in a dark room to make the participants to focus their attention on the experiments.

A computer with a 24 inch liquid crystal display (LCD) screens and a control device, namely the Omega Device, in one side (left or right according to the subjects preference) played the role of a fixed-base flight simulator.

The layout of the experiment environment is shown in Figure A.1.

The LCD screen was employed to display the simulation scenarios: an EFIS display for the disturbance rejection experiments and a synthetic view of a street with buildings for the obstacle avoidance experiments.

During the experiments, the subjects were sitting in the darkened room. The experiment coordinator was next to the subject following the experiment.

The experiments itself was run on MatLab and the Simulink Tool-

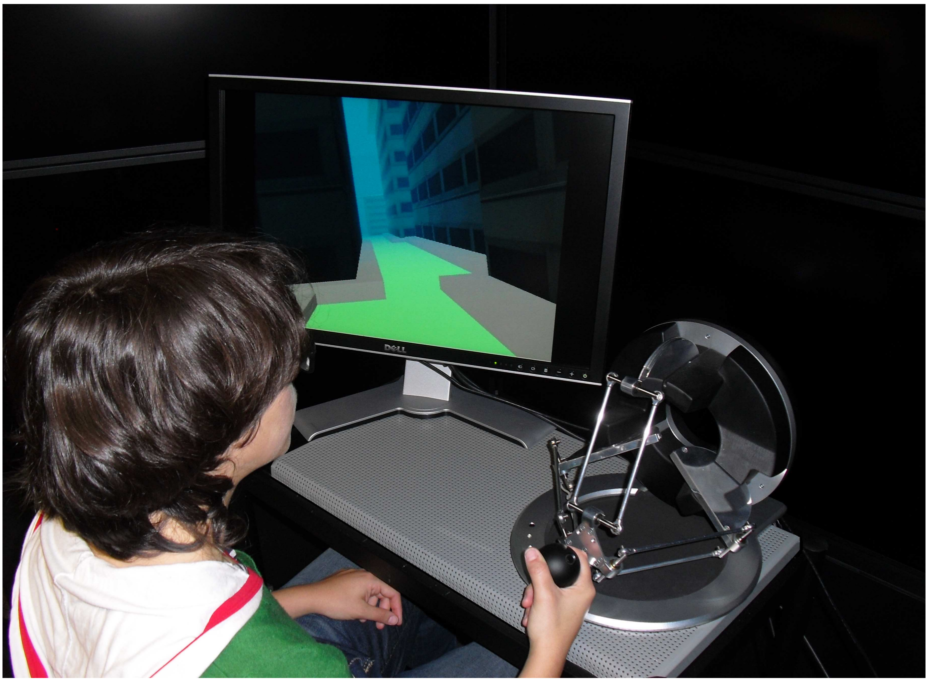

Figure A.1: The experimental setup.

box which ran at 200 Hz. The visualization ran at 20 Hz (see Section A.3 for details). The haptic loop ran around 3000 Hz (see Section A.2 for details).

A.1 The Aircraft Model

In all the experiments the Flight Dynamics and Control Toolbox [45] was employed. It is a graphical software environment for the design and analysis of aircraft dynamics and control systems based upon the complex non linear model developed in Simulink from M.O. Rauw. It is distributed exclusively across the Internet through the website *http://www.dutchroll.com*. In particular, for the disturbance rejection experiments the full non linear model was employed. While a linearization around a trim condition was used for the obstacle avoidance experiments.

The Beaver De Havilland Canada DHC-2 was the simulated aircraft employed. It is a fixed-wing aircraft with single propeller engine. The fully non linear model is made up by 12 Ordinary Differential Equations (ODE).

In the disturbance rejection experiments the aircraft model was trimmed to fly horizontally and the trim conditions were:

$$\begin{cases} V \simeq 50 m/s \\ H = 300 m \\ \gamma = 0 deg \Rightarrow \alpha = \theta \end{cases} \tag{A.1}$$

The engine runs at constant *1800 rpm*. To obtain the trim conditions shown in Equation A.1, the elevator had to be deflected by $\delta_{e,trim}$ and the manifold pressure (the thrust in case of the aircraft under consideration) is kept constant to MP_{trim}:

$$\begin{cases} \delta_{e,trim} = -0.2565 deg \\ MP_{trim} = 25" Hg \end{cases} \tag{A.2}$$

In all the simulations, the thrust is kept constant at the value of Equation A.2, while the elevator is deflected around the trim value of the same equation.

In the disturbance rejection experiments, the only considered dynamics was the longitudinal one and the lateral input (the aileron deflection δ_a and the rudder deflection δ_r) were kept to the zero value.

In the obstacle avoidance experiments, the only considered dynamics was the lateral one. Thus, values different from the zero for δ_a and δ_r were needed in order to make possible the control of the lateral dynamics. New trim values were needed:

$$\begin{cases} \delta_{e,trim} = 0.5856 deg \\ \delta_{a,trim} = 0.0661 deg \\ \delta_{r,trim} = -2.1933 deg \end{cases} \tag{A.3}$$

A.1.1 Technical Data

Before starting to work with an aircraft, important data must be known. The *flight envelope* depicts the boundaries of aircraft loading and flight conditions within which operation of the aircraft is satisfactory and beyond which some aspect becomes unacceptable. It shows at some particular velocities the maximum load factor that could be introduced by the maneuvers remaining handling qualities, engine behavior and structural loads acceptable. Figure A.2 depicts an example of the simplest flight envelope.

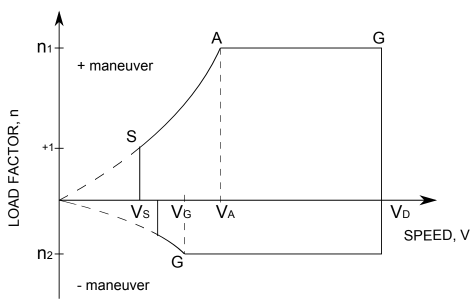

Figure A.2: The flight envelope.

V_S is the stall speed. Currently, this is interpreted as the minimum speed at which the steady horizontal flight ($n = 1$) is possible. It is the velocity that corresponds to the maximum lift coefficient $C_{L,max}$:

$$\begin{cases} n \cdot W = \frac{1}{2}\rho V_S^2 S C_{L,max} \\ W = m \cdot g \end{cases} \tag{A.4}$$

For:

$$\begin{cases} C_{L,max} = 2.2 \\ S = 23.23m^2 \\ \rho = 1.225Kg/m^3 \\ m = 2288.231Kg \\ g = 9.81m/s^2 \\ n_1 = 3.8 \\ n_2 = -1.52 \end{cases} \tag{A.5}$$

S is the wing area, ρ is the air density, m is the aircraft mass, g is the gravity acceleration, n_1 and n_2 are respectively the maximum positive and negative load factors.

V_A is the design maneuvering speed.

V_S is calculated for $n = 1$; while V_A, that is the velocity that corresponds to the maximum lift coefficient for the maximum aircraft load factor, is calculated for $n = n_1$. Similarly V_G is calculated for $n = n_2$.

V_D is the design diving speed. As long as this value is unknown, it was hypothesized to be:

$$V_D = V_{NE} + 10\% V_{NE} \tag{A.6}$$

where V_{NE} (*80.25 m/s*) is the never exceed speed.

A.1.2 Aicraft Natural Modes

By linearizing the complex non linear model around the trim conditions of Equation A.1, the following transfer function is obtained:

$$H_{Lon} = \frac{5.985s^3 + 2.2364s^2 - 1298.2s - 27.607}{s^5 + 5.7716s^4 + 15.229s^3 + 0.73354s^2 + 0.74834s} \tag{A.7}$$

Figure A.3 shows the Bode plot of the transfer function of Equation A.7.

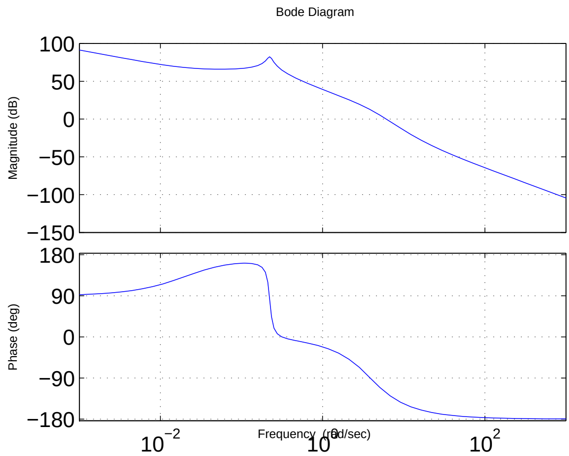

Figure A.3: Bode plot of the Beaver longitudinal dynamics.

While Figure A.4 shows the pole-zero map of Equation A.7.

The low damped couple of complex and conjugate poles (ζ about 0.06) represent the Phugoid mode poles. While the well damped one (ζ about 0.75) represent the Short Period mode poles. The Beaver longitudinal dynamics presents a non minimum phase zero as well.

By linearizing the complex non linear model around the trim conditions of Equation A.3, the following transfer function is obtained:

$$H_{Lat} = \frac{-9.9877s^3 - 10.4132s^2 - 6.1385s - 0.0184}{s^4 + 8.1578s^3 + 10.2490s^2 + 11.8186s} \tag{A.8}$$

Figure A.5 shows the Bode plot of the transfer function of Equation A.8.

While Figure A.6 shows the pole-zero map of Equation A.8.

The couple of complex and conjugate poles (ζ about 0.5) represent the Dutch Roll mode poles. While the real poles represents the

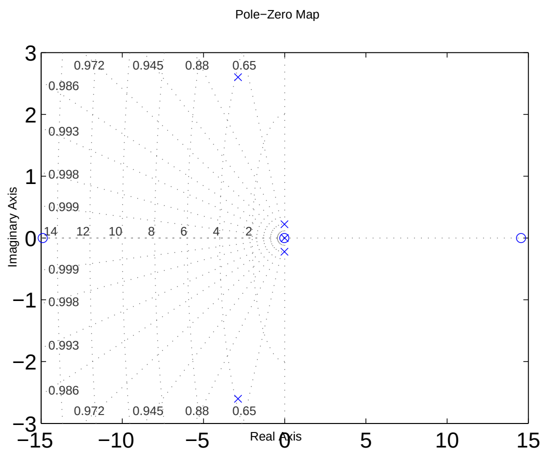

Figure A.4: Pole-zero map of the Beaver longitudinal dynamics.

low frequency (long time constant) Spiral mode and high frequency (fast time constant) Roll Subsidence mode.

The pilot or the autopilot has to damp the above longitudinal and lateral aircraft natural modes.

A.2 The Haptic Device

The control device employed in this work is the Omega Device (omega.3 produced by the Force Dimension, Switzerland). It is a high precision force feedback device and it is classified as an **impedance-like** haptic device. Some technical data is shown in Table A.1.

An S-Function was built to make the Omega Device communicate with the PC. The control loop which implemented the haptic device dynamics was realized in software. A Microsoft windows application constructed a thread which implemented all the haptic algorithms and was set to run as fast as possible; the software was executed in a dual core machine, thus one of the two cores was essentially devoted

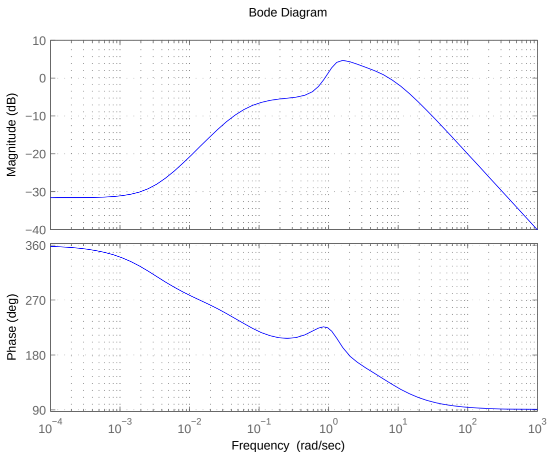

Figure A.5: Bode plot of the Beaver lateral dynamics.

workspace	translation	⊘ 160 x 110 mm
forces	translation	12.0 N
resolution	translation	< 0.01 mm
stiffness	closed-loop	14.5 N/mm

Table A.1: The Omega Device Specifications.

to executing the haptic control loop. A statistical measure of the thread execution frequency was recorded: the haptic loop execution frequency resulted to be around 3000 Hz. Due to this high activation frequency, no clitches or other undesired disturbances were noticed in the rendered force.

The stiffness and damping for respectively the longitudinal (x-axes of Figure 3.2) and the lateral (y-axes) constants were chosen heuristically and shown in the Table A.2:

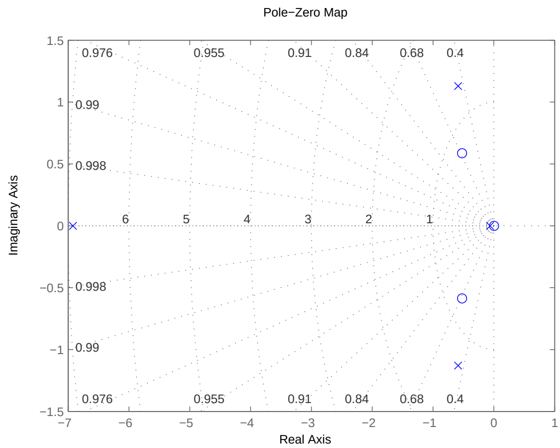

Figure A.6: Pole-zero map of the Beaver lateral dynamics.

Longitudinal Stiffness	$K_{S,x} = 240$ N/m
Longitudinal Damping	$K_{D,x} = 6Ns/m$
Lateral Stiffness	$K_{S,y} = 120$ N/m
Lateral Damping	$K_{D,y} = 6Ns/m$

Table A.2: The stick characteristics.

A.3 The 3D Visualization System

The out of window view of Figure 4.1 and the EFIS Display of Figure 3.3, were made up using DynaWORLDS. DynaWORLDS is an software project born at the Department of Electrical Systems and Automation at the University of Pisa, from an idea of Lorenzo Pollini and Gaetano Mendola, and later developed by DynamiTechs (www.dynamitechs.com) to build a low-cost, comprehensive distributed simulation and Synthetic Environment (SE) visualization toolset. Mathworks Real Time Workshop can be used effectively to automatically generate C code to be used for simulation. Network connections are based on TCP/IP and UDP/IP protocols, but the same data stream could be sent on any transmission channel simply by coding appropriate device drivers.

Synthetic environments can be created using an integrated framework of scene design, object animation, and control panel design. The world, or scene, can be designed by means of 3-D objects, whose geometry and surface properties are imported by commercial CAD file formats, lights, and cameras. Each object can be connected to a motion channel that affects its position, orientation, and scaling in 3-D space; can be linked to any one other so as to inherit some of its features (a robotic arm); and its position can be tracked with a trail. A link can be established even among objects, cameras, and lights so that one object can bring cameras (inside vision from a vehicle) and lights (car's headlight). Motion channels are the animation sources for the scene; a channel is the abstraction of a data stream that may have several sources: files, network sockets, I/O boards, or input devices such as joysticks or buttons. With motion channels, all these sources can be mixed to obtain very complex object animation.

A control panel can then be designed interactively on-screen using output devices: camera views, various instruments such as pointers, light indicators, or artificial horizons, and so on.

DynaWORLDS is also capable of drawing nonfixed geometry objects; trails, smoke, clouds, or typical augmented reality tools such as a guidance tube or data superimposed on recognized objects on the screen can be drawn using appropriate graphical plug-ins. Furthermore, particular transformations such as nonlinear scaling, squeezing (useful for displaying collisions between elastic objects), or bending (vital for representation of flexible structures) are only possible with custom software.

One of the most important requirements of a hardware-in-the-loop simulation environment is its capability to incorporate various input and output devices to allow full integration of hardware components and software-simulated systems. Only with custom software device drivers and the adoption of a common communication standard it is possible to virtually connect heterogenous systems in their interfaces and sampling time. Every new real-world device can be put in the simulation loop with ease and without relying on the non-standard interfaces adopted by other commercial applications. In the end, complete control over the final rendering makes environmental features such as viewing through fog or turbid water, or even the reproduction of night vision device images, feasible. Figures A.7 and A.8 show a couple of simulation examples.

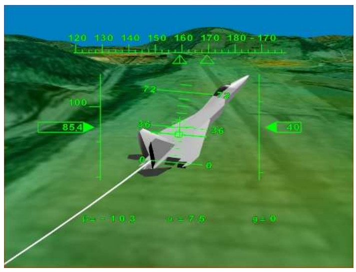

Figure A.7: Snapshot of a F-22 aircraft simulator.

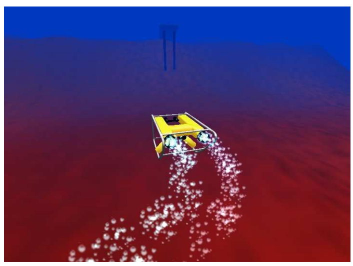

Figure A.8: Snapshot of an underwater vehicle simulator.

Appendix B

Omega Device Identification

This Appendix presents the results of the model identification procedure that was applied to the Omega Device.

The longitudinal transfer function $OD_{i,x}(s)$ of the actual Haptic device used in the disturbance rejection experiments (see Chapter 3) is shown in Equation B.1. It was identified by using frequency sweeps (from 0.0262 to 10 Hz) and the Empirical Transfer Function Estimate (ETFE) technique [49].

$$OD_{i,x} = \frac{3}{s^2 + 8.413s + 902.7} \tag{B.1}$$

The stiffness and damping constants (for both longitudinal and lateral identification procedure) are shown in Table A.2.

Figure B.1 show on the left side the real Omega Device Bode plot and on the right side the identified model Bode plot.

An example of the time response comparison between the real and the identified Omega Device for the longitudinal case obtained for a frequency sweep with amplitude of $3.2N$ is shown in Figure B.2.

As concerning the Omega Device lateral dynamics identification, the same procedure as above was employed. It resulted in the trans-

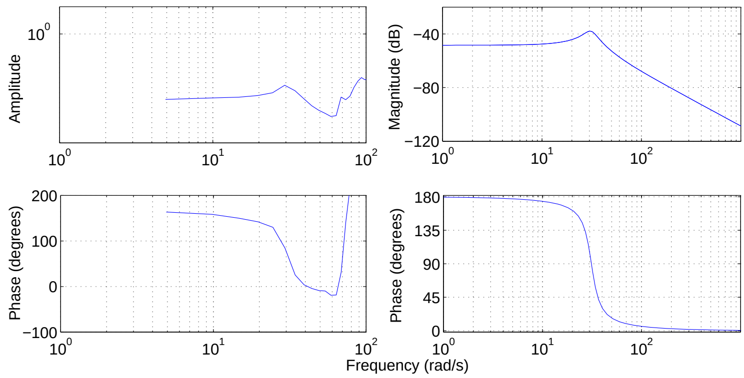

Figure B.1: The Real (on the left side) and Identified (on the right side) Omega Device longitudinal Bode plot.

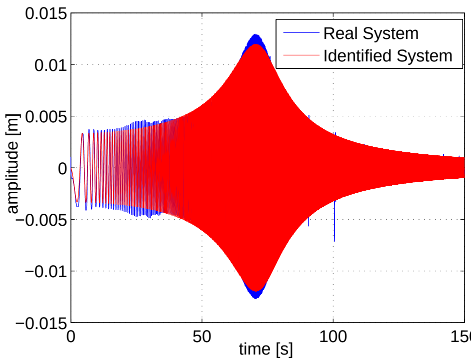

Figure B.2: Real Vs Identified Omega Device longitudinal dynamics time response comparison.

fer function $OD_{i,y}(s)$ of Equation (B.2) and it was used in the obstacle avoidance experiments (see Chapters 4 and 5).

$$OD_{i,y} = \frac{7.118}{s^2 + 26.76s + 864.8} \tag{B.2}$$

Appendix C

DHA Compensators Design

This Appendix presents the design of the DHA compensators employed in this work.

In particular, the Section C.1 shows the design of the DHA disturbance rejection compensator for the longitudinal dynamics which was employed in Section 3.5.2; the Section C.2 shows the design of the DHA disturbance rejection compensator for the lateral dynamics which was employed in Section 5.2.

C.1 DHA Design for Longitudinal Disturbance Rejection

McRuer presented a detailed study of human operator dynamics in compensatory tasks [80]. This research concentrated upon the effects of forcing function bandwidth and controlled element dynamics upon human operator describing functions (transfer functions and remnant). One very important product of the reported research was the "crossover model" of the human operator or pilot. This model essentially describes the ability of the human to adapt to different controlled elements and random appearing command inputs with different bandwidths.

It is mainly based on the assumption that in the area of the whole system crossover the human will adjust to different plant dynamics to yield the same human plus plant dynamics that is a simple integrator behavior. The Hess structural model which focus on the ability to adapt to different vehicle dynamics [79] is based on the McRuer crossover model.

The plant in this case is a combination of the control device dynamics and of the aircraft dynamics to control.

As concerning the longitudinal dynamics, the longitudinal model of the control device of Equation (B.1) and the linearized aicraft longitudinal model of Equation (A.7) has to be considered.

The pilot has to control the dynamics represented by the series of the previous transfer functions:

$$H_{Lon} = \frac{-17.96s^3 - 6.709s^2 + 3895s + 82.82}{s^7 + 14.18s^6 + 966.5s^5 + 5339s^4 + 1.375e004s^3 + 668.5s^2 + 675.5s} \tag{C.1}$$

The plant Bode plot is depicted in Figure C.1.

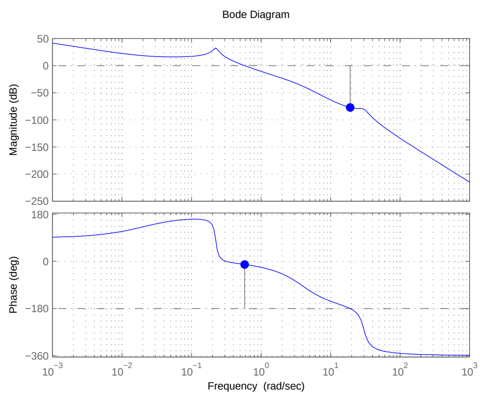

Figure C.1: The plant Bode plot.

The slope of the plant Bode plot (Figure C.1) around the crossover frequency (about *0.5 rad/sec*) is close to *-40 dB*. Thus the pilot model has to produce around the same frequency a positive slope of about *-20 dB* in order to get a simple integrator behavior (i.e. a *-20 dB* slope) of human plus plant dynamics.

Hess in [79] gives detailed indication on how to calculate the value of the new the human plus plant crossover frequency (in this case *3.18 rad/sec*) in case of $1/s^2$ (current case) behavior of the plant.

Through [79] is possible to calculate all the constants needed to build the human model (Figure C.2) that results in Equation (C.2):

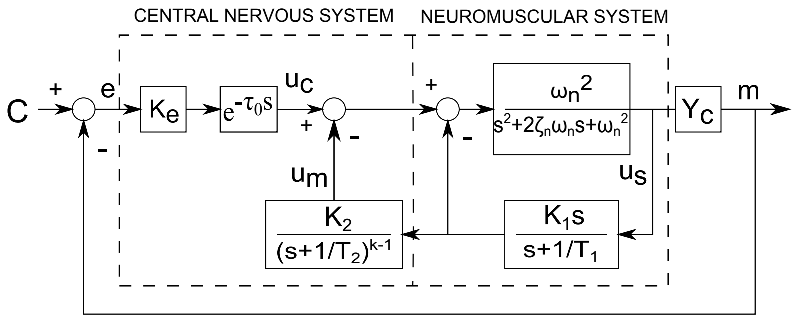

Figure C.2: The Hess Structural Model [79].

$$C_{Lon}(s) = \frac{6452s^2 + 2584s}{s^4 + 14.75s^3 + 209.5s^2 + 1089s + 13.04} \tag{C.2}$$

The Human plus Plant Bode plot is depicted in Figure C.3.

C.2 DHA Design for Lateral Disturbance Rejection

In this case a simpler compensator (a *phase lead network*) was chosen.

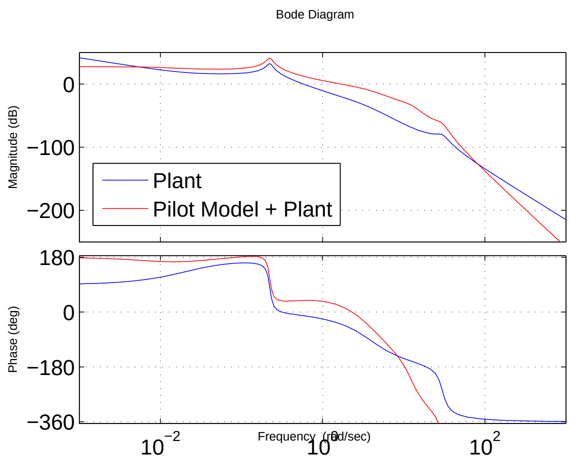

Figure C.3: Human plus Plant Bode plot.

The plant to control of Equation (C.3) is represented by the series of the lateral control device dynamics of Equation (B.2) (the input is the output force of the compensator and the output is the control device displacement which represents the aileron deflection) and the linearized (*sin(angle)*$\simeq$ *angle* and *cos(angle)*$\simeq$ *1*) lateral aircraft dynamics represented in Figure 5.2 (the input is the aileron deflection and the output is the lateral acceleration $\ddot{y}_B$) by considering $v_W = 0$.

$$H_{Lat}(s) = \frac{-697.4s^3 - 727.1s^2 - 428.6s + 1.284}{s^8 + 34.92s^7 + 1093s^6 + 7341s^5 + 9181s^4 + 1.024e004s^3 + 602s^2} \tag{C.3}$$

The compensator $C_{Lat}(s)$ of Equation (C.4) was designed in the linear domain using the Evans' Root Locus tool in order to have a good response time (about $0.6s$). Figure C.4 shows the root locus used for the design. In blue you can see the open loop poles, in red the compensator roots, in magenta the closed loop poles.

$$C_{Lat}(s) = \frac{102.1s + 0.4717}{s + 0.0048} \tag{C.4}$$

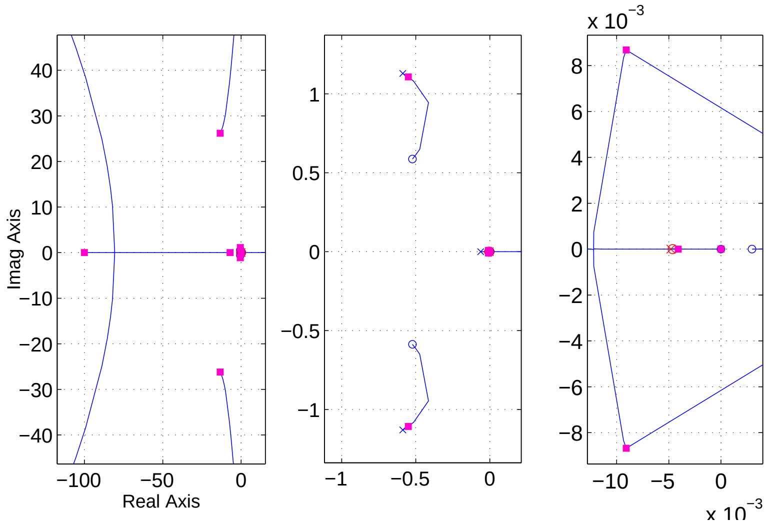

Figure C.4: The Evans' Root Locus used to design the compensator $C_{Lat}(s)$. From the left, the second and the third figures are a zoom around the origin.

Figure C.5 depicts the Bode plot of the plant and the compensated plant.

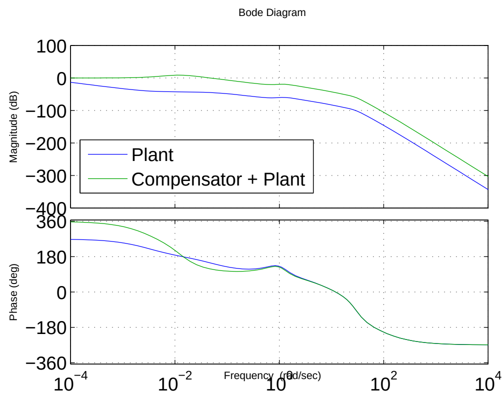

Figure C.5: Bode plot of the lateral plant compensated and not.

Appendix D

Experiments Background

D.1 The CAAF Experiment

As said in Section 3.6.1, the experiment consisted of three different force conditions: No Force condition with only compensation of gravity activated on the end-effector, Simple Force with Variable Stiffness CAAF (Equation (3.15)) and Double Force (twice as much force as in the Simple Force condition). Each condition was run as a separate block, i.e., the experiment consisted of three successive blocks.

The trials' (24 of 120 seconds each, 8 trials per force condition) order of presentation of the blocks was counter-balanced according to the Table D.1.

In total, the experiment lasted from 60 to 90 minutes (including instructions and breaks between blocks).

Before to start the real experiment each participant had to run a 5 minutes trial about the first block condition.

D.1.1 Instruction to subjects

> You are going to pilot a simulated aircraft through the use of the Omega Device which is a force feedback device, i.e. when you move the end-effector of it you can feel a force feedback. During the experiment you will watch at the electronic instrument display: on the right side you see the altitude, in the center the artificial horizon in which the angle between the aircraft and the horizon is shown (when this angle is zero it means that you're flying straight). The only dynamics that you have to control is the longitudinal dynamics (to make the aircraft to go up or down). To do this you need to move the stick forward or backward only: you have to pull the end effector to climb (to go up), to push the end-effector to dive (to go down); lateral or vertical movements do not affect the aircraft trajectory. The first 10 seconds of each trial, the aircraft is flying at constant altitude (300 ft). At time 9.5 s a 0.5 s duration disturbance (a vertical wind gust) affects the aircraft. The task of the experiment is to bring the aircraft at the initial altitude condition and to keep it there as much as possible.

D.1.2 Subjects detailed results

In Figure D.1, the three types of force were grouped: blue for No Force condition, green for VS CAAF-Simple Force condition, red for VS CAAF-Double Force condition.

The correspondence with the results provided in Section 3.6.1 in evident.

D.2 The CAAF VS DHA Experiment

As said in Section 3.6.3, in the CAAF VS DHA experiment, object of this section, a simple control task was prepared: the aircraft was initially flying leveled in trimmed condition at constant altitude (*300 ft*); three severe vertical wind gusts, which induce the aircraft to initiate a motion according to its Phugoid mode, are simulated by artificially injecting three control disturbances (elevator impulses) of randomized duration (2, 3 or 3.5 seconds), starting time and sign (upwards or downwards).

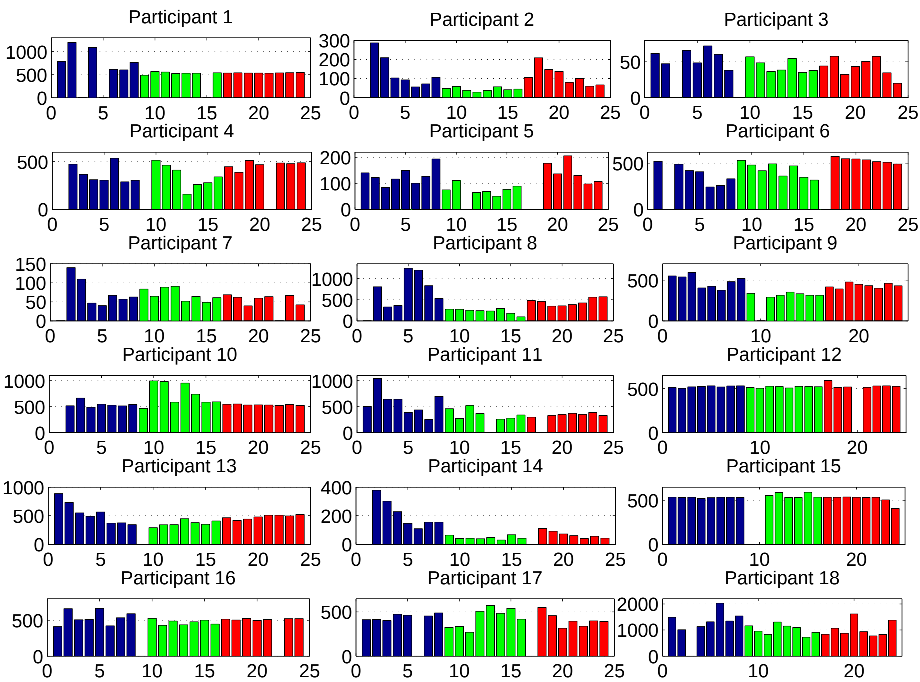

Figure D.1: CAAF Experiment detailed results. Find in the vertical axes the IAE about the task altitude. The missing bars refer to trials in which the aerodynamic stall happened (non-linear aircraft dynamics and naive participants, i.e. not professional pilots, were employed in this experiment).

The experiment consisted of three different force conditions: No Force condition (referred as *NoEF* condition) with only the spring-damper force on the end-effector, IHA condition (the Force Injection CAAF from Equation (3.19)) and DHA condition (see the Section 3.5.2 for details).

All the trials (36 of 60 seconds each, 12 trials per condition) have been mixed and counter-balanced to test natural reaction of the pilots to the three different conditions. Before starting the experiment, every pilot was asked to run a 5 minutes trial where he/she had to perform a slightly different altitude regulation task; the goal of this initial trial, was to let the pilot acquire enough knowledge of aircraft dynamics to be able to confidently pilot it. During this trial a simple spring-damper (the stiffness and the damping constants were chosen to be 1/6 of the NoEF case) behavior of the stick was employed. In total the experiment lasted 90 minutes.

No instructions were given about the three different force conditions to test natural reaction of the pilots to the three different conditions.

The following matrix shows an example about the force conditions planned for 4 of the 36 trials and for the 7 pilots:

In order to focus on the haptic cueing we made the experiment more difficult for the pilots by setting the Artificial Horizon inoperable (zero pitch and roll).

In each trial there were 3 impulses of 3 different randomized (Latin Square Method) amplitudes (2, 3, 4 seconds), at randomized starting times and always the same amplitude (4 cm displacement of the stick) which sign was randomly changed (+/- that is respectively upward or downward wind gust) all counterbalanced in a way that during the 36 trials every subject received the same number of positive and negative disturbances.

As a rule, the first impulse starting time was randomized between 6 and 11 seconds, the second one between 20 and 28 seconds, the third one between 40 and 46 seconds. As long as the time between each impulse and the next one was randomized between 14 and 23 seconds, after every impulse there might be enough time to re-establish the trim conditions.

By using for each trial counter-balanced force condition as in Table D.2 and similar planned amplitude, starting times and sign impulses to simulate the wind gusts, no learning about the impulses was ensured.

D.2.1 Instruction to professional pilots

You are going to pilot a simulated aircraft through the use of the Omega Device which is a force feedback device, i.e. when you move the end-effector of it you can feel a force feedback. During the experiment you will watch at the electronic instrument display: on the right side you see the altitude, in the left side the airspeed, in the center the artificial horizon set as inoperable. The only dynamics that you have to control is the longitudinal dynamics (to climb or dive only). The only needed commands are forwards or backwards (as in a typical aircraft control bar). In each trial there will be 3 vertical wind gusts of random duration, at randomized starting times and of randomized sign (upwards or downwards). The task of the experiment is to fly leveled in trimmed condition at constant altitude ($300ft$) although the presence of the randomized wind gusts by watching the altimeter only. In fact, the Artificial Horizon is set inoperable. Before to start the real experiment you will to run a 5 minutes trial to familiarize with the setup. During this trial, you have to fly at the altitude suggested by the magenta window: at the starting point you have to fly straight (0 degrees in the artificial horizon and 300 ft altitude), after about 10 seconds you have to fly at 310 ft altitude, after about 40 seconds you have to fly at 290 ft altitude, after about 40 seconds you have to fly at 300 ft altitude as in the initial conditions and so on till 5 minutes. You have just to follow the magenta marker which will move from one desired value of altitude to reach the other one. You are going to run 36 trials of 60 seconds each. In total the experiment lasts 90 minutes. At the end of the whole experiment you have some question to answer.

D.2.2 Subjects detailed results

In Figure D.2, in each horizontal axes the 3 types of force were grouped according to the legend colors.

The correspondence with the results provided in Section 3.6.4 in evident.

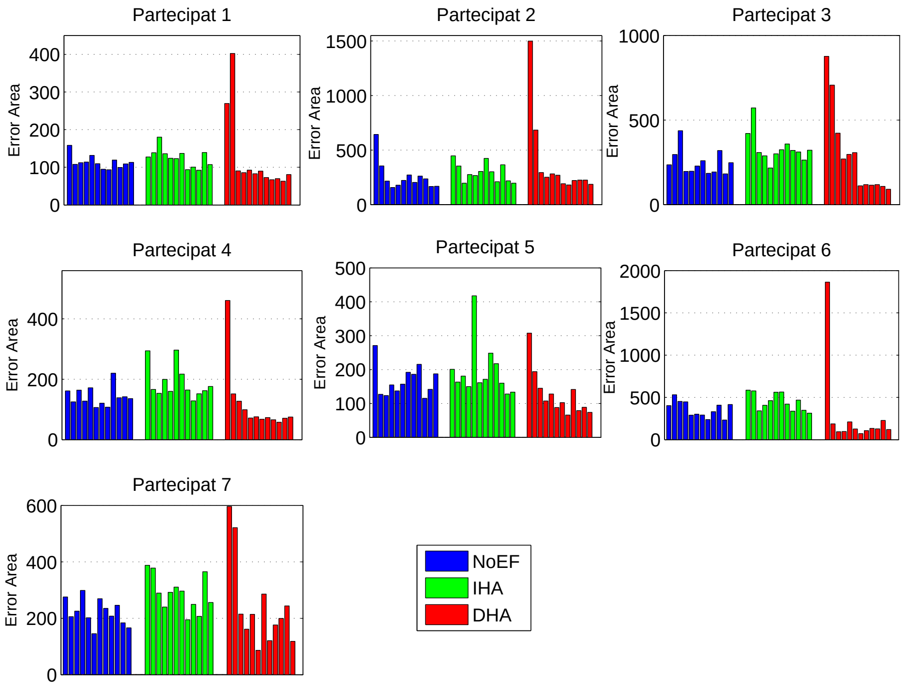

Figure D.2: The CAAF VS DHA Experiment detailed results.

D.3 The OAF VS DHA Experiment

In order to test the IHA-Obstacle Avoidance concept, several experiments about an obstacle avoidance task were run.

Ten naive subjects participated to the experiment.

A simple control task was prepared: the aircraft had to be flown in an urban canyon with buildings placed irregularly (non Manhattan-like) along the desired path; thus, the buildings constituted a narrow street with buildings in both sides. The task of the experiment was to get the end of the street by avoiding the collisions with them.

Five different scenarios (i.e. position of the N obstacles) were used to avoid the effect of learning in test subjects. An example about the employed scenario is depicted in Figure D.3.

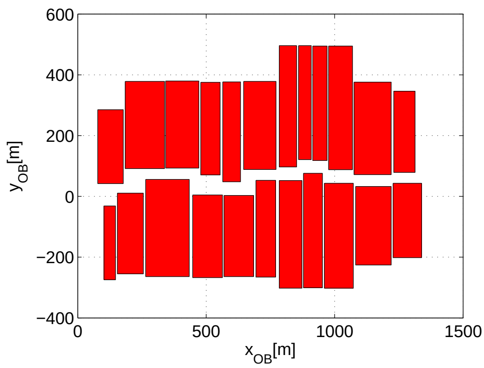

Figure D.3: One of the five employed scenarios.

To test the natural response to the different types of force no instructions were given to the participants about the force they were going to feel on the stick.

D.3.1 Instruction to subjects

> You are going to pilot a simulated aircraft through the use of the Omega Device which is a force feedback device, i.e. when you move the end-effector of it you can feel a force feedback. During the experiment you will watch at the screen in which you will see the scenario of the experiment: a sort of street with buildings in both sides. You will run 45 trials of about 2 minutes each in 3 different fog conditions: the first 15 trials are with pretty good visibility, the second 15 ones are with medium visibility, the third 15 ones are with very poor visibility. During the experiment you will feel through the Omega Device 3 types of forces. One type is only a spring and no aiding force is related to the obstacles. It is similar to the force usually felt on a normal joystick for games (when you leave the stick it comes back to the central position).

> The others two forces are with a sort of force feedback related to the obstacles. We will call it A Force and B Force. These forces instead try to move the stick themselves according to some kind of influence by the obstacles. In all trials the force conditions are all mixed and after each trial you will write which type of force you felt according to you: if you felt the Spring force or if you felt one of the two A or B. Step by step you will try to identify the difference you feel between the conditions A Force and B Force. Before starting each trial you have to push a button on the keyboard. At the end of the experiment you have some question to answer.

An example about the first five trials is given in Table D.3.

D.3.2 Subjects detailed results

In Figure D.4, in each horizontal axes the 3 types of force were grouped: blue for NoEF condition, green for IHA condition, red for DHA Force condition.

The correspondence with the results provided in Section 4.5 in evident.

D.4 The MIXED-CAAF/OAF VS DHA Experiment

In order to test the IHA-Mixed CAAF/OAF, several experiments about an obstacle avoidance task in windy conditions were run.

Seven naive subjects participated to the experiment.

The control task is the same as in the Obstacle Avoidance Experiment: the aircraft had to be flown in an urban canyon with buildings placed irregularly (non Manhattan-like) along the desired path; thus, the buildings constituted a narrow street with buildings in both sides. The task of the experiment was to get the end of the street by avoiding the collisions with them although the presence of 8 lateral wind gusts (4 towards left, 4 towards right). Again five

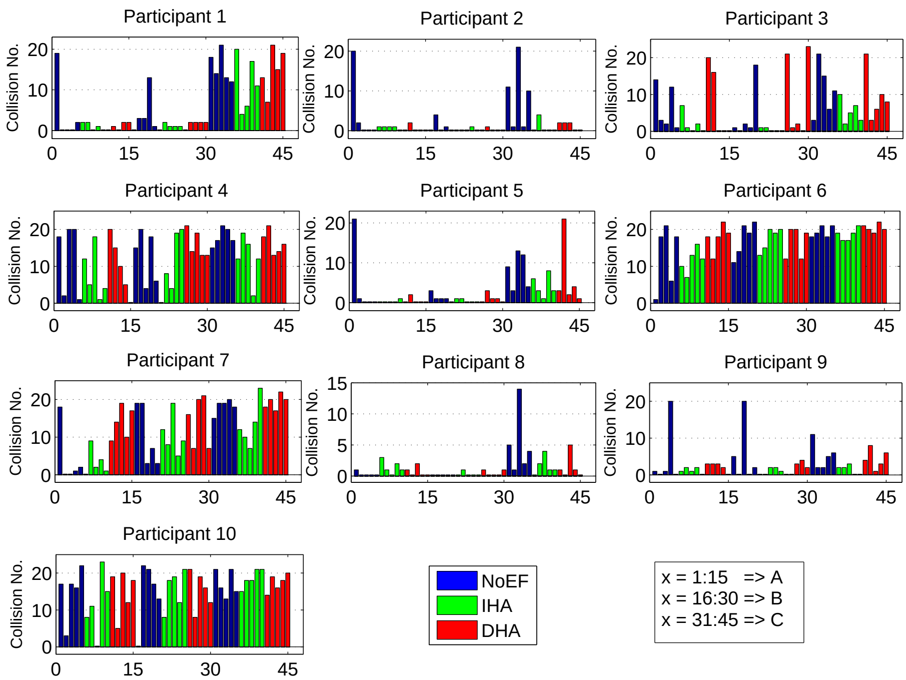

Figure D.4: The Obstacle Avoidance Experiment detailed results (A=Minimum Fog condition; B=Medium Fog condition; C=Maximum Fog condition).

different scenarios (i.e. position of the N obstacles) were used to avoid the effect of learning in test subjects.

To test the natural response to the different types of force no instructions were given to the participants about the force they were going to feel on the stick.

D.4.1 Instruction to subjects

> You are going to pilot a simulated aircraft through the use of the Omega Device which is a force feedback device, i.e. when you move the end-effector of it you can feel a force feedback. During the experiment you will watch at the scenario display which depicts a sort of street with buildings in both sides. You are already in the middle of the street and have just to avoid the obstacles on the sides by making turns. The only dynamics that you have to control is the lateral dynamics (to make the aircraft to go left or right). To do this you need to move the stick left or right only: forward or vertical movements do not affect the aircraft trajectory. The task of the experiment is to fly to the end of the street between the buildings by avoiding collisions with them. Sometimes, while you are flying, some sudden lateral wind gust will affect the aircraft and although this you have still to avoid the collisions with the buildings. You will run 60 trials of about 2 minutes each. The first 30 trials will be without/with lateral wind gusts (see later). The second 30 trials will be with/without lateral wind gusts. There will be two different visibility conditions: a medium visibility condition (some fog is present) and a very poor visibility condition (more fog is present). During the experiment you will feel through the Omega Device 3 types of forces. One type is only a spring and no aiding force is related either to the obstacles or to the wind gusts. The other two forces are with a kind of force feedback related to the obstacles and to the wind gusts. We will call it A Force and B Force. In all trials the force conditions are all mixed and after every trial you will write which type of force you felt according to you: if you felt the Spring force or if you felt one of the two A or B Forces. You will learn step by step about the A and B Forces and you will be more and more capable of distinguish them. At the end of the experiment you have some question to answer. In all trials the force conditions are all mixed and after each trial you will write which type of force you felt according to you: if you felt the Spring force or if you felt one of the two A or B. Step by step you will try to identify the difference you feel between the conditions A Force and B Force. Before starting each trial you have to push a button on the keyboard. At the end of the experiment you have some question to answer.

An example about the first five trials is given in Table D.4 clearly not shown to the participants.

D.4.2 Subjects detailed results

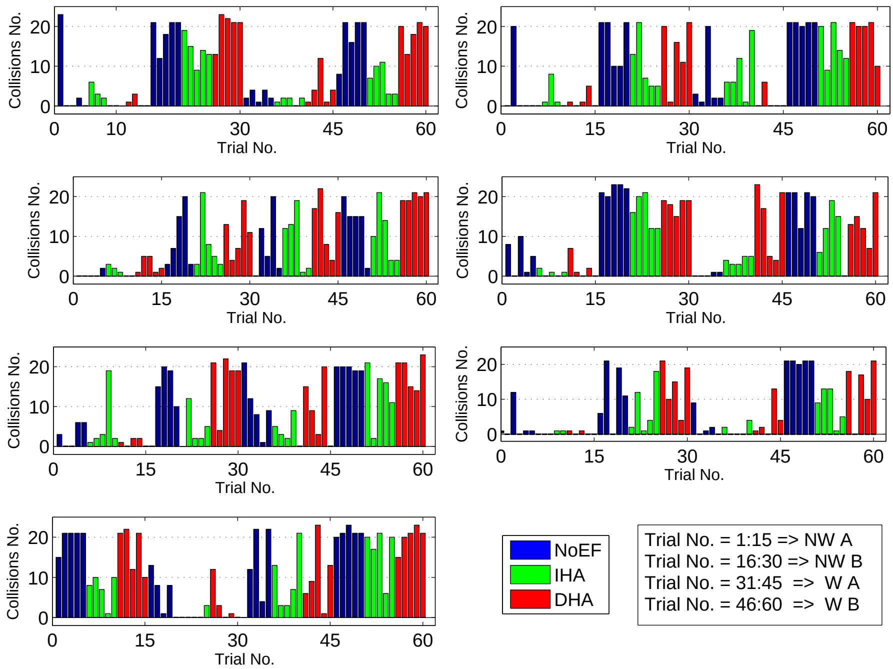

Figure D.5: The MIXED-CAAF/OAF VS DHA Experiment detailed results (NW=No Wind condition; W=Wind condition; A=Minimum Fog condition; B=Maximum Fog condition).

In Figure D.4, in each horizontal axes the 3 types of force were grouped: blue for NoEF condition, green for IHA condition, red for DHA Force condition.

The correspondence with the results provided in Section 5.6 in evident.

Subj No.	**Block 1**	**Block 2**	**Block 3**
1	1	2	3
2	1	3	2
3	2	1	3
4	2	3	1
5	3	1	2
6	3	2	1
7	1	2	3
8	1	3	2
9	2	1	3
10	2	3	1
11	3	1	2
12	3	2	1
13	1	2	3
14	1	3	2
15	2	1	3
16	2	3	1
17	3	1	2
18	3	2	1

Table D.1: The blocks order of presentation for each of the 18 participants (1=NoF; 2=Single VS CAAF Force; 3=Double VS CAAF Force).

Pilot No.	**1**	**2**	**3**	**4**	**5**	**6**	**7**
Trial No.1	1	3	2	2	1	3	3
Trial No.2	3	1	3	2	3	3	1
Trial No.3	2	2	3	2	1	1	2
Trial No.4	1	3	2	3	2	2	2

Table D.2: The blocks order of presentation for each of the 7 professional pilots. *1: NoEF*; *2: IHA*; *3: DHA*.

	Force Condition	Scenario Type
Trial No.1	1	1
Trial No.2	3	5
Trial No.3	2	4
Trial No.4	3	3
Trial No.5	1	5

Table D.3: Example of planned force conditions and scenario types for each one of the 10 participant. *1: NoEF*; *2: IHA*; *3: DHA*.

	Force Condition	Scenario Type
Trial No.1	2	1
Trial No.2	1	5
Trial No.3	0	4
Trial No.4	2	3
Trial No.5	0	5

Table D.4: Example of planned force conditions and scenario types for one of the 7 participants. *1: NoEF*; *2: IHA*; *3: DHA*.

Bibliography

[1] Lam, T.M., Boschloo, H.W., Mulder, M., van Paassen, M.M.: "Artificial Force Field for Haptic Feedback in UAV Teleoperation". In: *IEEE Transactions on Systems, Man and Cybernetics, Part A: Systems and Humans.* Vol. 39, Issue 6, pp. 1316 - 1330, Nov. 2009.

[2] Alaimo, S.M.C., Pollini, L.,Magazzú, A.,Bresciani, J.P., Robuffo Giordano, P., Innocenti, M., Bülthoff, H.H., "Preliminary Evaluation of a Haptic Aiding Concept for Remotely Piloted Vehicles". International Conference, EuroHaptics 2010, Proceedings, Part II, Amsterdam, July 2010, pp. 418-425.

[3] Kveraga, K., Boucher, L., Hughes, H.C., "Saccades operate in violation of Hick's law", Exp Brain Res. 2002 October; 146(3): 307-314. Published online 2002 August 10. doi: 10.1007/s00221-002-1168-8.

[4] Diolaiti, N., Melchiorri, C., "Tele-Operation of a Mobile Robot through Haptic Feedback". IEEE Int. Workshop on Haptic Virtual Environments and Their Applications (HAVE 2002). Ottawa, Ontario, Canada, 17-18 November 2002.

[5] Alaimo, S.M.C., Pollini, L., Bresciani, J. P., Bülthoff, H. H., "A Comparison of Direct and Indirect Haptic Aiding for Remotely Piloted Vehicles". Proceedings of the 19th IEEE International

Symposium in Robot and Human Interactive Communication (IEEE Ro-Man 2010), 541-547.

[6] Alaimo, S.M.C., Pollini, L., Bresciani, J. P., Bülthoff, H. H., "Augmented Human-Machine Interface: Providing a Novel Haptic Cueing to the Tele-Operator". The 3rd Workshop for Young Researchers on Human-Friendly Robotics, Max Planck Institute for Biological Cybernetics, Tübingen, Germany, October 28th-29th, 2010.

[7] Cox, T.H., Nagy, C.J., Skoog, M.A., Somers, I.A., "Civil UAV capability assessment", NASA, December 2004, on-line, Internet, available from http://www.nasa.gov/centers/dryden/pdf/111761main_UAV_Capabilities_Assessment.pdf.

[8] David R. Oliver and Arthur L. Money, "Defense Science Board Study on Unmanned Aerial Vehicles and Uninhabited Combat Aerial Vehicles" (Office of the Under Secretary of Defense For Acquisition, Technology, and Logistics Washington, D.C. 20301-3140, February 2004), on-line, Internet, available from www.acq.osd.mil/dsb/reports/ADA423585.pdf.

[9] Oliver, D. R. and Money, A. L. (2001). "Unmanned Aerial Vehicles Roadmap". Technical Report, Department of Defense, Washington DC.

[10] Nisser, T., Westin, C., "Human Factors challenges in Unmanned Aerial Vehicles (UAVs): a literature review", Lund University School of Aviation, Ljungbyhed, Sweden, 2008.

[11] Cooke, N. J. (2006), Human Factors of Remotely Operated Vehicles. Proceedings of the Human Factors and Ergonomics Society 50th Annual Meeting, pp. 166-169.

[12] Lam, T.M.: "Artificial Force Field for Haptic Feedback in UAV Teleoperation", Ph.D. thesis, Faculty of Aerospace Engineering, Delft University of Technology (TU Delft), Delft, The Netherlands, 2009.

[13] Royal Aeronautical Society (RAES), Human Factors Group, on-line, Internet, available from http://www.raes-hfg.com/crm/reports/sa-defns.pdf

[14] Peer, A., Buss, M., "A New Admittance Type Haptic Interface for Bimanual Manipulations". IEEE/ASME Transactions on Mechatronics, 13(4):416428, 2008.

[15] Endsley, M.R., "Measurement of situation awareness in dynamic systems", Human Factors, 1995, 37(1), 65-84.

[16] Endsley, M.R., Farley, T.C., Jones, W.M., Midkiff, A.H. and Hansman, R.J., "Situational awareness information requirements for commercial airline pilots", International Center for Air Transportation Department of Aeronautics & Astronautics, Massachusetts Institute of Technology, Cambridge, MA 02139 USA, September 1998.

[17] Tenney, Y.J., Adams, M.J., Pew, R.W., Huggins, A.W., and Rogers, W.H. (1992). "A principle approach to the measurement of situation awareness in commercial aviation". NASA contractor report 4451, Langley Research Center: NASA.

[18] Emerson, T.J., Reising, J.M., and Britten-Austin, H.G., "Workload and situation awareness in future aircraft". SAE Technical Paper (No. 871803). Warrendale, PA: Society of Automotive Engineers, 1987.

[19] Mouloua, M., Gilson, R., Kring, J., Hancock, P., "Workload, situational awareness, and teaming issues for UAV/UCAV op-

erations", Proceedings of the Human Factors and Ergonomics Society 45th Annual Meeting, 162-165, 2001.

[20] de Vlugt, E., "Identification of Spinal Reflexes". Ph.D. dissertation, Faculty of Design, Engineering, and Production, Delft University of Technology, Delft, The Nederlands, 2004.

[21] McCarley, J.S., Wickens, C.D., "Human Factors Implications of UAVs in the National Airspace", Institute of Aviation Aviation Human Factors Division University of Illinois at Urbana-Champaign, on-line, Internet, available from http://www.tc.faa.gov/logistics/grants/pdf/2004/04-G-032.pdf

[22] Hing, J.T., Oh, P.Y., "Development of an Unmanned Aerial Vehicle Piloting System with Integrated Motion Cueing for Training and Pilot Evaluation", J Intell Robot Syst (2009) 54, pp. 319. DOI 10.1007/s10846-008-9252-3

[23] Robuffo Giordano, P., Deusch, H., Lächele, J., Bülthoff, H.H., "Visual-Vestibular Feedback for Enhanced Situational Awareness in Teleoperation of UAVs", Proceedings of the American Helicopter Society 66th Annual Forum and Technology Display, 1-10, AHS International, Alexandria, VA, USA (05 2010).

[24] Nordh, R., Berrezag, A., Dimitrov, S., Turchet, L., Hayward, V., Serafin, S., "Preliminary experiment combining virtual reality haptic shoes and audio synthesis", International Conference, EuroHaptics 2010, Proceedings, Part I, Amsterdam, July 2010, pp. 123-129.

[25] Tadema, J., Theunissena, E., Koenersb, J., "Using perspective guidance overlay to improve UAV manual control performance", Enhanced and Synthetic Vision 2007, edited by Jacques G. Verly, Jeff J. Guell, Proc. of SPIE Vol. 6559, 65590C.

[26] Ren, W., Beard, R.W., "Satisficing approach to human-in-the-Loop safeguarded control", American Control , Portland, OR, USA, June 8-10, 2005.

[27] Sheridan, T.B., "Space teleoperation through time delay: review and prognosis", Robotics and Automation, IEEE Transactions on , vol.9, no.5, pp.592-606, Oct 1993. doi: 10.1109/70.258052

[28] Sheridan, T.B., Ferrell, W.R., "Remote Manipulative Control with Transmission Delay", IEEE Transactions on Human Factors in Electronics, Vol. HFE-4, Issue 1, pp. 25-29, Sept. 1963.

[29] Anderson, R.J., Spong, M.W., "Bilateral control of teleoperators with time delay", Proceedings of the 27th Conference on Decision and Control Austin, Texas, December 1988.

[30] Niemeyer, G., Slotine, J-J.E., "Telemanipulation with time delay", The International Journal of Robotics Research 2004, 23, 873. DOI: 10.1177/0278364904045563

[31] Tanner, N.A., Niemeyer, G., "Online tuning of wave impedance in telerobotics", Proceedings of the 2004 IEEE Conference on Robotics, Automation and Mechatronics, Singapore, 1-3 December, 2004.

[32] Chopra, N., Spong, M. W. (2005). "Synchronization of networked passive systems with applications to bilateral teleoperation". In Society of instrumentation and control engineering of Japan annual conference, Okayama, Japan, August 810.

[33] de Vries, S.C, "UAVs and control delays", TNO report, TNO Defence, Security and Safety, September 2005.

[34] Ruff, H.A., Draper, M.H., Lu, L.G., Poole, M.R., Repperger, D.W., "Haptic feedback as a supplemental method of alerting

UAV operators to the onset turbulence", Proceedings of the IEA 2000/ HFES 2000 Congress, 3.41 - 3.44.

[35] Zhu, W-H., Salcudean, S.E., "Stability guaranted teleoperation: an adaptive motion/force control approach", IEEE Transation On Automatic Control, Vol. 45, No. 11, 1951-1969, 2000.

[36] Hannaford, B., Ryu, J.H., "Time-Domain Passivity Control of Haptic Interfaces", In IEEE Transaction on Robotics and Automation, Vol. 18, No. 1, 2002.

[37] Lawrence, D.A., "Stability and transparency in bilateral teleoperation", In IEEE Transactions on Robotics,and Automation, Vol. 9, pp. 624-637, 1993.

[38] Goertz, R., "Electronically controlled manipulator", Nucleonics, vol. 12, pp. 4647, November 1954.

[39] Ganjefar, S., Momeni, H., Janabi-Sharifi, F., "Teleoperation systems design using augmented Wave-Variables and Smith predictor method for reducing time-delay effects", In Proceedings of the IEEE international symposium on intelligent control (pp. 333338), Vancouver, Canada, 2002.

[40] Draper, J.V., Kaber, D.B., Usher, J.M., "Telepresence", Human Factors, Vol. 40, 1998.

[41] Sheridan, T.B., "Teleoperation, telerobotics and telepresence: a progress report". Control Engineering Practice, 1995. 3(2): p. 205-214.", Human Factors, Vol. 40, 1998.

[42] Pollini, L. Innocenti, M.: "A synthetic environment for dynamic systems control and distributed simulation", *IEEE Control Systems Magazine*, Vol 20, Num. 2, pp. 49-61, April 2000.

[43] Peer, A.: "Design and Control of Admittance-Type Telemanipulation Systems", Ph.D. thesis, Institute of Automatic Control Engineering, Technische Universität München, 2008.

[44] Schauss, T., Vittorias, I., Passenberg, C., Peer, A., Buss, M.: "Tutorial for Telerobotic Summer School 2010 - Control Group", Institute of Automatic Control Engineering, Technische Universität München, July 26-30, 2010, Munich, Germany.

[45] Rauw, M.O.: "FDC 1.2 - A Simulink Toolbox for Flight Dynamics and Control Analysis", Zeist, The Netherlands, 1997 (second edition: Haarlem, The Netherlands, 2001). Distributed exclusively across the Internet *http://www.dutchroll.com*.

[46] Sangyoon L., Sukhatme, G.S., Kim, G.J., Chan-Mo P., "Haptic control of a mobile robot: a user study", Intelligent Robots and Systems, 2002. IEEE/RSJ International Conference on, vol.3, pp. 2867- 2874, 2002. DOI: 10.1109/IRDS.2002.1041705.

[47] Roskam, J., *Airplane Flight Dynamics and Automatic Flight Cotrols Part I*, DARcorporation Design, Analysis, Research, 120 East 9th Street, Suite 2, Lawrence, Kansas 66044, U.S.A, 2001.

[48] Stevens, B.L., Lewis F.L., *Aircraft Control and Simulation*, 2nd ed., John Wiley & Sons Inc., 111 River Street, Hoboken, New Jersey 07030, U.S.A, 2003.

[49] Ljung, L., *System Identification: Theory for the User*, second edition, Prentice Hall, New Jersey, 1999.

[50] Lam, T.M., Mulder, M., van Paassen, M.M., "Collision Avoidance in UAV Tele-operation with Time Delay". Systems, Man and Cybernetics, 2007. ISIC. IEEE International Conference on, pp.997-1002, 7-10 Oct. 2007. DOI: 10.1109/ICSMC.2007.4413867.

[51] Lam, T.M., Mulder, M., van Paassen, M.M., "Haptic Interface For UAV Collision Avoidance", The International Journal of Aviation Psychology, 17(2), 167-195.

[52] Hosman, R.J.A.W., Benard, B., Fourquet, H., , "Active and passive side stick controllers in manual aircraft control". Systems, Man and Cybernetics, 1990. Conference Proceedings, IEEE International Conference on, pp.527-529, 4-7 Nov 1990. DOI:10.1109/ICSMC.1990.142165.

[53] Alaimo, S.M.C., Pollini, L., Bresciani, J. P., Bülthoff, H. H, "Evaluation of Direct and Indirect Haptic Aiding in an Obstacle Avoidance Task for Tele-Operated Systems". 18th World Congress of the International Federation of Automatic Control (IFAC WC), 28th August - 2nd September 2011 (accepted).

[54] Hokayem, P.F., Spong, M.W., "Bilateral teleoperation: an historical survey", Automatica 42, pp 20352057, 2006.

[55] Farkhatdinov, I., Ryu, J-H., An, J., "A preliminary experimental study on haptic teleoperation of mobile robot with variable force feedback gain", IEEE Haptics Symposium 2010, 25-26 March, Waltham, Massachusetts, USA.

[56] Horan, B., Creighton, D., Nahavandi, S., Jamshidi, M., "Bilateral haptic teleoperation of an articulated track mobile robot", System of Systems Engineering, 2007. SoSE '07. IEEE International Conference on, San Antonio, TX, 2007.

[57] Horan, B., Najdovski, Z., Nahavandi, S., "Multi-point Multi-hand Haptic Teleoperation of a Mobile Robot", The 18th IEEE International Symposium on Robot and Human Interactive Communication, Toyama, Japan, Sept. 27-Oct. 2, 2009.

[58] de Stigter, S., Mulder, M., van Paassen, M.M., "Design and Evaluation of a Haptic Flight Director", Journal of Guidance, Control, and Dynamics, Vol. 30, No. 1, JanuaryFebruary 2007.

[59] Van Erp, J.B.F., Van Veen, H.A.H.C., Jansen, C., Dobbins, T., "Waypoint Navigation with a Vibrotactile Waist Belt", ACM Trans. Appl. Percept., 2(2):106117, 2005.

[60] Montano, F., "Integrazione di Active Sticks nell'architettura fly-by-wire dell'Alenia Aermacchi M-346", Universita' degli Studi di Palermo, Palermo, Italy, 2006.

[61] James, T., "Multi-mission/multi-agency reconfigurable UAV", Unmanned Systems, Winter, 41-42, 1994.

[62] Sheridan, T.B., "Telerobotics, automation, and human supervisory control", Cambridge, MA, The MIT Press, 1992.

[63] Wickens, C.D., "Engineering Psychology and Human Performance", 2nd ed., New York, Harper Collins, 1992.

[64] Ferrell, W. R., Sheridan, T. B., "Supervisory control of remote manipulation", IEEE Spectrum, 8188, 1967.

[65] Kim, W. S., "Experiments with a predictive display and shared compliant control for time-delayed teleoperation", In Proceedings of the annual international conference of the IEEE engineering in medicine and biology society, pp. 19051906, 1990.

[66] Miyazaki, F., Matsubayashi, S., Yoshimi, T., Arimoto, S., "A new control methodology towards advanced teleoperation of master-slave robot systems", Proc. IEEE Int. Conf. Robot. Autom. Vol.3 (1986), pp. 997-1002.

[67] Furuta, K., Kosuge, K., Shiote, Y., Hatano, H., "Master-slave manipulator based on virtual internal model following control

concept", Robotics and Automation. Proceedings. 1987 IEEE International Conference on, pp. 567 - 572.

[68] Raju, G. J., Verghese, G. C., Sheridan, T. B. (1989). "Design issues in 2-port network models of bilateral remote manipulation". In Proceedings of the IEEE international conference on robotics and automation (Vol. 3, pp. 13161321).

[69] Hirche, S., Buss, M., "Transparent data reduction in networked telepresence and teleaction systems, Part II: Time-delayed communication". Presence: Teleoperators & Virtual Environments, 16(5): 532-542, 2007.

[70] Yokokohji, Y., Imaida, T., Yoshikawa, T. (2000). "Bilateral control with energy balance monitoring under time-varying communication delay. In Proceedings of the IEEE international conference on robotics and automation (Vol. 3, pp. 26842689), San Francisco, CA, USA.

[71] Artigas, J., Preusche, C., Hirzinger, G., "Time domain passivity for delayed haptic telepresence with energy reference", Proceedings of the 2007 IEEE/RSJ International Conference on Intelligent Robots and Systems, San Diego, CA, USA, Oct 29 - Nov 2, 2007.

[72] Stramigioli, S., Secchi, C., van der Schaft, A.J., Fantuzzi, C., "Sampled data systems passivity and discrete Port-Hamiltonian systems", IEEE TRANSACTIONS ON ROBOTICS, VOL. 21, NO. 4, AUGUST 2005.

[73] Franken, M., Stramigioli, S., Reilink, R., Secchi, C., Macchelli, A., "Bridging the gap between passivity and transparency", In Proc. of Robotics: Science & Systems, 2009.

[74] Mark B. Tischler, Advances in Aircraft Flight Control, Ed. (London, UK: Taylor & Francis, 1996).

[75] Gibson, J.C., Hess, R.A.: Stick and Feel System Design. Advisory Group for Aerospace Research & Development. AGARDograph 332. Canada Communication Group, Hull, Canada (1997).

[76] Lippay, A.L., Kruk R., King, M., Murray, M.: Flight Test of a Displacement Sidearm Controller. Annual Conference of Manual Control, 17 June 1985.

[77] Schmidt, A., Lee, D., "Motor Control and Learning, A behavioral Emphasis"', 4th Ed., Human Kynetics, 2005.

[78] Lam, T.M., Mulder, M., van Paassen, M.M., Mulder, J.A., van Der Helm, F.C.T., Force-stiffness Feedback in UAV Teleoperation with Time Delay. In: AIAA Guidance, Navigation, and Control Conference, Chicago, Illinois, August 2009.

[79] Hess, R.A., "Theory for Aircraft Handling Qualities Based Upon a Structural Pilot Model", Journal of Guidance, Control, and Dynamics, Vol. 12, No. 6, 1988, p. 792.

[80] McRuer, D., Weir, D.H., "Theory of Manual Vehicular Control" Man-Machine Systems, IEEE Transactions on , vol.10, no.4, pp.257-291, Dec. 1969. doi: 10.1109/TMMS.1969.299930

[81] Hosman, R.J.A.W., Benard, B., Fourquet, H., "Active and Passive Side-Stick Controllers in Manual Aircraft Control" System, Man and Cybernetics, Conference Proceedings, IEEE International Conference on, pp.527-529, Nov. 1990. doi: 10.1109/ICSMC.1990.142165

[82] Mayer, J., Cox, T.H., "Evaluation of Two Unique Side Stick Controllers in a Fixed-Base Flight Simulator" NASA Dryden Flight Research Center Edwards, California.

[83] Bicchi, A., Buss, M., Ernst, M.O., Peer, A., *The Sense of Touch and its Rendering Progress in Haptics Research* , Springer Tracts in Advanced Robotics Volume 45, 2008, DOI: 10.1007/978-3-540-79035-8.

[84] Reichenbach, A., Thielscher, A., Peer, A., Bülthoff H.H., Bresciani, J-P. (2009), *Seeing the hand while reaching speeds up on-line responses to a sudden change in target position.* The Journal of Physiology 587(19) 4605-4616.